ANALYSIS OF THE SPIRAL STRUCTURE IN DISK GALAXIES USING THE FFT TRANSFORM

Carlos Barberà Escoí

UNIVERSITAT ROVIRA i VIRGILI

Analysis of the spiral structure in disk galaxies using the FFT transform

CARLOS BARBERÀ ESCOÍ

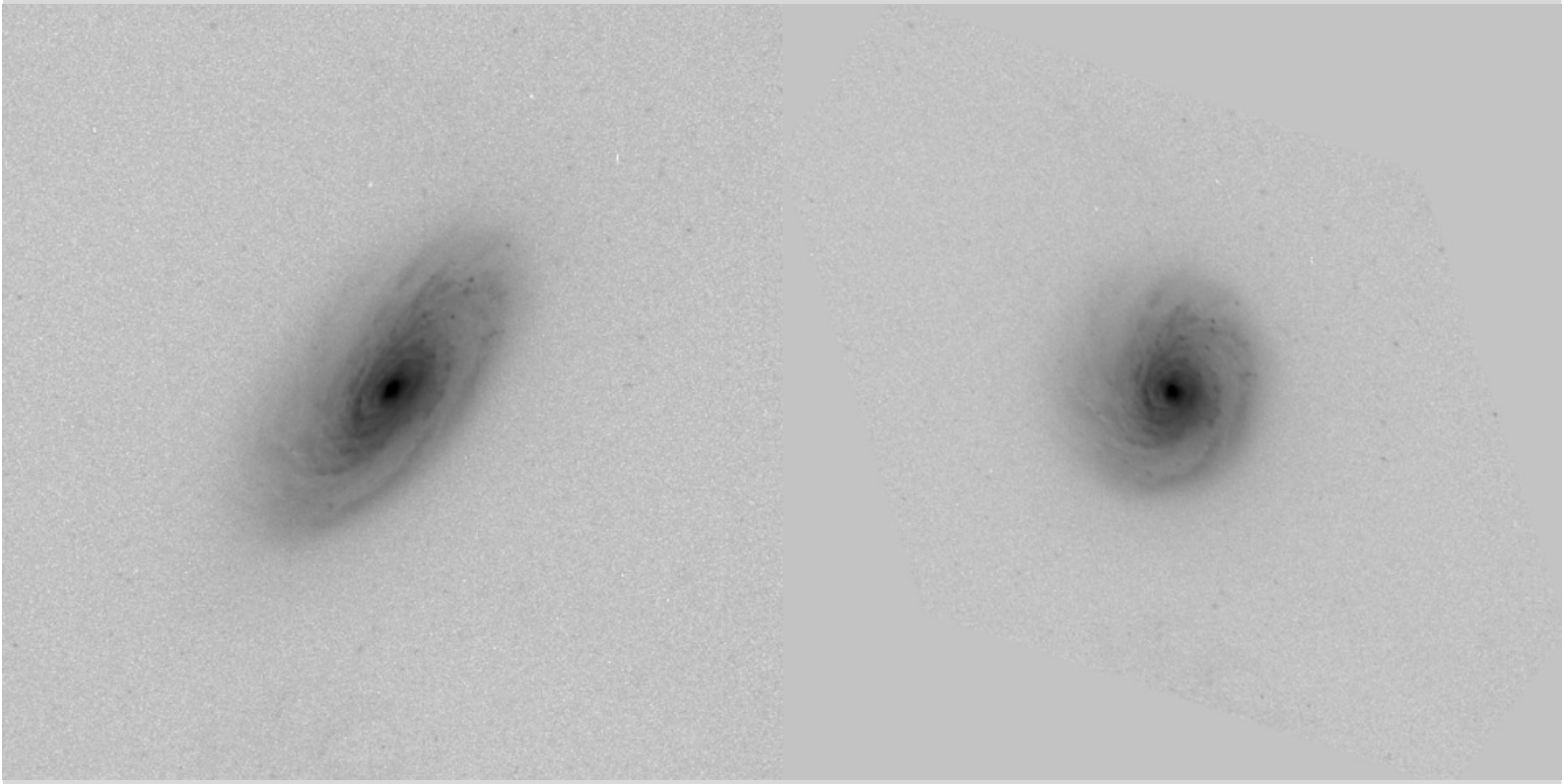

DOCTORAL THESIS
2018

UNIVERSITAT ROVIRA I VIRGILI
ANALYSIS OF THE SPIRAL STRUCTURE IN DISK GALAXIES USING THE FFT TRANSFORM
Carlos Barberà Escoí

Carlos Barberà Escoí

ANALYSIS OF THE SPIRAL STRUCTURE IN DISK GALAXIES USING THE FFT TRANSFORM

DOCTORAL THESIS

Supervised by Dr. Carlos García-Gómez
Department of Computer Engineering and Mathematics

UNIVERSITAT ROVIRA i VIRGILI

Tarragona
2018

UNIVERSITAT ROVIRA I VIRGILI
ANALYSIS OF THE SPIRAL STRUCTURE IN DISK GALAXIES USING THE FFT TRANSFORM
Carlos Barberà Escoí

UNIVERSITAT ROVIRA I VIRGILI
DEPARTAMENT D' ENGINYERIA INFORMÀTICA I MATEMÀTIQUES
Av. Països Catalans, 26
43007 Tarragona
Tel. 34 977 559 703
Fax. 34 977 559 710

I STATE that the present study, entitled "Analysis of the Spiral Structure in Disk Galaxies using the FFT Transform", presented by Carlos Barberà Escoí for the award of the degree of Doctor, has been carried out under my supervision at the Department of Computer Engineering and Mathematics of this university.

Tarragona, February 23, 2018
Doctoral Thesis Supervisor:

Dr. Carlos García-Gómez

UNIVERSITAT ROVIRA I VIRGILI
ANALYSIS OF THE SPIRAL STRUCTURE IN DISK GALAXIES USING THE FFT TRANSFORM
Carlos Barberà Escoí

To my wife Inma and sons Carles and Àlex
for unconditional love and support

UNIVERSITAT ROVIRA I VIRGILI
ANALYSIS OF THE SPIRAL STRUCTURE IN DISK GALAXIES USING THE FFT TRANSFORM
Carlos Barberà Escoí

Acknowledgments

I would like to express my sincere gratitude to my doctoral thesis and research supervisor, Dr. Carlos García-Gómez, for his constant support, guidance, encouragement and perspective to my thesis. I have learned and enjoyed working with him during all this time. Over many years, this professional and personal relationship has evolved into a life-long friendship reinforced by the health problems that both of us have successfully overcome.

I would also like to thank Dr. Lia Athanassoula for her calm, wise advice and enthusiasm on scientific research. Special thanks to Jean-Charles Lambert for always being available to help on Unix issues and for transforming my stays in the Laboratoire d'Astrophysique de Marseille on dear moments.

On a more practical level, I would also like to thank my office mate, office neighbours and the rest of collegues and staff of the Department of Computer Engineering and Mathematics for all the cofees, lunches and good moments we have had together.

Finally, my family deserves all my gratitude for their love, support and patience. My wife Inma has been my best friend and helped me get through this long period in the most positive way. My sons Carles and Alex, watching me juggle with family and work. This thesis would not have been possible without your support.

UNIVERSITAT ROVIRA I VIRGILI
ANALYSIS OF THE SPIRAL STRUCTURE IN DISK GALAXIES USING THE FFT TRANSFORM
Carlos Barberà Escoí

Contents

Contents

Chapter 1

Introduction

In this chapter, we introduce and motivate the need for the research conducted in this thesis. To this end, in Section 1.1 we introduce and justify this thesis object of research. Section 1.2 situates the subject of study and introduce the common notation used in our field of research. Section 1.3 gives a complete vision on the different theories which try to explain the spiral structures of galaxies. Section 1.4 focuses on the relevant observations and their interpretations suggested by the theories. Section 1.5 shows the mathematical basis of the methods which are the main subject of this thesis. Finally, the structure of the rest of this thesis report is presented in Section 1.6

1.1 Motivation

Our motivation is to give a quantitative classification of disk spiral galaxies according to their morphology, particularly on the presence (or not) of a central bar-shaped structure.

A galaxy is a vast collection of stars, gas and dust held together by mutual gravitational attraction. Galaxies are found in a wide range of shapes, sizes and mass, but can usefully be classified into groups according to their morphologies. The first and most famous classification was made by Hubble (1926), hnown as the Hubble sequence. He identified four main types of galaxies: elliptical, lenticular, spiral and irregular.

1.2 Galaxy classification

Elliptical galaxies have smooth, featureless light distributions in three dimensions. Their projected shapes are elliptic. They are denoted by the letter E followed by a number from 0 to 7, which describes their degree of ellipticity on the sky, then E0 corresponds to a round galaxy and E7 would be a strongly elliptical galaxy. The most common shape is close to E3. This classification depends on the intrinsic shape of the galaxy, as well as the angle in which the galaxy is observed. Hence, some galaxies with Hubble type E0 may be actually elongated.

Lenticular galaxies consist of a bright central bulge surrounded by an extended flattened disk with no gas, dust, bright young stars, or spiral arms. These galaxies are basically a transition class between elliptical and spiral galaxies and are labeled by the notation S0 in Hubble's classification scheme.

Approximately two thirds of all galaxies are spiral galaxies, Eskridge & Frogel (1999). 60% according to Buta (1989). Spiral galaxies consist of a flattened prominent disk of bright young stars, gas, and dust; a near-spherical halo of stars; and a central non-disk-like concentration of stars named bulge which may or may not be present. Disks are thin and show a clear spiral structure called spiral arms. The spiral arms vary greatly in their length and prominence. Moreover, many spiral galaxies contain also a bar-like structure extending from the central bulge. Approximately two thirds of all spiral galaxies show clearly a central bar so Hubble assigns the symbol S to spiral galaxies and denotes as SB the barred spiral ones. As in the case of elliptical galaxies, Hubble divided spiral galaxies into a sequence of four types called Sa, Sb, Sc, Sd. From a to d the spiral arms become wider while the bulge becomes smaller.

Irregular galaxies are those which do not fit into any category because they show no particular pattern. Hubble denoted irregular galaxies by the Irr symbol. A minority of Irr galaxies are spiral or elliptical galaxies that have been violently distorted by a recent encounter with a neighbour. However, the majority of Irr galaxies are simply low-luminosity systems rich in gas such as the Magellanic Clouds. These galaxies are designated Sm or Im to indicate their kinship to the Magellanic Clouds.

In 1959 Grard de Vaucouleurs, de Vaucouleurs (1959) complemented the Hubble classification system by introducing a more elaborated classification system for spiral galaxies. De Vaucouleurs introduced the notation SA for spiral galaxies without bars, maintaining

the Hubble's notation SB for barred spirals, and introducing a new category denoted SAB for an intermediate class containing weakly barred spirals. Lenticular galaxies are also classified as unbarred (SA0) or barred (SB0).

All those different approaches on galaxy classification show the importance of understanding the physical properties of spiral galaxies. A better comprehension of all the phenomena related to the spiral structure will allow a better understanding of spiral galaxies. Note that the spiral arm structure is the main classification subject. Spiral arms have a central role because they are the primary site of star formation, so their strength and shape provide important clues to the dynamics of the gas and stars within the galactic disk. Moreover, spiral arms may be the main force that drives the secular dynamic evolution of galactic disks.

These are the main classification schemes used to comprehend the rich structure of spiral galaxies. All these schemes are however, quite qualitative. Our aim is to give a more quantitative scheme of classification that could provide better clues to understand the spiral structure of disk galaxies

1.3 Spiral structure theories

1.3.1 Density waves

The first approach on the origin and evolution of the spiral structures was made in 1929 by the Swedish astronomer Bertil Lindblad, Lindblad (1929) who recognised that spiral structure arises through the interaction between the orbits and the gravitational forces of the stars of the disk. Lindblad and his collaborators focused their research on individual orbits and resonance efects associated to these orbits, but they did not study the cumulative effect into the galaxy dynamics properly. So their work was not well suited to quantitative analysis. Goldreich & Lynden-Bell (1965) looked at the spiral structure as an instability of the total combination of gas and stars triggered by an increase in gas density. This theory can explain multiarmed structures but cannot explain long bisymmetric arms arising from the center of certain galaxies. Oort (1962) recognised the truly nature of the problem. He showed that spiral structures come from a different rotation of the stellar disk, but a cummulative effect and persistence theory is still needed. Lin & Shu (1964), (1966) made the crucial step. They recognised that spiral structure in a stellar disk could be regarded

as a density wave, a wavelike oscillation that propagates through the disk in pretty much the same way that waves propagate over the ocean surface. As a result, the combination of both the Lindblad theory, where the spiral rotating pattern remains unchanged over many orbital periods, and the density wave theory, leads to the hypothesis that spiral structure is a quasi-stationary density wave in a frame of reference rotating around the center of the galaxy at a definite angular speed and unchanged amplitude. In this theory, the persistence of a regular grand design may be maintained despite the presence of differencial rotation. In addition, it is shown that a two-armed spiral pattern is only possible when the basic rotation curve is similar to that of the Milky Way system. The presence of a symmetric structure in galaxy disks is a signature of a spiral density wave. This differencial rotation can't explain star formation so Roberts (1969) suggested the existence of an additional stationary two-armed spiral shock wave that may form the triggering mechanism for the gravitational collapse of gas clouds, leading to star formation. In this scenario, the density falls down very quickly after the collapse and the star formation must be restricted to very narrow regions. Observations must show regions of luminous, newly born stars with HII regions lying on the inner side of each gaseous spiral arm. Newly born stars cause strong radiation fields, that ionize hidrogen gas. Ionized hydrogen gas is also known as HII, so the star forming regions are known as HII regions. Assuming that HII regions lie in spiral arms, the study of their distribution in spiral galaxies can help us understand the mechanism that controls the star formation on a large scale, mainly the spiral structure. This shock wave effect should take place in the concave or convex part of the arms according to the sense of rotation ot the spiral on the disk. If the spiral rotates at a lower speed than the galaxy disk, the shock should be in the concave part of the arms. If the spiral rotates faster than the galaxy, the shock should be placed in the convex part.

However, those theories present some problems. First they are based on Lin & Shu (1964) approximation which uses very twisted spirals. Toomre (1969) shows that any existing spiral wave in the disk of a galaxy must somehow be replenished to persist. Otherwise, dissipation would erase any spiral structure on the long term. Several sources of such replenishment are proposed. Toomre (1981) proposes a possible mechanism called swing amplification that occur in a thin disk of stars with a Gaussian spread of radial velocities. During swing amplification events, spiral patterns grow and decay while swinging around from leading to trailing orientation. Such events have been frequently seen in numerical sim-

ulations of the dynamical behaviour of galactic disks such as Sellwood & Carlberg (1984). Those authors showed the second and more important problem: the importance of gas and star interactions to form spiral galaxy patterns. They describe how gas fluctuations can agree with swing amplification theory. Spiral instabilities increase star velocity dispersion heating the disk until it is stable. Dissipation comes through gas accretion or star formation. This balance between cooling and heating is responsible for instabilities that maintain transient spiral patterns. So, interstellar gas is linked to spiral structure. The absence of interstellar gas and the asbsence of spiral arms are the principal features that distinguish lenticular or S0 galaxies from spiral ones.

Moreover interstellar gas is not uniformly distributed, its distribution is much more complex. Gas accumulates in little clouds, that through inelastic collisions, form giant molecular clouds which, in turn collapse to form stars. This process take place in spiral arms. So models that combine large scale effects like density waves with small scale effects like cloud-cloud collisions and supernova explosions can help us understand how global galactic shocks can be formed and persist. Levinson & Roberts (1981) introduced a cloud-particle model that embodies both concepts, density wave and stochastic star formation. They show that compression ridges associated with galactic shocks on the large scale are the products of the interaction of cloud-cloud collisions and supernova explosions. In this model, the collisional mean free path for gas clouds is about 100 or 200kpc. It seems certain that local processes can play a significant and observable role in global spiral structure.

Roberts & Hausman (1984) continued the study of the spiral pattern and star formation with numerical models showing that large scale galactic shocks are possible in a cloudy interestellar medium, even if the collisional mean free path is as long as 2 kpc. Thus, the value of the gas cloud system's collisional mean free path has remarkably little effect on galactic structure. When the cloud collisions are the main star formation mechanism, the population of young stellar associations formed during this procesus show a stable spiral pattern. In contrast, when the star formation is dominated by supernova explosions the spiral structure is unsteady. Later, the same authors Hausman & Roberts (1984) studied the gas cloud system's kinematics and concluded that the global density distribution and velocity field are pretty much independent of stellar parameters. They show that the distribution of young stellar associations is quite sensitive to assumptions about the mean lifetimes of bright stars and the susceptibility of their parent clouds, to repeated closely

spaced acts of star formation. Well defined spiral arms exhibited by the stellar associations are possible only when the average delay time between star-triggering events and stellar burnout are rather short (maximum time delay $\leq$ 20Myr). Beyond this delay time, the amount of stellar associations spreads on the disk and washes out the spiral pattern. The mean velocity field of clouds shows tipped oval streamlines similar to Roberts' theoretical model, Roberts (1969). By varying the parameters which describe star formation and cloud-star interactions, the authors can reproduce a wide variety of spiral pattern morphologies. Kimura & Tosa (1985) showed that the global distribution of molecular clouds in a galaxy, specially the existence of clouds in the interarm region, mainly depends on the lifetime of molecular clouds regardless of the amplitude of the density wave.

More recently, Roberts & Stewart (1987) showed that the distribution of giant molecular clouds only can present large-scale galactic shock structures when the mean free path between cloud-cloud collisions is short ($\lambda_c \sim$200pc). For longer mean free path ($\lambda_c \sim$1000pc) they find more symmetric, less shocklike, density and velocity profiles. Those theories seem to have great interest for galactic spiral patterns studies.

Trying to explain the enhance star formation rate in spiral arms, Cepa & Beckman (1990) show evidences that the accepted spiral density wave theory is not enough to explain star formation rate in grand-design galaxies. They put in evidence that an additional specific triggering effect is needed, perhaps associated with the supersonic propagation of the density wave through the gas. They found high HII densities in the arms and very low HII densities in the corotation and in the Lindblad resonance radii. Therefore, some nonlinear star formation rate enhancement mechanism is needed. Other authors focused on the study of the inner strong and symmetric spiral arms presented in most galaxies with spiral density waves. Elmegreen & Elmegreen (1995) found that only the strong symmetric part of the arms end at corotation, with weaker or bifurcated arms extending beyond.

Opposite to grand-design spiral galaxies with well-defined spiral arms, flocculent spiral galaxies have weak and poorly structured arms. This fundamental difference makes flocculent galaxies an important class of objects in the study of galactic structure. Thornley (1996) found low-level, two-arms spiral structure in the inner disks of a sample of nearby flocculent galaxies, that can be the result of self-excited spiral denstiy waves maintained by feedback between the stellar disk and the more dissipative, self-gravitating gas disk. Elmegreen *et al.* (1999) confirms this two-armed structure with an arm-interarm contrast increasing with

radius, as they do in grand-design galaxies. But the contrast is much smaller, indicating that they density waves are very weak. This result is consistent with the modal theory of spiral density waves, Bertin *et al.* (1989a) (1989b), which maintains that density waves are intrinsic to the disk. This denotes the importance of careful kinematic studies of spiral galaxies over all degrees of structure.

Gnedin *et al.* (1995) focused on the gravitational torque depending on the non-axisimetric mass distribution due to massive spiral arms. If persistent, the gravitational torque would remove most of the angular momentum from the inner two scale lengths of the disk and deposit it in the outer part of the disk. The inner part of the disk would contract, and the outer part would expand. This tendency could be modified by infall of new material into the disk.

The wide range of spiral arms needs a detailed morphological classification to help further studies. This is the main reason which led Elmegreen & Elmegreen (1982) to introduce a 12-division classification system for spiral arm structure independent of the Hubble galaxy type. This classification is based on the regularity of the spiral arm structure and stresses the properties of arm continuity, length, and symmetry. The classification starts from arm class 1 for chaotic appearance and no symmetry fragmented arms, with differing pitch angles, to arm class 12 for two long and sharpy defined symmetric arms, dominating the total appaerance. Pitch angle measures how tightly the spirals arms are wound and it is defined as the angle between the line tangent to a circle and the line tangent to a logarithmic spiral at a specified radius. In a later paper Elmegreen & Elmegreen (1987) reduced the number of classes by elimination of arm classes 10 and 11, because these were not directly related to the spiral structure. According to this classification, they derive the fractions of all spiral galaxies that have grand-design spirals with bars or companion galaxies and, the fraction of spiral galaxies in various environments that have purely flocculent arms. That is it, they determine what effect companions or bars may have on spiral arm structure. They show that most galaxies appear to have symmetric continuous arms and that bars are correlated with spiral density waves.

It is interesting to point out the corelation between bar and spiral structure in galaxies. Elmegreen & Elmegreen (1989) showed that the presence of a strong, long and flat-shaped bar in early-type galaxies is able to produce strong and symmetric arms, which extend out to the corotation resonance and can fill the entire disk outside the bar. While weak, short

and exponential-shaped bars which tend to occur in late-type galaxies, may not be able to propagate outwards in the region immediately beyond the bar. This difference in bar-spiral correlation is consistent with the theoretical prediction that short-wavelength trailing spirals propagate outwards beyond corotation and inwards inside corotation.

Sellwood (2012), Sellwood & Carlberg (2014) collect previous contributions to spiral wave theory to present their broad picture where apparent rapidly changing spirals result from the superposition of a small number of relativey long-lived coherent waves. The evolution of each disturbance, through a resonant scattering feature, creates the seeds for a fresh instability. Their simulations present considerable evidence to support their broad picture, but some details are still not substantaited.

Another recent scenario is based on N-body simulations of a cold, unbarred, collisionless stellar disk. D'Onghia *et al.* (2013) showed that the spiral patterns are not material entities but statistically long-lived density waves induced by local density perturbations. In particular, it is very difficult to produce persistent grand-design two-arm spiral structure in these simulations of an isolated stellar disk.

1.3.2 Self-propagation star formation theory

The density wave theory combined with interstellar clouds collision which collapse to form stars seems attractive for symmetric two-armed spirals. Another way to approach the spiral structure formation issue is to see it as the result of star formation rather than the origin. From this point of view, high-mass young stars, which are created in spherical shells of gas, quickly evolve and, at the end, they die as supernova that generates shock wave fronts. Those shock waves will start new star formation. This process will be referred to a self-propagating star formation. When this process occurs in a differentially rotating disk, regions of star formation are naturally drawn out into spiral features. Thus, spiral features are continually replaced by new ones as they wind up and disappear. The formed structure is not the attempted classical two-armed symmetric spiral pattern, but it is asymmetric and broken. In Lin & Shu (1964), (1966) density wave model need a mechanim to create and maintain the density waves, self-propagating star formation model of spiral structure introduce random spirals which may well complement the ordered structure induced by density waves. This new approach, where sequential star formation causes waves of star formation to propagate through the galaxy, was proposed by Mueller & Arnett (1976)

and the physical process that explains this self-propagation star formation mechanism was theoretically described by Elmegreen & Lada (1977). Miller (1978) confirms this theory showing the quantitative agreement with a series of numerical experiments for an axisimetric disk. This experimental confirmation requires quantization conditions for matching growth rates and to agree with the radial extension and wavenumber of the disturbances.

This model of deterministic sequential star formation of Mueller & Arnett (1976) was modified by Gerola & Seiden (1978). They replaced a stochastic sequential star formation depending only, on the probability of star formation, in the neighborhood of a new star and showed that stochastic star formation can form large scale spiral patterns. Furthermore, this method can distingish different types of galaxies according to their rotating velocity. Comins (1981) improved the method by replacing the constant probability of star formation from supernova shocks by a variable probability that decreases with the galactic radius as galaxy gas distribution does. In this case, the method becomes less effective, so it is more difficult to form large scale spiral structures, and only works for radii between the inner and outer Linblad resonances in a dynamiacal model. A new extension comes from Seiden *et al.* (1982) who includes a two-component gas, active and inactive. The active component is the gas that is available for star formation. The inactive gas can be activated by supernovae, ionization front shocks or stellar winds after a certain time. This two-component gas is essential to get feedback from the interaction between the stars and gas. Those authors show that their method can explain the gas distribution observed in the galaxy and, at the same time, produce two-armed large and symmetric structures. However they are not stable, and the galaxy alternates from very active star formation situations to less active situations.

Nozakura & Ikeuchi (1984) propose a new model based upon the viewpoint that the global spatial structure of a galaxy is produced by the local physical process and its propagation. They show that spiral structures can be regarded as dissipative structures formed within phase transition of the interstellar gas that become spiral as a result of the differencital rotation.

Junqueira & Combes (1996) performed self-gravitating simulations of the coupled stellar and gaseous components, to investigate the role of gas dynamics in the gravitational instabilities of galaxy disks. Spiral structure needs a cooling mechanism to subsist. Gas with its dissipative character, acts as a regulator and can prolong the phase of dynamical instability

to account for the spiral density waves observed in so many spiral galaxies. They suggest that the gravitational coupling between the stars and gas plays a fundamental role in the formation and dissolution of stellar bars, depending on the gaseous mass concentration and on the degreee of dissipation.

Other authors suggest that asymmetric components in disk galaxies are related to the mass accreation rate of galaxies, and thereby, constrain their mass evolution, Zaritsky & Hans-Walter (1997)

1.4 Comparing theory with observations

Spiral arms are formed by different components. The stellar component is formed by old star and young star associations (OB associations). We can find also HII regions, molecular clouds and a diffuse gas component. Each of these components is considered as a spiral arm tracer. In this paragraph we will show the relevant observations on spiral structure and their interpretation with the proposed theories.

1.4.1 Star arms

The accurate way to study a stellar arm is to count every individual star and analyse its spatial distribution according to its age. However, this is a huge work and the actual optical resolution is not enough to identify every star separately. Nevertheless, Dixon (1971) applied this method on M33 and showed that the star distribution along the southern arm of M33 is in agreement with a density waves, where old stars are placed in the inner part. Since this method is limited to very close galaxies, Dixon *et al.* (1972) proposed a new method to study spiral structure in more distant galaxies. The goal is to use colour index UB and BV as indicators. The first one can be used as a star's age indicator and the second one can indicate how interstellar extintion affects the stars. They show that the use of those index is congruent with counting stars. Following this method, Schweizer (1976) performs photometric studies for some close spiral galaxies and he shows that disk colors are very uniform with no color gradient. In contrast, arms are significantly more blue than the disks and have a highly composite spectrum. The ratio of arm intensity to disk intensity increases with radius, which explains the well-known outward bluing of spiral galaxies. He detected broad spiral paterns in the underlying disks of the galaxies.

These patterns represent variations in the surface mass density of the disk, which increases with radius, reaching about ±20% to ±30% of the mean surface mass density, in the zone of the outermost HII regions. He found that these asymmetries in the surface brightness across spiral arms is less pronounced and less frequent than one would expect. However, thanks to photographic improvements, Yuan & Grosbol (1981) measured color variation and surface brightness across a spiral arm and showed that variation is relatively smooth and symmetric, with little dependence on the distance to the center of the galaxy. Their observations are consistent with the two natural consequences of the density wave theory, namely continuous process of star formation within a cloud behind the shock, and the tendency of new stars to fall back to smaller distances to the center after their formation. Due to lower angular momentum of the cloud behind the shock.

Elmegreen & Elmegreen (1984) used blue and near-infrared surface photometry to measure disk scale lengths, spiral arm amplitudes and spiral arm color variations in 34 spiral galaxies. They found that spiral arm morphology correlates with photometric changes in the galaxy images and show that star formation and stellar density enhances the color evolution in star systems. The following results were obtained: extreme flocculent galaxies have very little structure in their old stellar population disks. Galaxies with strong developed arms can show stellar variations often exceeding 60%. For intermediate-type spiral galaxies the blueness of the arms is independent of the arm amplitude, so star-formation mechanism may be independent of these density variations, or star-formation rate would have to saturate to the same value of the stellar density amplitude.

A more modern approach to study spiral structure in disk galaxies was proposed by Elmegreen *et al.* (1989). This procedure involves removing the central part, mainly the galaxy disk, in order to emphasize the spiral arms and other nonaxisymmetric structures. So, the spiral structure can be studied; comparing the maxima and minima positions with theoretical predictions, and determining inner and outer resonances. This technique has been applied to grand-design galaxies like M51, M81 and M100 with good results, but is still an issue. Notice that the minima in intensity are not necessarily at the position of resonances, they can be originated by the superposition of two different components, if there is a phase coupling.

Substracting one galactic component can introduce errors on the remaining image, so, it is a risky procedure. It is possible to obtain all galactic components of a disk galaxy without

removing any component. A Fourier decomposition of the galaxy image using a suitable set of basic functions, like logarithmic spirals, offers the possibility to measure the amplitude of spiral and bar structure in galaxies. Danver (1942) has discussed the mathematical form of the spiral arms in galaxies. After analysing six types of simple mathematical spirals, he chooses the logarithmic spiral as the best fit to express the form of the arms. Despite this innovative work, subjective pattern recognition methods were widely used and sometimes lead to erroneous conclusions. Simien *et al.* (1978) have studied the distribution of HII regions and OB associations in M31. They have reached the noteworthy conclusion that the most probable spiral pattern of M31 is not the classical two-armed trailing spiral suggested by Arp (1964) but a one-armed leading spiral obtained by Kalnajs (1975) thanks to a Fourier analysis of the observed structure. This demonstrates the importance of using an objective algorithm to decide the best fit to describe the spiral structure of galaxies. This method was applied to galaxy images by Iye *et al.* (1982), Takase *et al.* (1989), Considère & Athanassoula (1982) and Considère & Athanassoula (1988), but unfortunately it is not extensively developed.

1.5 Two-dimensional Fourier analysis

In this work, we use the method proposed by Kalnajs (1975) of a two-dimensional Fourier analysis of the HII regions distribution as an objective method to study the properties of spiral galaxies. The method consists of choosing a logarithmic spiral basis of functions and calculating the Fourier coefficients of the HII region distribution on that basis. It is important to stress that, in this method, the specific form of the basis functions does not constrain the analysis. The basis functions only give a reference system in which we can obtain parameters to describe the distribution of HII regions.

The observed HII region distribution, which has all the objective information, shows the presence of a specific structure and plenty of points scattered all over the galaxy plane. It is difficult to decide which of those points follow a pattern and which points are someway random, not following any pattern. We are not looking for a method to clean those disturbing random points, but for a method that, objectively, manages to find out the structure from all the distribution points.

Thanks to this method, we can find out the parameters of the logarithmic spiral functions

that best represent the observed HII region distribution, between all the basis of functions. So, we can derive the main spiral pattern (signal) from the observed HII regions distribution that appears somehow randomly distributed on the galaxy plane (noise).

1.5.1 Mathematical equations

The logarithmic spiral basis function are given by $f(u,\theta) = exp[i(pu + m\theta)]$ in the logarithmic polar coordinates (u,θ), where $u = ln(r)$. The angular periodicity number m indicates the number of arms, and p is the logarithmic radial frequency or a measure of the direction and tightness of winding. The tightness of the arms winding is measured by the pitch angle i by the relation $tan(i) = -m/p$

1.5.2 Equations for HII regions

Let $\sigma(r,\theta)$ the HII region density on the galaxy plane, the galaxy mass is given by:

$$M = \int_0^{+\infty} \int_0^{2\pi} \sigma(u,\theta) r d\theta dr \tag{1.1}$$

Changing the radial coordinate r by its natural logarithm u the previous equation is:

$$M = \int_0^{+\infty} \int_0^{2\pi} \mu(u,\theta) d\theta du \tag{1.2}$$

where $\mu(u,\theta) = \sigma(u,\theta)e^{u^2}$ or in polar coordinates $\mu(r,\theta) = \sigma(r,\theta)r^2$

Each of the N HII regions, with polar coordinates (r_j,θ_j) in the galactic plane, is treated as a point with weight $1/N$ in order to normalize the total mass to unit. Then the density can be expressed as a sum of delta-functions

$$\mu(u,\theta) = \frac{1}{N} \sum_{n=1}^{N} \delta(u - u_j)\delta(\theta - \theta_j) \tag{1.3}$$

The Fourier transform of such distribution is expressed by

$$A(p,m) = \int_{-\infty}^{+\infty} \int_{-\pi}^{+\pi} \mu(u,\theta) e^{-i(pu+m\theta)}\, d\theta du \tag{1.4}$$

where replacing $\mu(u,\theta)$ by (1.3)

$$A(p,m) = \int_{-\infty}^{+\infty}\int_{-\pi}^{+\pi} \frac{1}{N}\sum_{n=1}^{N} \delta(u-u_j)\delta(\theta-\theta_j)e^{-i(pu+m\theta)}\,d\theta du \tag{1.5}$$

exchanging integrals and summation we have

$$A(p,m) = \frac{1}{N}\sum_{n=1}^{N}\int_{-\infty}^{+\infty}\int_{-\pi}^{+\pi} \delta(u-u_j)\delta(\theta-\theta_j)e^{-i(pu+m\theta)}\,d\theta du \tag{1.6}$$

As the Fourier transform of the delta function is given by

$$F_x\left[\delta(x-x_0)\right](k) = \int_{-\infty}^{+\infty}\delta(x-x_0)e^{-ikx}\,dx = e^{-ikx_0}$$

finally, we get the Fourier coefficients in the expansion of our observed distribution $\mu(u,\theta)$

$$A(p,m) = \frac{1}{N}\sum_{j=1}^{N} e^{-i(pu_j+m\theta_j)} \tag{1.7}$$

$A(p,m)$ are complex functions. The angular frequency m is an integer number that represents the number of arms in the studied galaxy structure. For $m = 0$ (axisymetric case), $m = 1$ (one-armed component), $m = 2$ (two-armed component) and so on. The radial frequency p is related tho the pitch angle i of the spiral, $tan(i) = -m/p$ and takes values, regularly spaced, in the interval $(-p_{max}, p_{max})$. We consider $p_{max} = 128$ because for this value we get a pitch angle $i = 0.45°$ that corresponds to a very coiled (winding) spiral. For $i = 45°$, p is 1. For spirals wider than 45°, p takes values between 0 and 1. For our study we calculate $A(p,m)$ for $p \in (-128, 128)$ and for $m = 0$ to 8.

To recover the mass density we perform the inverse Fourier transform of the coefficients A(p,m) given by the following expression

$$\mu(u,\theta) = \frac{N}{4\pi^2}\sum_{-\infty}^{+\infty}\int_{-\infty}^{+\infty} A(p,m)e^{-i(pu+m\theta)}\,dp \tag{1.8}$$

Fixing the angular frequency m we recover the mass density related to this m-armed

spiral using the inverse Fourier transform

$$\mu_{m_o}(u,\theta) = \frac{N}{4\pi^2}\int_{-\infty}^{+\infty} A(p,m_o)e^{-i(pu+m_o\theta)}\,dp \tag{1.9}$$

and multiplying by $1/r^2$ we get the function $S_m(r,\theta)$

$$S_m(r,\theta) = \mu_m(r,\theta)\frac{1}{r^2} \tag{1.10}$$

since S_m is a complex function, to recover the density distribution of the m-armed structure by taking the real part

$$\sigma(r,\theta) = Re\left[S_{m_o}(r,\theta))\right] \tag{1.11}$$

Now, we can recover the original galaxy.

1.5.3 Equations for galaxy images

Once we have developed the transforming method for HII regions, we now implement it for galaxy images. There are many reasons to use galaxy images. The increasing number of available galaxy image catalogs allows us to work with samples big enough for statistical studies. Galaxy images give much more information and this information comes from the whole galaxy disk and not only from the HII regions. We are not limited by the number, sizes and masses of the HII regions, we have homogeneous information covering the whole galaxy. Moreover, the availability of galaxy images, for the same galaxy, with different pass-bands opens the possibility to study the reliability and performance of our methods to different color images.

For each galaxy image we have a matrix representing the observed light intensity distribution in the plane of the sky, as measured in units of the sky brightness. Those digital images are NxN matrices centered at the galaxy center. First of all, we need to clean the image subtracting foreground stars and normalizing to the sky background using the brightest pixel of the image. In this way, we obtain a relative intensity matrix $I(x,y)$ of the galaxy, which will be the basis of our analysis. From this relative intensity matrix $I(x,y)$, we perform a polar coordinates interpolation with logarithmic radial coordinates ($u = ln(r)$) to obtain a new data matrix, $I(u,\theta)$. Where $u \in (-\infty,\infty)$ and $\theta \in [0,2\pi]$. The first step to perform in this interpolation is to define the 2-dimensional grid for the variables

(u, θ). We must keep in mind that we will use this grid to compute the Fourier transform of the function $I(u, \theta)$ in order to obtain the corresponding coefficients in the frequency domain (p, m). Since in Fourier's theory the spatial domain and the frequency domain are related, we are going to adapt our spatial domain grid to have enough resolution in the frequency domain. As we have already seen for the case of HII regions, the optimal domain for the radial frequency p is $p \in (-128, 128)$. So the starting consideration to generate the grid is to fix $p_{max} = 128$. In other words, we want that all our Fourier transformed image fits in the fixed interval for p. To meet this restriction, according to the sampling theorem, the maximum value for the radius is defined by $u_{max} = 1/2\Delta p$ where $\Delta p = 2p_{max}/n$ is the frequency sampling step and n is the size of the sampling grid for the variables (u, θ). It worth noting that the relative intensity matrix $I(x, y)$ of the galaxy image is a NxN matrix while the interpolated one, $I(u, \theta)$, is a nxn matrix. For technical reasons of the Fast Fourier Transform routine we use, we must add also a 2π factor. Therefore, in our case $u_{max} = \pi/\Delta p$. The last parameter that needs to be fixed is the sampling number n. This value is linked to the size of the initial galaxy image matrix NxN. Lower values of n will not profit all the information of the galaxy image, giving not enough accurate results. So, we need to take n big enough for good accuracy but not too big for computation time considerations. After different tests, for our galaxy images, values from 2^{10} provide enough accurate results, therefore we agree to fix $n = 2^{11}$. We should take into account that the sampling number must be a power of two to use Fast Fourier Transform routines.

With this relative intensity matrix in polar coordinates, we can proceed as in the case of HII regions, calculating the Fourier transform coefficients with bidimensional techniques. We have that the transformed image is defined as

$$A(p, m) = \int_{-\infty}^{+\infty} \int_{0}^{2\pi} I(u, \theta) e^{-i(pu+m\theta)} \, d\theta du \tag{1.12}$$

where angular and radial frequencies take the same values as for HII regions.

Opposite to the case of HII regions, where we worked with very few data points coming mainly from the spiral structure, here we have much more information coming from all the galaxy components including the background disk or $m = 0$ component. Some galaxy components as the galaxy bulge, must be removed prior the transformation. The galaxy bulge is the brightest part, and not removing it could result in a very strong axisymmetric

component that will disguise the weak non axisymmetric component that contain all the information from the galaxy spiral structure. The goal is to keep only the information coming from the galaxy disk where all the spiral structure can be found. The galaxy disk will be fitted with logarithmic spirals by Fourier thecniques. Afterward, our deprojecting techniques try to render the disk circular. The bulge is nearly spherical and looks round on the plane of the sky. Therefore, if we do not remove the bulge and the bulge-dominated region, when trying to deproject the galaxy, we will stretch it, given an elongated structure which will be interpreted as a bar structure, giving strong spurious signals in the $m = 2$ components that will bias the results. Furthermore, for strongly barred galaxies, if we keep this inner structure, our methods try to circularize the bar, not the external disk, resulting in biased results as well. For these cases, in order to ged good values of the PA and IA, it is necessary to eliminate a circular region enclosing the whole bar, also if an inner ring is also present, this should be eliminated as well.

Despite the size of the inner part of the galaxy, we must remove it for all the galaxies before proceed with our computations. This is relevant because, in this new scenario, our relative intensity function $I(u, \theta)$ will abruptly fall to zero, at the radius of the removed inner part of the galaxy, resulting in a jump discontinuity. Calculating the Fast Fourier Transform in these circumstances will produce a strong numerical effect known as the Gibbs phenomenon, adding spurious terms to the Fourier series of the function. We propose to localy apply a sinus filter to gently decrease our function values to zero.

$$I_f(u,\theta) = \begin{cases} I(u,\theta) & \text{for } u \geq u_{min} \\ I(u,\theta) sin^2\left(\dfrac{\pi e^u}{2e^{u_{min}}}\right) & \text{for } u < u_{min} \end{cases}$$

Where u_{min} is the radius of the removed inner part of the galaxy.

Once dealed with these problems for the lower grid values of u, we can concentrate in the other end of the grid. For grid values of u approaching the disk galaxy limit, no filter is needed because the relative light intensity slowly falls down to the sky background. Finaly, for grid values overcoming the galaxy disk limits we set the function value to the relative light value of the sky backgrond, ie, to zero. So, once fixed the radius of the removed inner part, u_{min} and the radius of the disk galaxy extend, u_{ext} the final working function is:

$$I_f(u,\theta) = \begin{cases} 0 & \text{for} \quad u_{ext} < u \leq u_{max} \\ I(u,\theta) & \text{for} \quad u_{min} \leq u \leq u_{ext} \\ I(u,\theta) sin^2\left(\dfrac{\pi e^u}{2e^{u_{min}}}\right) & \text{for} \quad -u_{max} \leq u < u_{min} \end{cases}$$

After all these previous remarks and considerations, we can calculate the Fast Fourier Transform and move to the frequency domain where we will work with the complex functions $A(p,m)$ to extract information that will help us to first deproject the galaxy images from the sky and calculate the position and inclination angles. Secondly, to measure bar strength on disk galaxies and classify them according to their bar mophology and finally. Third, to measure and identify the spiral structure of disk galaxies.

1.6 Structure of the Thesis

This thesis is structured as compendium of four papers that we present in Chapter 2. Three of them are related to deproject disk galaxies from the plane of the sky to the plane of sight and the last one to quantify the bar strength on disk galaxies. The first one uses information from HII regions distribution to find the deprojection angles. Presenting two deprojection methods and applies them to a sample of 88 disk galaxies. The second and third papers present two new methods for galaxy deprojection, BAG1 and BAG2, based on Fourier analysis of their images. After testing the methods, we aply them to two galaxy samples; Frei *et al.* (1996) sample with 79 galaxies, and Ohio State Univerrity Bright Spiral Galaxy Survey with 158 galaxies. We have compared the resulting deprojection angles of BAG1 and BAG2 with data from the Third Reference Catalogue of Bright Galaxies (RC3) **?** and other estimations found in the literature. We found that our deprojection methods perform very well, except in cases where the galaxy is nearly face-on, where only the estimates from kinematics are reliable.

Chapter 3 summarize the main conclusions and some conslusion on the bar distribution as well as the future directions of research to go further using Fourier technique to quantify morphological structures on disk galaxies.

Chapter 2

Contributions of the Thesis

The main contribution of this thesis are included in this chapter. We include a complete copy of the fourth papers that present our research. The doctoral candidate is author of those fourth journal articles published and indexed in ISI-JCR.

2.1 Analysis of the distribution of HII regions in external galaxies. IV. The new galaxy sample. Position and inclination angles

García-Gómez, C., Athanassoula, E., and **Barberà, C.**, Analysis of the distribution of HII regions in external galaxies. IV. The new galaxy sample. Position and inclination angles. *Astronomy and Astrophysics* 389, 68-83 (2004) EDP Sciences. DOI: 10.1051/0004-6361:20020460

A&A 389, 68–83 (2002)
DOI: 10.1051/0004-6361:20020460

Astronomy & Astrophysics

Analysis of the distribution of HII regions in external galaxies

IV. The new galaxy sample. Position and inclination angles⋆

C. García-Gómez[1], E. Athanassoula[2], and C. Barberà[1]

[1] D.E.I.M., Campus Sescelades, Avd. dels Països Catalans 26, 43007 Tarragona, Spain
[2] Observatoire de Marseille, 2 place Le Verrier, 13248 Marseille Cedex 04, France

Received 12 February 2002 / Accepted 19 March 2002

Abstract. We have compiled a new sample of galaxies with published catalogs of HII region coordinates. This sample, together with the former catalog of García-Gómez & Athanassoula (1991), will form the basis for subsequent studies of the spiral structure in disc galaxies. In this paper we address the problem of the deprojection of the galaxy images. For this purpose we use two deprojection methods based on the HII region distribution and compare the results with the values found in the literature using other deprojection methods. Taking into account the results of all the methods, we propose optimum values for the position and inclination angles of all the galaxies in our sample.

Key words. galaxies: structure – galaxies: spiral – galaxies: ISM – ISM: HII regions

1. Introduction

Catalogs of HII regions of spiral galaxies can be used to obtain a great deal of information on their underlying galaxies. For instance, we can study the radial profile of the distribution of HII regions and compare it with the radial distribution of the light in different wavelengths. We can study also the number distribution of HII regions according to their flux and use this information to study the star formation rate in galaxies. Yet more information can be obtained by Fourier analyzing the spatial distribution of the HII regions. The distribution can then be decomposed into components of a given angular periodicity, whose pitch angles and relative amplitude can be calculated. Using such results for a large sample of galaxies should provide useful information on the properties of spiral structure in external galaxies. With this aim, we started in 1991 a study of all catalogs published until that date (García-Gómez & Athanassoula 1991, hereafter GGA; García-Gómez & Athanassoula 1993; Athanassoula et al. 1993). Since then, however, a large number of new catalogs has been published, nearly doubling our initial sample. This warrants a reanalysis of our previous results, particularly since the new published catalogs extend the initial sample specially towards barred and ringed galaxies, which were sparse in the first sample. The new sample contains also a large number of active galaxies.

In this paper we will concentrate on the fundamental step of the deprojection of the HII region positions from the plane of the sky onto the plane of the galaxy, determining the position angle (hereafter PA) and the inclination angle (hereafter IA) of each galaxy using several methods of deprojection. In future papers we will study the spiral structure of the galaxies which have a sufficient number of HII regions and use the whole sample to study the global properties of the spiral structure in external galaxies. This paper is structured as follows: In Sect. 2 we present the new sample and in Sect. 3 we discuss the different methods of deprojection used to obtain the values of PA and IA. In Sect. 4 we give the PA and IA values adopted for the galaxies in our sample and finally in Sect. 5 we compare the values of the PA and IA obtained by using the different methods of deprojection.

2. The sample

Several new catalogs of the distribution of HII regions in external galaxies have been published in the last decade. These come mainly from the surveys of Hα emission in Seyfert galaxies from Tsvetanov & Petrosian (1995), Evans et al. (1996) and González Delgado et al. (1997), from the Hα survey of southern galaxies from Feinstein (1997) and the Hα survey of ringed galaxies by Crocker et al. (1996). There have also been a considerable number of studies of the HII region distribution in individual

Send offprint requests to: C. García-Gómez,
e-mail: cgarcia@etse.urv.es

⋆ Tables 2 and 3 are only available in electronic form at http://www.edpsciences.org

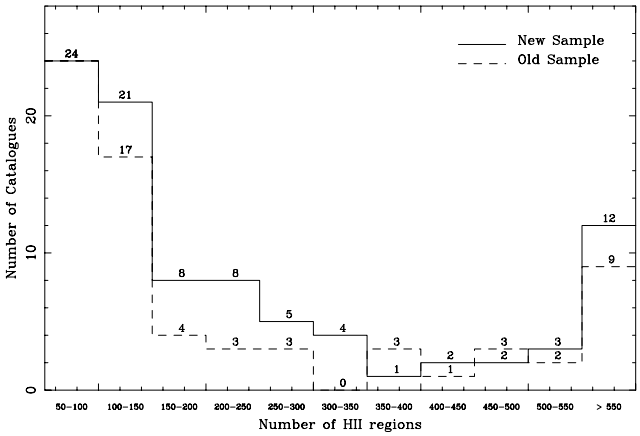

Fig. 1. Distribution of galaxies as a function of number of HII regions.

galaxies: NGC 157, NGC 3631, NGC 6764 and NGC 6951 (Rozas et al. 1996); NGC 598 (Hodge et al. 1999): NGC 3198 (Corradi et al. 1991); NGC 3359 (Rozas et al. 2000b); NGC 4321 (Knapen 1998); NGC 4258 (Courtès et al. 1993); NGC 4736 (Rodrigues et al. 1998); NGC 5194 (Petit et al. 1996); NGC 5457 (Hodge et al. 1990; Scowen et al. 1992); NGC 6184 (Knapen et al. 1993); NGC 7331 (Petit 1998) and NGC 7479 (Rozas et al. 1999).

From these studies we have retained all galaxies with an inclination less than 80° and with a sufficient number of HII regions listed. Indeed, more than 50 HII regions are necessary to allow a study of the spiral structure. Nevertheless, we included also five galaxies with fewer HII regions because we judged that they described fairly well the galaxy disc. In Fig. 1 we show the number of catalogs as a function of the number of HII regions they have. The solid line corresponds to catalogs of the new sample, and the dashed line corresponds to the sample used in GGA (1991). From this figure we see that the quality of the two samples is roughly the same.

The properties of the galaxies selected for our study and of their HII region catalogs are listed in Table 1. Column 1 gives the galaxy name. Columns 2 and 3 the Hubble type (T) and the Hubble stage (S) from the RC3 catalog (de Vaucouleurs et al. 1991). Column 4 gives the arm class (AC) as defined in Elmegreen & Elmegreen (1987). Column 5 classifies the spiral structure (SS) seen in the HII region distribution, which we obtain by eye estimates as in GGA (1991). If we can see a clear grand design spiral we give a classification Y in Col. 5 and N on the contrary. Intermediate cases are classified as R. Finally, in Col. 6 we give the number of HII regions in the catalog (N) and in Col. 7 a key for the reference of this particular catalog. The number distribution of galaxies as a function of galaxy type is shown in Fig. 2. The solid line corresponds to the number distribution of types for the galaxies of the new sample, while the dashed line corresponds to the sample used in GGA (1991). As in the previous paper the peak is for galaxies of type Sbc. Nevertheless, this sample

Table 1. General properties of the galaxies in the new sample.

Name	T	S	AC	SS	*N*	Ref.
ESO 111-10	PSXT4..	3.7	-	N	64	1
ESO 152-26	PSBR1..	1.0	-	Y	236	1
ESO 377-24	.SAT5*P	5.0	-	N	59	2
IC 1438	PSXT1*.	0.7	-	Y	44	1
IC 2510	.SBT2*.	2.3	-	N	70	2
IC 2560	PSBR3*.	3.3	-	R	137	2
IC 3639	.SBT4*.	4.0	-	N	112	2
IC 4754	PSBR3*.	2.6	-	N	114	1
IC 5240	.SBR1..	1.0	-	N	119	1
NGC 0053	PSBR3..	0.6	-	N	66	1
NGC 0157	.SXT4..	4.0	12	Y	707	8
NGC 0210	.SXS3..	3.0	6	Y	518	1
NGC 0598	.SAS6..	6.0	5	N	1272	18
NGC 1068	RSAT3..	3.0	3	N	110	3
NGC 1097	.SBS3..	3.0	12	Y	401	6
NGC 1386	.LBS+..	-0.6	-	N	44	2
NGC 1433	PSBR2..	2.0	6	R	779	1
NGC 1566	.SXS4..	4.0	12	Y	679	2
NGC 1667	.SXR5..	5.0	-	N	46	3
NGC 1672	.SBS3..	3.0	5	N	260	6
NGC 1808	RSXS1..	1.0	-	N	206	2
NGC 1832	.SBR4..	4.0	5	R	206	1
NGC 2985	PSAT2..	2.0	3	N	110	3
NGC 2997	.SXT5..	5.0	9	R	373	5
NGC 3081	RSXR0..	0.0	6	N	75	6
				N	58	2
NGC 3198	.SBT5..	5.0	-	N	104	9
NGC 3359	.SBT5..	5.0	5	Y	547	4
NGC 3367	.SBT5..	5.0	9	R	79	3
NGC 3393	PSBT1*.	1.0	-	R	80	2
NGC 3631	.SAS5..	5.0	9	Y	1322	8
NGC 3660	.SBR4..	4.0	2	N	59	3
NGC 3783	PSBR2..	1.5	9	N	58	2
NGC 3982	.SXR3*.	4.6	2	N	117	3
NGC 4051	.SXT4..	4.0	5	N	123	6
NGC 4123	.SBR5..	5.0	9	N	58	5
NGC 4258	.SXS4..	4.0	-	Y	136	16
NGC 4321	.SXS4..	4.0	12	Y	1948	12
NGC 4507	PSXT3..	3.0	5	N	92	2
NGC 4593	RSBT3..	3.0	5	Y	112	2
				R	45	5
NGC 4602	.SXT4..	4.0	-	N	218	2
			-	N	46	5
NGC 4639	.SXT4..	4.0	2	R	190	6
NGC 4699	.SXT3..	3.0	3	N	104	3
NGC 4736	RSAR2..	2.0	3	N	168	3
				N	90	17
NGC 4939	.SAS4..	4.0	12	Y	250	2
				Y	206	6
NGC 4995	.SXT3..	3.0	6	R	142	3
NGC 5033	.SAS5..	5.0	9	R	423	6
NGC 5194	.SAS4P.	4.0	12	Y	477	7
NGC 5364	.SAT4P.	4.0	9	R	174	5
NGC 5371	.SXT4..	4.0	9	Y	100	3

Table 1. continued.

Name	T	S	AC	SS	N	Ref.
NGC 5427	.SAS5P.	5.0	9	Y	300	2
				Y	164	1
				R	78	6
NGC 5457	.SXT6..	6.0	9	Y	1264	13
				Y	248	14
NGC 5643	.SXT5..	5.0	-	N	214	2
NGC 5861	.SXT5..	5.0	12	N	55	5
NGC 6070	.SAS6..	6.0	9	N	61	5
NGC 6118	.SAS6..	6.0	-	N	117	5
NGC 6221	.SBS5..	5.0	-	Y	173	2
NGC 6300	.SBT3..	3.0	6	N	977	1
				N	317	6
NGC 6384	.SXR4..	4.0	9	R	283	5
NGC 6753	RSAR3..	3.0	8	Y	541	1
NGC 6764	.SBS4..	3.5	5	R	348	8
NGC 6782	RSXR1..	0.8	-	Y	296	1
NGC 6814	.SXT4..	4.0	9	Y	734	15
				Y	131	6
NGC 6902	.SAR3..	3.1	-	R	467	1
NGC 6935	PSAR1..	1.1	-	N	166	1
NGC 6937	PSBR5*.	4.9	-	Y	213	1
NGC 6951	.SXT4..	4.0	12	Y	664	8
NGC 7020	RLAR+..	-1.0	-	N	68	1
NGC 7098	RSXT1..	1.0	-	R	188	1
NGC 7219	RSAR0P.	0.0	-	Y	139	1
NGC 7267	PSBT1P.	1.0	-	N	122	1
NGC 7314	.SXT4..	4.0	2	N	151	6
				N	117	2
NGC 7329	.SBR3..	3.0	-	R	349	1
NGC 7331	.SAS3..	3.0	3	N	252	10
NGC 7479	.SBS5..	5.0	9	R	126	11
NGC 7531	.SXR4..	2.8	3	R	549	1
NGC 7552	PSBS2..	2.0	-	N	78	5
NGC 7590	.SAT4*.	4.0	-	N	129	2

(1) Crocker et al. (1996), (2) Tsvetanov & Petrosian (1995), (3) González Delgado et al. (1997), (4) Rozas et al. (2000a), (5) Feinstein (1997), (6) Evans et al. (1996), (7) Petit et al. (1996), (8) Rozas et al. (1996), (9) Corradi et al. (1991), (10) Petit (1998), (11) Rozas et al. (1999), (12) Knapen (1998), (13) Hodge et al. (1990), (14) Scowen et al. (1992), (15) Knapen et al. (1993), (16) Courtés et al. (1993), (17) Rodrigues et al. (1998), (18) Hodge et al. (1999).

contains many more earlier type galaxies than the previous one. Indeed, in the previous sample most galaxies are of type Sbc and later, while in the new one most are Sbc and earlier.

In Fig. 3 we compare the arm class classification of Elmegreen & Elmegreen (1987) with our classification of the arm structure present in the HII region distribution. The left panels refer to the galaxies in the new sample and the right panels to the galaxies in the GGA (1991) sample. The upper panels correspond to galaxies classified as Y,

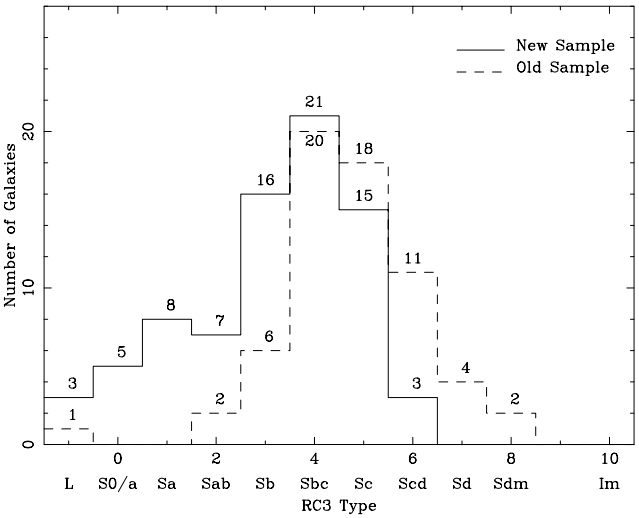

Fig. 2. Distribution of galaxies as a function of galaxy type.

the second row of panels correspond to the galaxies classified as N and the third row contains the galaxies classified as R. The last row contains the distribution of all the galaxies according to arm class. The figure shows that galaxies classified with higher number in the arm class have a tendency to have well developed arms in the distribution of HII regions. There are, however, exceptions as e.g. NGC 5861 which has been given an arm class 12 by Elmegreen & Elmegreen (1987), but has no apparent spiral structure in the HII region distribution.

We should also note that our new sample is formed mainly by barred and ringed galaxies. This is shown in Fig. 4 where we can see the number distribution of galaxies as a function of bar type as given in the RC3 catalog. In the upper panel we show the distribution of bar types of the galaxies of the GGA (1991) sample. In the middle panel we show the distribution for the new sample and in the lower panel the distribution of bar types of the two samples combined. While the first sample was biased towards non-barred galaxies (upper panel), the new catalog is biased towards barred and/or ringed galaxies (middle panel). This gives a quite uniform total distribution (lower panel).

Our final aim is to study the spiral structure outlined by the HII region distribution. Obviously, this cannot be done with a catalog with a number of HII regions lower than 50, and only the richer catalogs will be considered for this purpose in a forthcoming paper. Nevertheless, useful information on the galaxies can be obtained even from the less rich catalogs, as e.g. the orientation of the galaxies as seen in the sky and the radial scale of the distribution, which can be compared with the radial scale length of galaxy discs (Athanassoula et al. 1993).

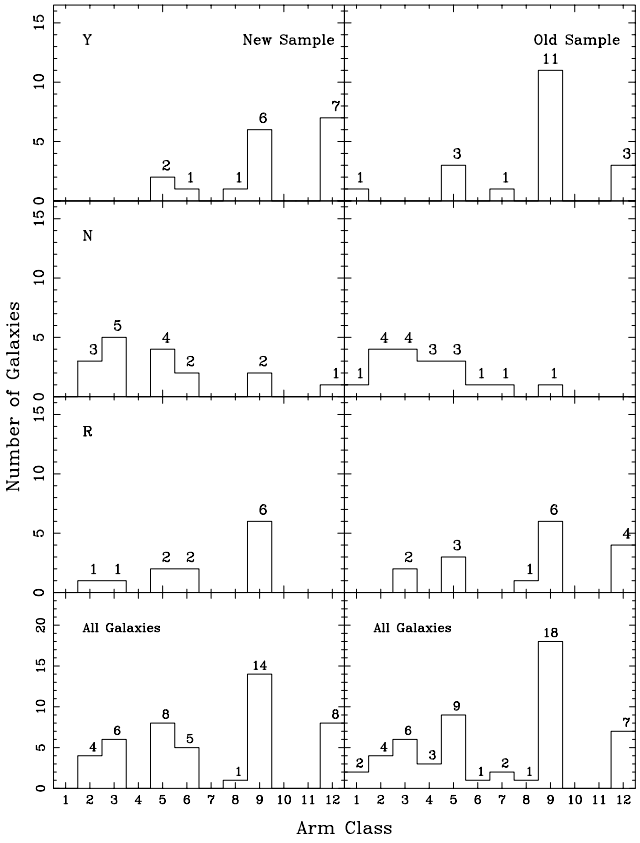

Fig. 3. Comparison of the arm classification of Elmegreen & Elmegreen (1987) with our own classification of the arm structure present in the HII region distribution. The histograms give the number of galaxies as a function of the Elmegreen & Elmegreen (1987) arm class. Left panels are for the new sample and right ones for the old one. The upper panels contain galaxies with prominent spiral structure in their HII region distribution. The second row, galaxies with no such structure. The third row contains galaxies which are intermediate or unclassifiable, and the fourth row, all galaxies together.

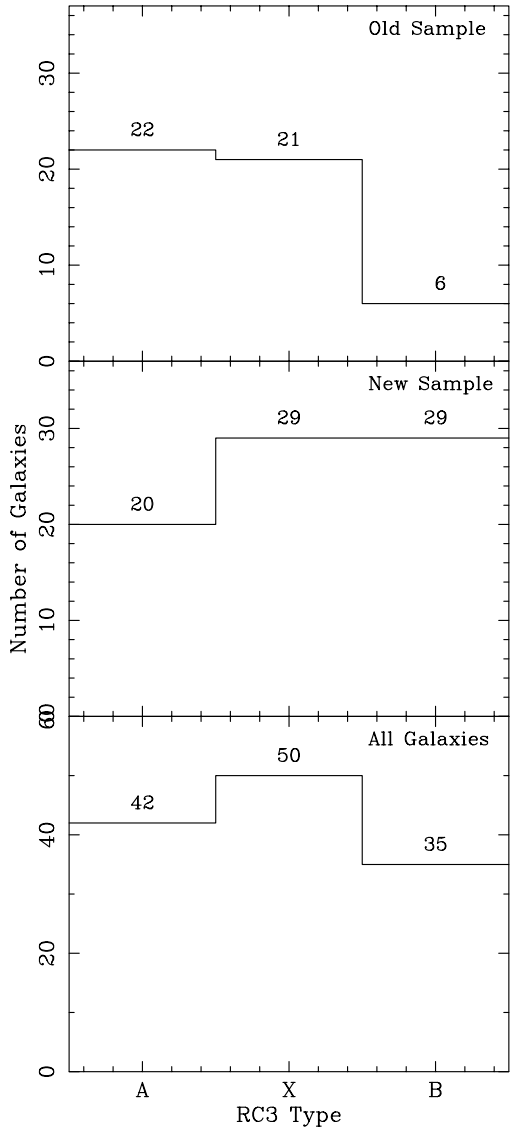

Fig. 4. Distribution of galaxies according to the bar type classification of the RC3 (1991) catalog.

3. Deprojection methods

The first step in order to study the distribution of HII regions is to deproject the images of the galaxies. For this we need two angles, namely the position angle (PA) – which is the angle between the line of nodes of the projected image and the north, measured towards the east – and the inclination angle (IA) – which is the angle between the line perpendicular to the plane of the galaxy and the line of sight –. An IA of zero degrees corresponds to a galaxy seen face-on.

Two basic groups of methods have been used so far to determine these angles. The first one is based on photometry and images, and the second one on kinematics. The most standard way to use images is to fit ellipses to the outermost isophotes and measure their axial ratio. This method, which is often used in the literature, is well suited for discs which are not warped, and requires photometric images with high signal-to-noise ratio in the outer parts, where the influence of non axisymmetric components like arms and bars is minimum. Several variants have also been proposed: Danver (1942) used a special display table to rotate the galaxy images until they were circular. Grosbøl (1985) applied the one dimensional Fourier transform to the intensity distribution in the outer parts of disc galaxies and adopted the deprojection angles that minimized the bisymmetric Fourier component.

Another classical method uses a two dimensional velocity field of the galaxy. Assuming that the emission comes from a thin planar disk, which is in circular motion around the galaxy center, we can select the deprojection angles that minimize the departures from such a flow. This method is particularly well adapted for HI kinematics, which covers the whole galaxy disk. During the last decade, however, this method has been applied also to

data coming from CO and Hα kinematics, which are generally more restricted to the central parts. This method is specially well suited for measuring the PA. In the case of warps, a tilted ring model can be used, but the values of the deprojection angles will not be uniquely defined, as they will change with galactocentric radius.

Searching in the literature, we can also find other kind of methods to derive the deprojection angles that do not use the techniques described above. Comte et al. (1979) used a plot of the HII region distribution of M 101 in a $\log(r) - \theta$ plane to fit a straight line to the arms, using the hypothesis that the arms are well described by logarithmic spirals. Iye et al. (1982) applied the two dimensional Fourier analysis to the galaxy NGC 4254, using a photometric image, and chose the deprojection angles that maximize the axisymmetric component. Considère & Athanassoula (1982) also applied Fourier analysis but used instead published catalogs of HII regions. The criterion that they used was to maximize the signal to noise ratio in the $m = 2$ component. This same criterion was used by Considère & Athanassoula (1988) but using instead photometric galactic images.

In this paper we will use two methods, which were already introduced by GGA (1991). For our first method we use two dimensional Fourier analysis of the galaxy image. We decompose the HII region distribution in its spiral components using a basis formed of logarithmic spirals. Since the deprojected galaxy should be more axisymmetric than the projected one, we can calculate the deprojection angles are as the angles that maximize the ratio:

$$\frac{B(0)}{\sum_{m=1}^{N} B(m)}, \tag{1}$$

where the $B(m), m = 0, \ldots, N$ are defined as:

$$B(m) = \int_{-\infty}^{\infty} \mid A(p,m) \mid \ \mathrm{d}p \tag{2}$$

and the function $A(p,m)$ is the Fourier transform of the HII region distribution, considered as a two dimensional distribution of δ-functions of the same weight:

$$\begin{aligned} A(p,m) \ &= \ \int_{-\infty}^{+\infty} \int_{-\pi}^{+\pi} \frac{1}{N} \\ &\quad \times \sum_{j=1}^{N} \delta(u-u_j)\delta(\theta-\theta_j)\mathrm{e}^{-i(pu+m\theta)} \ \mathrm{d}u\mathrm{d}\theta \\ &= \ \frac{1}{N}\sum_{j=1}^{N} \mathrm{e}^{-i(pu_j+m\theta_j).} \end{aligned} \tag{3}$$

In the above (r_j, θ_j) are the polar coordinates of each HII region on the galaxy plane, $u_j = \ln r_j$ and N is the total number of HII regions. The details of this method are outlined in GGA (1991). It is clear that this method will work mainly for distributions which have a clear signal of all the components of the spectrum, specially the $m = 0$ component which corresponds to the background disk distribution.

Our second method was also described in GGA (1991). This method is specially devised for HII region distributions. If an axially symmetric distribution of points is divided in N_s equal sectors, like cake pieces, and it is sufficiently rich, then we expect to have a roughly equal number of HII regions in each piece, when viewing it from a line of sight perpendicular to the disc. If the same distribution of points is now viewed from a skew angle and we again use sectors, which are of equal surface in the plane perpendicular to the line of sight, then the number of HII regions will *not* be the same in all sectors. Thus the correct deprojection angles will be those for which the number of points in each sector is roughly the same, or, in other words, when the dispersion around the mean value is minimum.

None of the methods described are free from systematic errors. In fact they all work perfectly well for the theoretical case of a razor thin, axisymmetric disc in circular motion around its center but present more or less important problems for galaxies deviating from this idealized case. When we fit ellipses to the isophotes, the presence of strong bars and/or spiral arms can bias the results, if the isophotes are not sufficiently external. However, Athanassoula & Misiriotis (2002) show that even for very strong bars the isophotes in the outermost part of the disc are sufficiently circular to be used for deprojection. If we use the velocity fields in HI, the external parts of the galaxy may be warped, in which case the deprojection angles will be ill defined. Our methods also can suffer from systematic problems. For instance, in the case of the first method, if the HII region distribution delineates mainly the $m = 2$ arms and there are only few regions in the background disk, the ratio (1) will not be well defined and the method can find difficulties. Our methods can also find problems in the case of highly irregular distributions, as well as in strongly barred galaxies where many HII regions are concentrated in the bar region. In these cases our methods will erroneously tend to circularize the bar. A similar difficulty appears when many HII regions are located in some galaxy rings. Buta (1995) using his Catalog of Southern Ringed Galaxies showed that rings need not be circular. The outer features have an average intrinsic axis ratio of 0.87 ± 0.14 while the inner features an average of 0.84 ± 0.10. This indicates that some rings must have an oval nature. Our methods, however, will tend to circularize these structures when they dominate the HII region distribution. Thus they will attribute to a face on case an IA of 12.5 degrees if there was an outer ring of axial ratio of 0.87 and of 9.8 degrees if there was an inner ring of axial ratio 0.84. Of course if only part of the HII regions are in the ring component, then the error could be smaller. In such cases, where HII regions delineate the several components, we obtain secondary minima in the results obtained by our methods. It is thus necessary to check if some of these minima give better results than the principal minimum, which can be strongly biased by some of the effects described above.

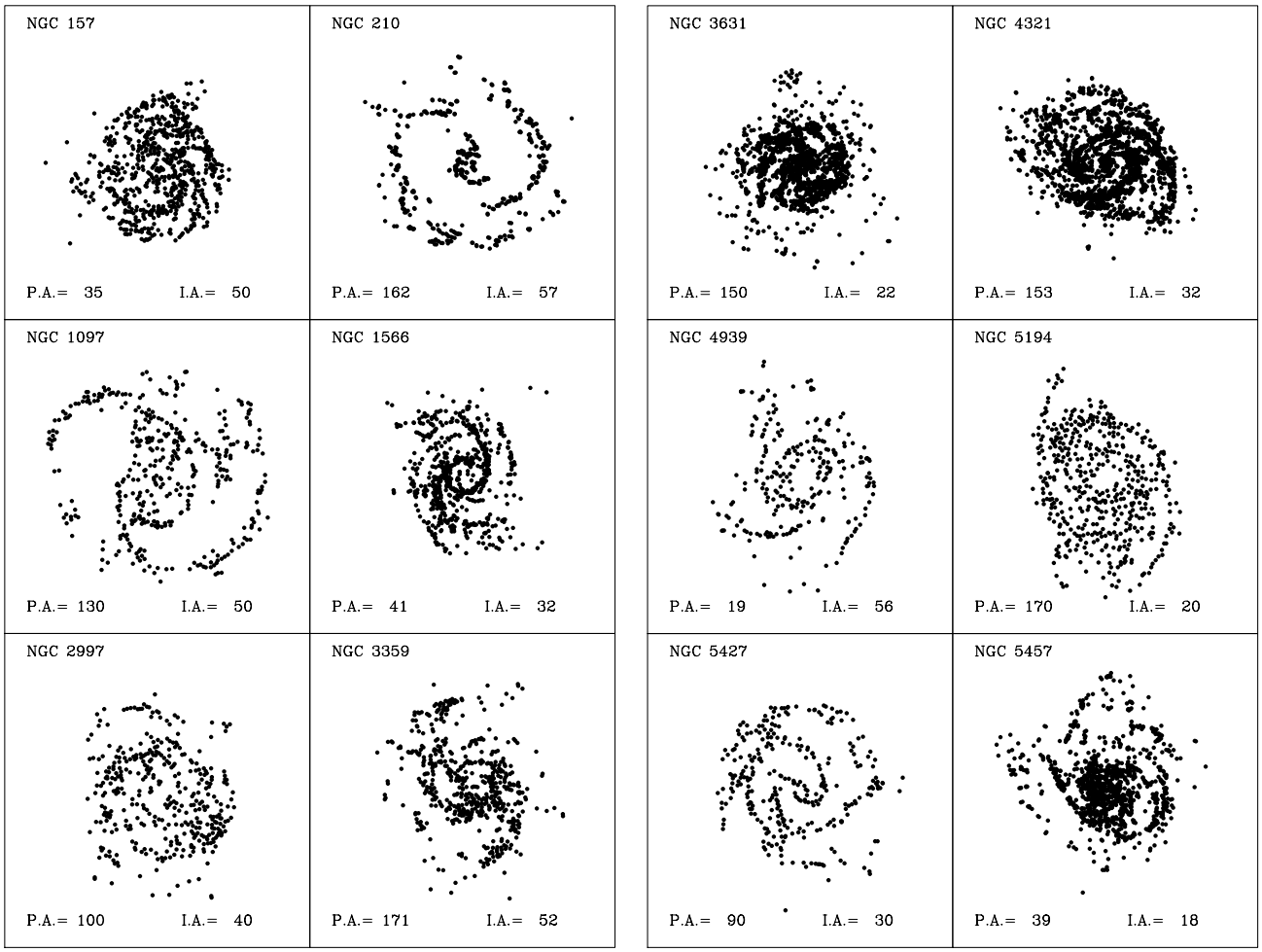

Fig. 5. Deprojected HII region distribution of the galaxies in our sample with rich catalogs and clear spiral structure.

Fig. 5. continued.

Thus, instead of relying on a single method in the crucial step of deprojecting the galaxy image, a comparison of the values given by the different methods is in order. In this way we can choose the pair of deprojection angles that suit best a particular galaxy. Our two methods, in conjunction with the literature values, were used in our first sample of HII region distribution of spiral galaxies (GGA, 1991). In this paper we will use this procedure to the HII region catalogs published in the last decade. We should, however keep in mind that our new sample has a high fraction of barred and ringed galaxies, where our two methods may not perform as well as for the galaxies in the GGA (1991) sample (see Fig. 4).

4. Notes on individual galaxies

In this section we give some comments on the deprojection angles chosen for each individual galaxy. This information is shown in Table 2. In Col. 1 we give the galaxy name. In Cols. 2 and 3 we show the PA and IA obtained using our two methods. In the first row we show the values for our first method, while in the second row those for our second method. If there are more than one catalog for a particular galaxy, the values found using our methods are displayed in the following lines. In Cols. 4 and 5 we show the main values of PA and IA respectively found in the literature. In Col. 6 we give a key to describe the method used to obtain the literature values. P is used for photometric values, KH is used for values determined using HI velocity field, KC for values determined using a velocity field in CO, KO for optical velocity fields, KS is used when the values come from slit spectra determinations and finally O is used for methods different to the previous ones. In Col. 7 we give a key for the reference where this particular determination can be found. This key is resolved in Table 3. Finally in Cols. 8 and 9 we give the adopted values of the PA and IA respectively. This same structure is repeated in the second group of columns. Using the finally adopted values we can deproject the catalogs of HII regions. The deprojected distribution of the richer catalogs showing with spiral structure are shown in Fig. 5 while in Fig. 6 we present the rest.

ESO 111-10: this is a galaxy with apparent small size and the catalog of HII regions is not very rich.

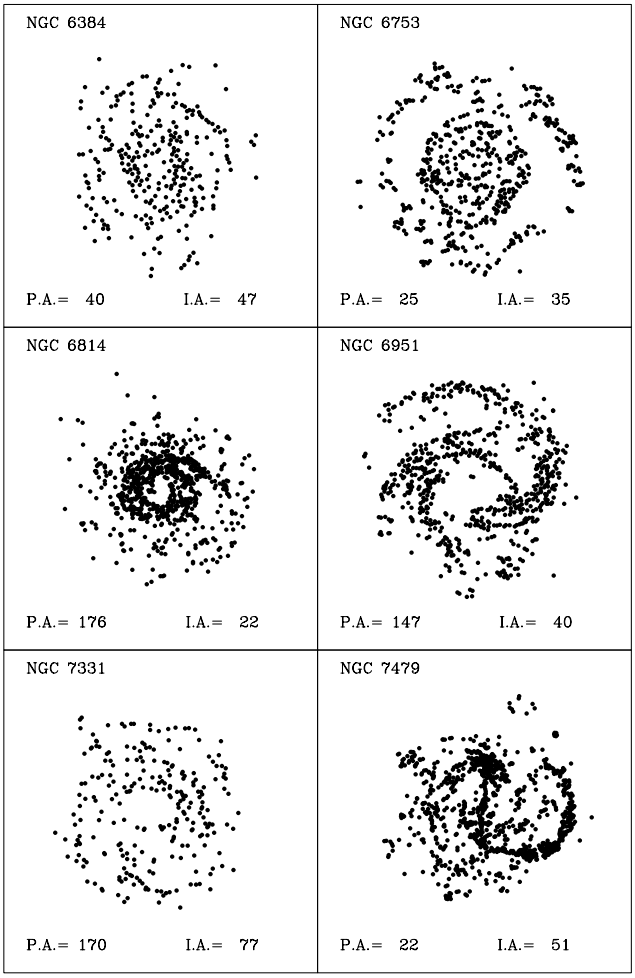

Fig. 5. continued.

Nevertheless, our two methods give a good agreement when we use a secondary minimum for the second method. We adopt the mean of both methods, which agrees well with RC3.

ESO 152-26: for this galaxy the HII regions are placed mainly in the arms and in the inner ring. Our two methods give the same value for the position angle and close values for the inclination angle. Eye estimates, however, show that the value of the PA is not satisfactory, presumably because our methods try to circularize the ring. We thus use the PA from the photometry of Crocker et al. (1996) and the mean of our IAs, which is also the mean of the literature values.

ESO 377-24: this is a small sized and not very inclined galaxy. The number of HII regions in the catalog is also small and both methods give a minimum at values more appropriate for a more inclined galaxy. Using secondary minima for both methods we get a reasonable agreement with the values from RC3 (1991). We finally adopt the values from the second method, which are in agreement with the photometry and close to the values of the first method.

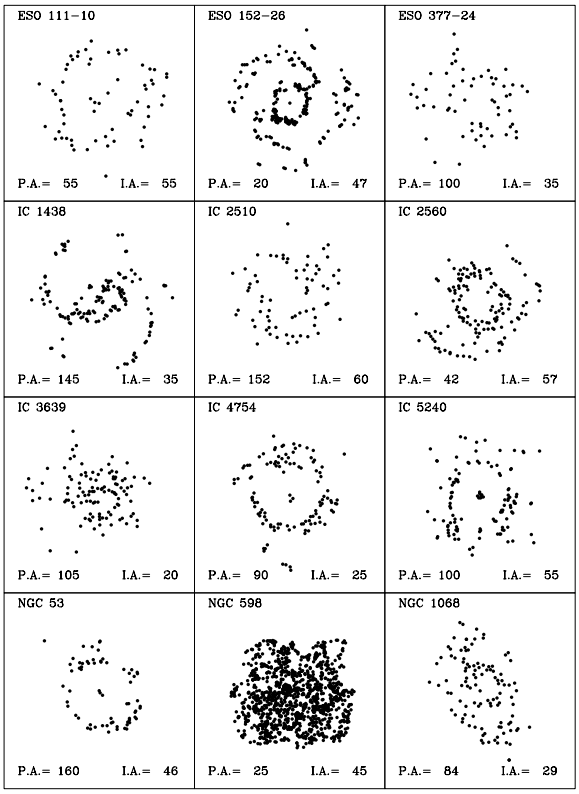

Fig. 6. Deprojected HII region distribution of the rest of the galaxies in our sample.

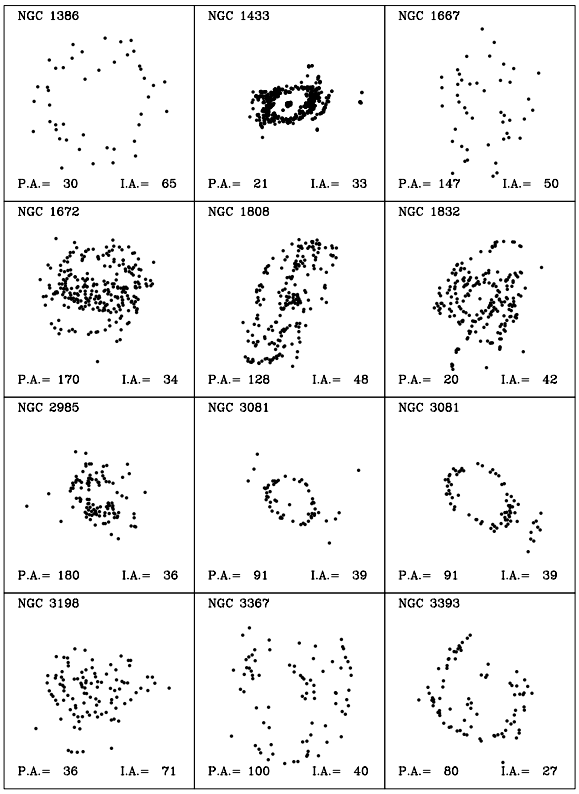

Fig. 6. continued.

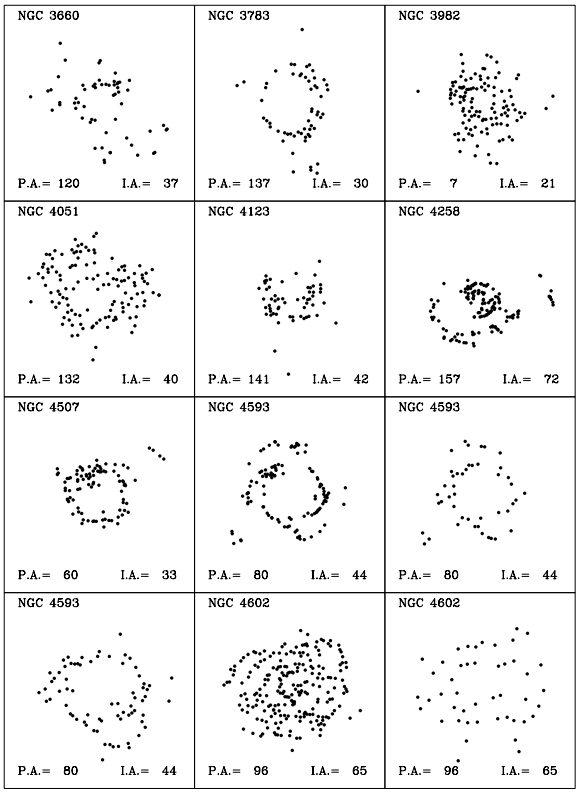

Fig. 6. continued.

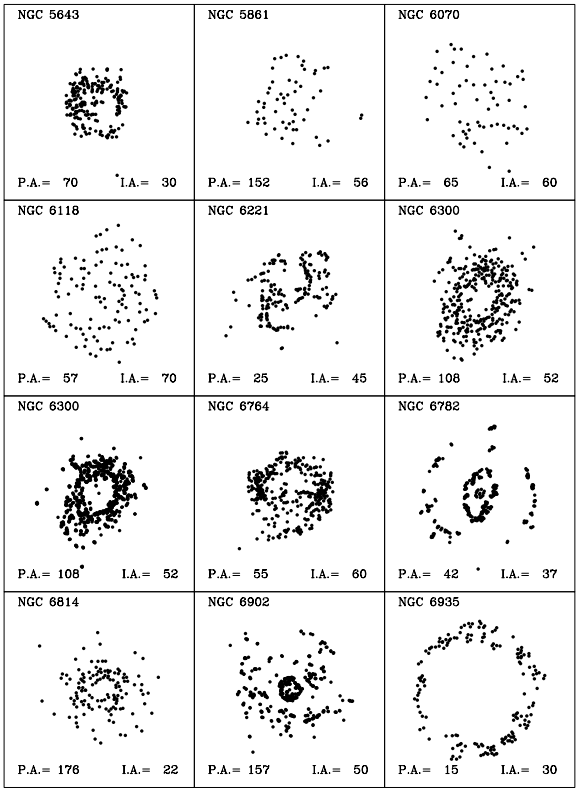

Fig. 6. continued.

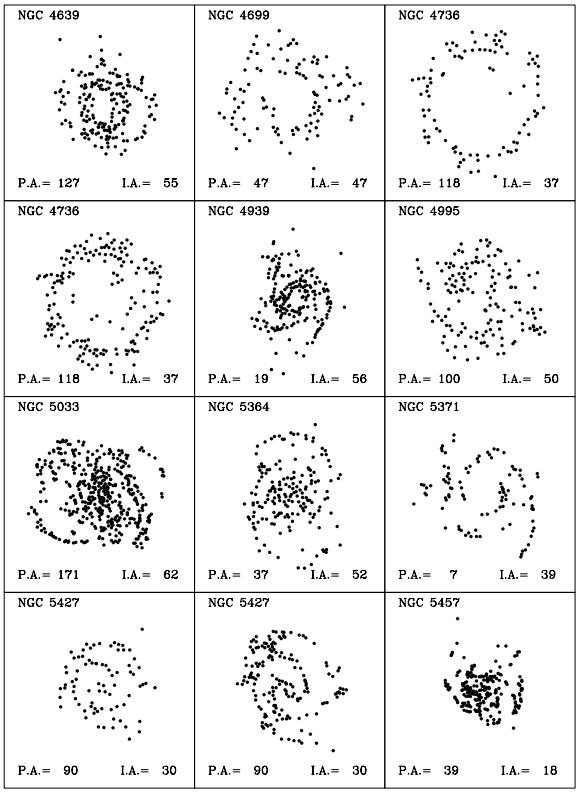

Fig. 6. continued.

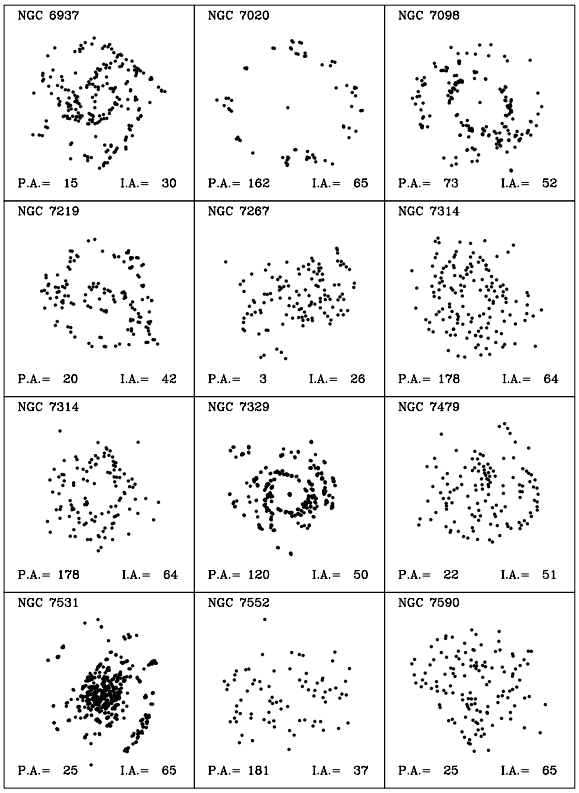

Fig. 6. continued.

IC 1438: the HII regions are placed mainly in the arms and the ring of this nearly face-on galaxy. The two methods are in good agreement. But as there is no background disk of HII regions, the first method may be biased by the presence of the spiral structure. We thus keep the PA from the second method, which coincides with that found by Crocker et al. (1996). For the IA we take the average of our two methods.

IC 2510: this is a galaxy of a very small apparent size. Nevertheless, as it is quite inclined, our two methods give results in good agreement and we keep the mean of the two, which is, furthermore, in good agreement with the literature values.

IC 2560: our two methods are in good agreement for this galaxy and we adopt the mean of their values, which agrees well with the PA given in the RC3 (1991) and the Lauberts-ESO catalogs (1982), and with the IA of the former.

IC 3639: this is a nearly face-on galaxy in a small group. The catalog of HII regions is quite irregular and does not show any spiral structure. We adopt the values from our second method, which are in agreement with the PA of Hunt et al. (1999) and the average IA of all methods. Note, however, that there is a lot of dispersion around the mean values, which could mean that our estimate is not very safe.

IC 4754: this is a ringed, small size galaxy. Nearly all of the HII regions of the catalog are placed in the external ring. Our methods are in agreement for the IA and the agreement for the PA is only reasonable, but the values from the PA are poorly determined as the projected catalog looks quite round. We prefer to keep the values from the second method, which are in agreement with two of the photometric values for the PA and all the values for the IA.

IC 5240: this case is quite similar to the previous one. Again the HII regions are placed mainly in the external ring, but as the galaxy is quite inclined, both methods are in reasonable agreement. As before, we keep the values from the second method, whose PA is in excellent agreement with all the literature values, and the IA with the results of the Lauberts ESO catalog (1982).

NGC 53: the HII regions are placed only in the outer ring and their number is quite low. On the galaxy image, it seems that the inner ring is not oriented as the main disk, but along the bar. Our first method tends to circularize this ring which is not necessarily circular. So, we keep the mean values from the photometry of the RC3 (1991) and the Lauberts ESO catalog (1982).

NGC 157: this galaxy seems to be a bit irregular and this is reflected in the rich catalog of HII regions. Nevertheless the two methods are in excellent agreement between them and in fair agreement with the literature values Thus, we keep the mean of our values.

NGC 210: the HII regions trace very well the arms and the inner ring. Our two methods are in agreement with the literature values and thus we keep the mean of our values.

NGC 598: our two methods are in good agreement but the values that they give are not in agreement with the rest of the literature values, probably due to an incomplete sampling of the galaxy disk in the HII region catalog from Hodge (1999). Thus, we prefer to keep the mean of the kinematically derived values.

NGC 1068: the HII regions are placed only in the inner bright oval, and the values obtained using both methods, while in agreement, are inadequate. The values given by Sánchez-Portal et al. (2000) also pertain to the inner bright oval. Thus, we take the mean of the values from the velocity fields.

NGC 1097: our two methods agree well for the values of IA, but the discrepancy is higher for the PA. The first method gives rounder arms, so its PA and IA values must have been highly influenced by a Stocke's effect (Stocke 1955), while the second gives a rounder central part. These latter values agree very well with the HI kinematical values from Ondrechen (1989) as well as with three of the photometrical estimates, so we will adopt the values from the second method.

NGC 1386: our two methods give identical results for this quite inclined galaxy, which are furthermore in agreement with the photometric estimates. We adopt the values from our two methods.

NGC 1433: the HII regions trace very well the inner ring of this galaxy. Both methods try to circularize this inner ring giving a strong disagreement with the kinematical values. We adopt the values from the velocity fields.

NGC 1566: this galaxy was also studied in the first paper, where we used the catalog by Comte et al. (1979) which traces also the external arms. For this new catalog, the HII regions are placed mainly in the inner oval part and the results of our methods disagree. The values obtained from the first catalog by GGA (1991) are in good agreement with the values from the kinematics, so we adopt the mean values of the GGA values and the optical velocity field from Pence et al. (1990).

NGC 1667: this galaxy has a small apparent size, with a catalog with a low number of HII regions. Nevertheless, as the galaxy is quite inclined, the two methods are in reasonable agreement and we give the mean of both methods.

NGC 1672: our second method does not converge, probably due to the strong bar present in this galaxy. On the other hand our first method gives a PA value in good agreement with the photometric values form RC3 (1991) and the Lauberts-ESO catalogs (1982), but the value obtained for the IA value seems too high. We keep the values from the RC3 catalog.

NGC 1808: there is a good agreement between the two methods, but the HII regions trace only the inner bright oval part and there are no regions in the outer arms or disk. The outer disk in the galaxy image seems to be much less inclined. For this reason we prefer to keep the kinematic values from Koribalski et al. (1993).

NGC 1832: this galaxy was studied also in the first paper, but using a catalog with a low number of

HII regions. Using this new catalog, the two methods are in good agreement, and there is a rough general agreement with the rest of the values from the literature. Thus we keep the mean of our two methods.

NGC 2985: the HII region distribution is quite irregular, but despite this fact, the first method gives values in reasonable agreement with the RC3 (1991) catalog. The second method does not work. We adopt the mean between our first method and RC3 (1991).

NGC 2997: this galaxy was also studied in the first paper using a similar catalog. Using the new catalog we find values for the IA that are in reasonable agreement between them, while the values for the PA are not so well constrained. The mean of the two methods are in agreement with the kinematical values from Milliard & Marcelin (1981) and the photometric values from the RC3 (1991) and, to a lesser extent, with the rest of the values. We adopt the mean of our two methods.

NGC 3081: for this galaxy we have two catalogs with distributions of similar shape, the HII regions being mainly in the inner ring. As both methods try to circularize this ring we prefer to adopt the mean of the values from the photometry and kinematics from Buta & Purcell (1998).

NGC 3198: there is a good agreement between our two methods for this quite inclined galaxy. There is also a general agreement with the rest of methods. The projected HII region distribution, however, seems somewhat irregular, and this may bias our two methods, giving higher values from the PA. For this reason we prefer to adopt the mean values from the HI kinematical studies of Bosma (1981) and Begeman (1987). Note that these are in good agreement with our second method and reasonable agreement with the first.

NGC 3359: our methods are not adequate for this galaxy because a lot of HII regions are located in the bar region. We thus keep the mean of the kinematical values from the Hα velocity field from Rozas et al. (2000b) and HI velocity fields from Gottesman (1982) and Ball (1986).

NGC 3367: the values given by the various methods cover a broad range of values. Our two methods give the same value for the IA, which is furthermore in agreement with the value from Danver (1942). The average of the two values of the PA are in agreement with the photometry from Grosbøl (1985). We thus adopt the mean of our two methods.

NGC 3393: the situation for this galaxy is highly unsatisfactory. The PA of 160 is mainly reflecting the orientation of the bar, so it can be dismissed. The estimate of 41 degrees comes from the outer isophote, but this seems to be heavily distorted, partly by the arms. Our methods should suffer from Stocke's effect (1955). Since our purpose in the following pages will mainly be to study the spiral structure and our two methods agree well, we will adopt their average for our future work. We stress, however, that this is due to the lack of any better estimate.

NGC 3631: this is a nearly face-on galaxy, and thus although we use a very rich catalog, the values of PA and IA are not very well constrained. We adopt the value of the PA derived in the kinematical analysis of Knapen (1997). However, the kinematic analysis did not give a value for the IA, so we adopt the mean of our methods for this angle, which is in rough average with the photometric values.

NGC 3660: the catalog of HII regions is quite poor and the values of PA and IA are not very well constrained. Nevertheless, the two methods are in good agreement and in rough agreement with the photometric values from RC3 (1991). We adopt the mean of our two methods.

NGC 3783: the HII regions of this catalog populate an inner ring. Nevertheless, our two methods are in good agreement with the only PA value that we found in the literature and with the IA of RC3 (1991). There is also a rough agreement with the IA values from other studies. We adopt the mean of our methods.

NGC 3982: this is a small apparent size galaxy nearly face-on and the HII region catalog is quite poor. Both our methods have two clear minima, however, and are in good agreement between them. Moreover, they are in rough agreement with the photometry, so we adopt the mean values of all methods.

NGC 4051: the HII region distribution is somewhat irregular and the first method gives results only in rough agreement with the values from the second method. We finally adopt the kinematical values of Listz & Dickey (1995), which are in general agreement with most of the photometric values.

NGC 4123: the number of HII regions is quite low and the HII region distribution traces mainly the bar region. The first method does not work properly, so should be neglected. The values from our second method are in good agreement with the values from the kinematics. Seen the poor quality of the HII region catalog we adopt the mean values from the kinematics.

NGC 4258: as our two methods are in agreement for this quite inclined galaxy we adopt their mean value which is in agreement with the results of the velocity fields of van Albada (1980) and van Albada & Shane (1975).

NGC 4321 (M100): this galaxy is not very inclined and thus the value of the PA is not well constrained. On the other hand, there is a rough agreement about the IA for the rest of the methods. We adopt the kinematical values of Guhatakurta (1988).

NGC 4507: the galaxy has a small size and the HII regions populate a ring. Our two methods do not work properly because they try to circularize the ring. We adopt the deprojection angles obtained in the photometric study of Schmitt & Kinney (2000).

NGC 4593: this is a strongly barred galaxy for which there are three published catalogs of HII regions. Our two methods are in good agreement for the richer catalogs but the first method gives discordant results in the second catalog and the second method does not work at all. Thus we discard the values from the second catalog. The mean of our values are also in general agreement with the photometric values, except for the case of the I photometry

by Schmitt & Kinney (2000) who give a higher PA value than the rest. We adopt the mean values of the results of our two methods applied to the first and third catalog.

NGC 4602: all values of the PA are in rough agreement, except for the value given by Mathewson & Ford (1996), which by eyeball estimate does not look very reasonable. We adopt an average value of our two methods and both catalogs, which also agrees with RC3 (1991) and Danver (1942).

NGC 4639: there is good agreement between the values obtained by our methods. Thus, we take the average values. This is also in agreement with the literature values.

NGC 4699: we adopt the average of our two methods, which is in good agreement with the photometric values.

NGC 4736: for this galaxy, we have two catalogs. In both cases, nearly all the HII regions are placed in the external ring. Our four results are only in rough agreement and they are, furthermore, not very reliable since they pertain to the ring. Thus, we prefer to adopt, the mean values given from the velocity fields (Bosma et al. 1977; Mulder & van Driel 1993; Buta 1988) which are in good agreement between them and also with the average of our two methods and the two catalogs.

NGC 4939: we have two catalogs of similar richness for this galaxy. It is quite inclined and the two methods are in rough agreement for both catalogs. We take the averages of our two methods and the two catalogs, which is in agreement with the photometric values and the value given in GGA (1991).

NGC 4995: our two methods give identical results, which we adopt, since they are also in good agreement with the photometric values from RC3 (1991) and Grosbøl (1985).

NGC 5033: a number of estimates are available for the deprojection angles of this galaxy, and all cluster in a relatively narrow range of values. The results of our two methods are in good agreement between them and with the rest of the estimates. The deprojection of the HII region distribution is particularly sensitive to the adopted value of the IA. We tired several averages of the individual estimates both straight and weighted by our judgment of the quality which resulted in identical values. We adopt these mean values.

NGC 5194 (M 51): our two methods are in good agreement, but the values of the position angles in particular, using the primary minima, are quite discordant with the values obtained from the analysis of the velocity fields. Note that they are also similar to some of the derived photometric values. The deprojected galaxy using our values looks quite good, as already noted in GGA (1991). There is, however, a secondary minimum, which is in agreement with the values derived from the velocity fields. With these values we get also a round deprojected galaxy. We adopt the value from Rots et al. (1990), which are as stated, in agreement with the average of the secondary minima value.

NGC 5364: we take the average values from our two methods, which is in agreement with the rest of the values in the literature.

NGC 5371: the galaxy was too big to fit in the CCD frame used by Gonzàlez-Delgado et al. (1997), so that, the PA values found using this catalog can not be very reliable. We thus adopt for this galaxy an average of the photometric values.

NGC 5427: here the two methods and the three catalogs give different results, which again are very different from the literature values. This is not surprising as the galaxy is not very inclined and there is no derived velocity field in the literature. For lack of any stronger criteria and looking at the deprojected images obtained with all these values, we decided to adopt the result of the first method and the richer catalog. However, it should be stressed that these are very ill defined values.

NGC 5457 (M 101): this galaxy is nearly face-on. Thus, the values of the PA are not well constrained. Our methods prefer a galaxy completely face on but, as the galaxy is quite asymmetrical, we have decided to adopt the values obtained by the HI high resolution study of Bosma et al. (1981).

NGC 5643: the catalog of HII regions has an irregular distribution. The outer parts look also irregular in the galaxy images. Thus, our two methods as well as the photometric values are very unsafe. For lack of any stronger criteria, we adopt the results of the first method, which give a rounder deprojected object. It should nevertheless stressed that is a very unsafe estimate.

NGC 5861: there are very few HII regions in this catalog, so we adopt the values given by Grosbøl & Patsis (1998). It should, nevertheless be noted that, although the catalog is poor, our results are in fair agreement with the photometric ones.

NGC 6070: there is a good agreement between our two methods and the results available in the literature. We adopt the average of our two methods.

NGC 6118: for this galaxy we have, as in the former case, a good agreement between our methods and the literature values. Thus, we adopt the average of our two methods.

NGC 6221: the HII regions trace mainly the arms and give a rather irregular distribution, so that our second method is not reliable. There is a good agreement between our first method and the photometric value from Pence & Blackman (1984). We finally adopt our first method values. Note that the IA is in good agreement with the remaining photometric values.

NGC 6300: the results of the kinematical values of Ryder et al. (1996) and of Buta (1987b) are in perfect agreement, so we adopt these values. Our two methods are less reliable, since the HII regions are mainly lying in a ring for both catalogs. Nevertheless, it is worth noting that there is a reasonable agreement between our values and the adopted ones and also with the rest of the values.

NGC 6384: our two methods agree between them and we have adopted the average of their values. Our IA values

agree well with the photometric ones, while the PA does so reasonably well. The IA given by Prieto et al. (1992) seems more reliable than that of Sánchez-Portal et al. (2000), since the data extend further out in the region which is less influenced by the oval bar. This agrees with the mean of our values. The PA we adopt is somewhat higher than those given by the photometry. The deprojected catalog, however, has a round shape and thus we keep our values.

NGC 6753: our two methods agree reasonably well between them, so we take the average values which are in good agreement with the photometric values.

NGC 6764: our two methods give identical results and also agree quite well with the available photometric values, so we adopt our values.

NGC 6782: we adopt the average of our two methods, which is in reasonable agreement with the photometric values, as in the previous galaxy.

NGC 6814: this is a nearly face-on galaxy and as a result the values of the angles are not well constrained. We have two catalogs of different richness. As the PA can not be well constrained using our methods, we have decided to adopt the values from the kinematics of Listz & Dickey (1995) which are in fair agreement with the values obtained by our methods for the less rich catalog from Evans et al. (1996). Note that the richer catalog of Knapen et al. (1993) has a well delineated strong northern arm which can bias our results.

NGC 6902: we adopt the average of our two methods which is in good agreement with the results given in the RC3 (1991) catalog, and agrees also with the average of the rest of the literature determinations.

NGC 6935: the HII regions trace the outer ring only. Our second method does not work, and converges to a value with too high inclination, so we neglect it. We adopt the result from the first method which is in good agreement with the inclination of the RC3 (1991) catalog.

NGC 6937: no reasonable minimum was found by the first method and we adopt the values from the second method, which agree well with the inclination of the RC3 catalog, but not so well with the values quoted by Crocker et al. (1996).

NGC 6951: we take the average of our two values which are in good agreement with the values derived by Grosbøl (1985).

NGC 7020: the few available estimates agree well with our two methods, so we take the average of our two values.

NGC 7098: our two methods try to circularize the inner ring so that, even though they agree well between them, they are not very meaningful. We thus adopt the average of the photometric results.

NGC 7219: the first method does not work very well, so we list a secondary minimum. Our adopted values are the average of the two methods and are in reasonable agreement with the few available literature values.

NGC 7267: the few HII regions are mainly in and around the bar and not in the surrounding disc. We thus adopt, the value given by Crocker et al. (1996), which is in reasonable agreement with the other photometrically determined estimates.

NGC 7314: our two methods applied to the two catalogs give results in very good agreement. We thus adopt their mean value, which is also in good agreement with the few results available in the literature.

NGC 7329: our second method converges to an inclination angle which seems too large. We thus neglect it and take the result of the first method, which is in reasonable agreement with the little that is available in the literature.

NGC 7331: the results of our two methods agree very well between them, and with the main kinematic estimates. We thus adopt the average of our two methods.

NGC 7479: this is a difficult galaxy since, on top of a bar, there is a major $m = 1$ asymmetry, clearly seen in the deprojected image for both catalogs. This can bias our methods, thus we prefer to adopt the kinematical value from Laine & Gottesman (1998), which is in good agreement with the results given by our second method.

NGC 7531: this galaxy is quite inclined, so it is crucial for the PA to be accurate. Our first method gives a value which is, by visual inspection, not acceptable. We thus adopt the result of our second method, which is in good agreement with the kinematic values.

NGC 7552: the HII regions are mainly concentrated in and around the bar region and thus can not give useful information for the deprojection. We thus adopt the values from RC3 (1991).

NGC 7590: our two methods give results that coincide, so we adopt their average values, as they are also in reasonable agreement with the few available photometric estimates.

5. Discussion

In this section we compare the different methods used to determine the deprojection angles (PA, IA). Our aim is to see whether any one is inferior or superior to the others. We compared 7 methods, or groups of methods. Our two methods (method 1 and 2) constitute a group each. The values obtained by Danver (1942) form group D, those by Grosbøl (1985) form group G, and the values from the RC3 catalog form group RC3. The sixth group (kinematics, K) includes all the values obtained using information from HI or optical velocity fields. Finally the seventh group (photometry, P) includes all results obtained fitting ellipses to the outer parts of the galaxies. The values in these last two groups do not constitute homogeneous samples, but the methods used by the different authors are very similar. Moreover, the kinematical method is quite reliable, specially for the determination of the PA.

For comparing any two methods we fitted a straight line to all pairs of values, using a maximum likelihood algorithm which minimizes the χ^2 merit function

$$\chi^2(a,b) = \sum_{i=1}^{N} \frac{(y_i - a - bx_i)^2}{\sigma_{iy}^2 + b^2\sigma_{xi}^2}, \quad (4)$$

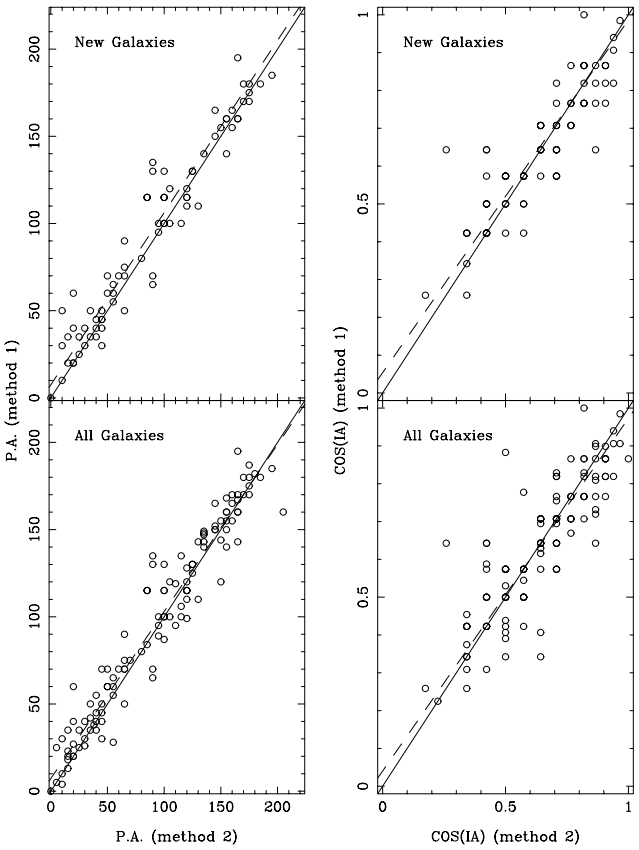

Fig. 7. Correlations between the values of the PA and IA derived using our two methods. Solid line. Diagonal (perfect correlation). Dashed line. Best fitting weighted linear correlation.

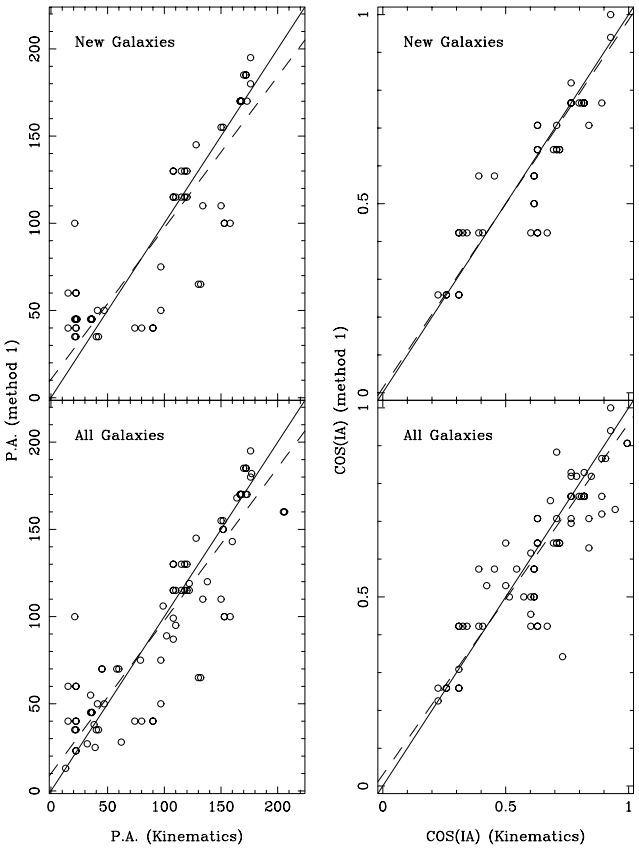

Fig. 8. Same as Fig. 7 but for the correlations between our first method and the results from HI kinematics.

where σ_{xi}^2 and σ_{yi}^2 are the errors for the ith value (Press et al. 1992).

When using our values, we assigned a weight to each catalog of HII regions as follows: If the catalog is very irregular with a small number of HII regions we assigned a weight of 0.1. If the number of HII regions is small but the catalog looked quite regular we assigned a weight of 0.3. If the catalog has a fair number of HII regions, but the distribution has some irregularities, we assigned a weight of 0.6 and, finally, if the catalog looked regular and had a fair number of HII regions we assigned a value of 1.0. We introduced a further weight, this time for the PA values of all the methods, to take into account the fact that for galaxies nearly face on, it is difficult for any of the methods to assign a reliable value of the PA. We thus assigned a low weight to the PA values of nearly face-on galaxies and a weight of 1. for all the rest. The errors were taken as the inverse of the weights, or, in cases with two weights, as the inverse of their product. In all the correlations we discarded the galaxy NGC 5194. For this galaxy, the values determined for the PA and IA using the kinematical information are in clear disagreement with the values determined using any of the other methods. This must be due to the strong interaction with the companion, NGC 5195.

Table 4. Weighted mean orthogonal distances for the PA correlations (upper triangle) and cos(IA) (lower triangle).

	1 st	2nd	RC3	G	D	K	P
1st		7.1	10.5	11.3	9.6	13.3	16.5
2nd	7.4		9.1	8.9	6.2	11.4	14.1
RC3	9.9	10.1		6.2	5.7	9.3	10.1
G	9.2	9.0	6.1		11.6	16.0	17.8
D	13.7	11.9	5.9	12.1		9.4	20.7
K	9.5	9.7	5.0	6.8	9.7		15.8
P	12.9	16.2	7.7	10.1	11.3	10.9	

Some illustrative correlations between pairs of methods are shown in Figs. 7 to 9. In Fig. 7 we compare the results of our two methods, in Fig. 8 our first method to the kinematical values and in Fig. 9 our first method to the photometrical determined values. To compare quantitatively the results of these and all the remaining correlations (not shown here) we used correlation coefficients as well as the weighted mean of the orthogonal distances of all the points to the best fitting straight line. The results of the comparison are shown in Tables 4 and 5. Tables 6 and 7 give the coefficients a and b of the linear regressions. In all cases the values above and to the right of the main diagonal correspond to the PA, and the values under and to the left of the main diagonal correspond to the cos(IA).

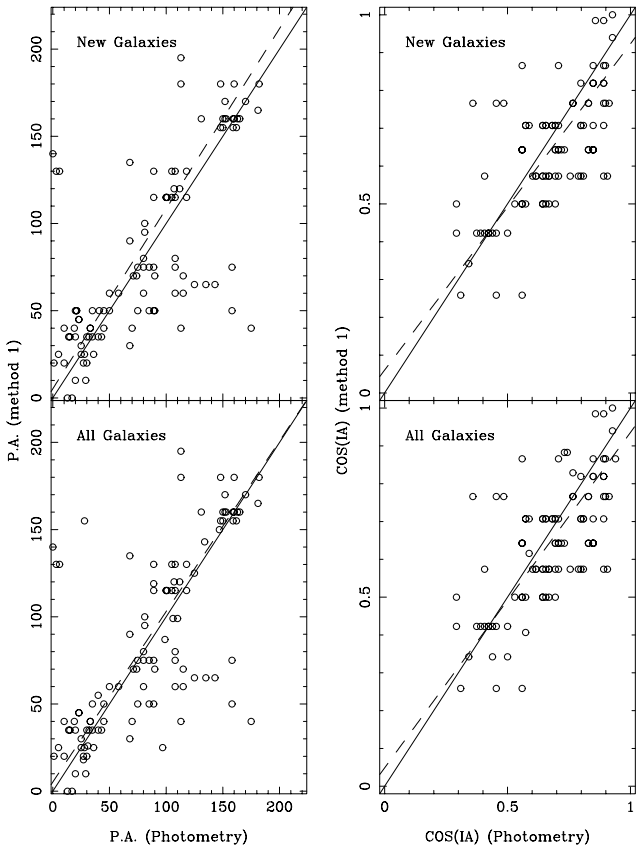

Fig. 9. Same as Fig. 9 but for the correlations between our first method and the results from the photometry.

We chose the *cos*, rather than the angle, since the former is uniformly distributed. Note that the values of the orthogonal distances and of the coefficient a for the case of cos(IA) have been rescaled so as to make them directly comparable to the corresponding values of the PA. For the comparisons we pooled together the data of the galaxies of the new sample presented in this paper and the galaxies of the previous sample (GGA, 1991). Obviously a perfect fit between two methods would imply a correlation coefficient of 1, a weighted mean of the orthogonal distances of zero, as well $a = 0.$ and $b = 1$. Random errors will introduce a scatter, which would lower the correlation coefficient and raise the value of the weighted mean of the orthogonal distances. Systematic differences, as would occur e.g. if a given method systematically overestimated or underestimated the geometric angles, would change the values of the coefficients a and b.

We note that, although no two methods we have used agree perfectly, there are also no glaring discrepancies. No method seems to overestimate or underestimate either of the deprojection angles. Also no method seems to give systematically smaller correlation coefficients, which would be indicative of a large random error in the results of this method. All correlations range between acceptable and good. The worst correlation coefficient, 0.51, is found when comparing the cos(IA) of Danver and Grosbøl.

Table 5. Weighted correlation coefficients for the PA correlations (upper triangle) and cos(IA) (lower triangle).

	1 st	2nd	RC3	G	D	K	P
1st		0.92	0.94	0.87	0.94	0.96	0.79
2nd	0.98		0.96	0.89	0.96	0.92	0.83
RC3	0.87	0.88		0.96	0.98	0.88	0.89
G	0.89	0.77	0.84		0.89	0.79	0.75
D	0.85	0.91	0.94	0.51		0.94	0.59
K	0.98	0.85	0.93	0.86	0.89		0.81
P	0.77	0.69	0.83	0.68	0.82	0.71	

Table 6. Zero points of the best fitting straight line for the PA correlations (upper triangle) and cos(IA) (lower triangle).

	1 st	2nd	RC3	G	D	K	P
1st		7.2	12.2	5.7	8.5	9.9	5.2
2nd	7.2		3.0	−0.1	1.0	−4.1	−4.8
RC3	−8.8	−19.0		4.1	−1.4	−8.2	4.5
G	−3.1	9.3	−19.5		14.6	1.2	15.6
D	9.5	−8.5	17.1	7.3		−2.0	−2.5
K	5.3	−6.9	22.4	−10.2	15.5		−26.5
P	8.7	4.3	13.3	29.2	−12.7	7.7	

Table 7. Slopes of the best fitting straight line for the PA correlations (upper triangle) and cos(IA) (lower triangle).

	1 st	2nd	RC3	G	D	K	P
1st		0.96	0.89	0.87	0.90	0.87	0.97
2nd	0.93		0.95	1.01	0.97	0.98	1.04
RC3	1.02	1.12		0.94	1.01	1.03	1.01
G	0.99	0.93	1.12		0.85	1.02	0.91
D	0.88	1.03	0.79	0.88		1.02	1.03
K	0.93	1.04	0.81	0.91	0.92		1.30
P	0.88	0.91	0.89	0.83	1.28	0.91	

This, however, is not due to one or several discordant galaxies, but rather to the fact that the galaxies are relatively few and are all clustered at low inclination angles. Nevertheless, the correlation is quite acceptable, as witnessed by the orthogonal distances and the coefficients of the regression line. It could be expected that two methods that rely on similar principles would give results closer to each other than methods based on different principles. We thus found it particularly gratifying to note the good agreement between either of our two methods and the kinematics, which is considered to give very reliable determinations and relies on very different assumptions.

One can thus conclude that all methods are acceptable for statistical analysis of samples of disc galaxies. In particular our two methods are as good as the other methods used so far and can give equally reliable estimates of the deprojection parameters. On the other hand if we are interested in the PA and IA of a particular galaxy it is best to apply several methods. The reason is that the different methods suffer from different biases – i.e. warps in the

external parts, non elliptical isophotes or not well defined backgrounds – which might be more or less important in a particular case.

Acknowledgements. In preparing this paper we made extensive use of the CDS Strasbourg database. CGG and CB acknowledge financial support by the Dirección de Investigación cintífica y Técnica under contract PB97-0411

References

Afanasiev, V. L., Sil'chenko, O. K., & Zasov, A. V. 1989, A&A, 213, L9
Aguerri, J. A. L., Muñoz-Tuñón, C., Varela, A. M., & Prieto, M. 2000, A&A, 361, 841
Alonso-Herrero, A., Simpson, C., Ward, M., & Wilson, A. S. 1998, ApJ, 495, 196
Arsenault, R., Boulesteix, J., Georgelin, Y., & Roy, J.-R. 1988, A&A, 200, 29
Athanassoula, E., García-Gómez, C., & Bosma, A. 1993, A&AS, 102, 229
Athanassoula, E., & Misiriotis, A. 2002, MNRAS, in press [astro-ph/0111449]
Atherton, P. D., Reay, N. K., & Taylor, K. 1985, MNRAS, 216, 17
Balkowski, C. 1973, A&A, 29, 43
Baumgart, Ch. W., & Peterson, Ch. J. 1986, PASP, 98, 56
Baldwin, J. A., Wilson, A. S., & Whittle, M. 1987, ApJ, 319, 84
Ball, R. 1986, ApJ, 307, 453
Becker, R., Mebold, U., Reif, K., & van Woerden, H. 1988, A&A, 203, 21
Beckman, J. E., Bransgrove, S. G., & Phillips, J. P. 1986, A&A, 157, 49
Begeman, K. G. 1987, Ph.D. Thesis
Begeman, K. G. 1989, A&A, 223, 47
Begeman, K. G., Broeils, A. H., & Sanders, R. H. 1991, MNRAS, 249, 523
Bergeron, J., Petitjean, P., & Durret, F. 1989, A&A, 213, 61
Blackman, C. P. 1979a, MNRAS, 186, 701
Blackman, C. P. 1979b, MNRAS, 186, 717
Blackman, C. P. 1981, MNRAS, 195, 451
Blackman, C. P. 1982, MNRAS, 200, 407
Blackman, C. P. 1983, MNRAS, 202, 379
Blackman, C. P. 1984, MNRAS, 207, 9
Bland-Hawthorn, J., Gallimore, J. F., Tacconi, L. J., et al., ApSS, 248, 9
Boroson, T. 1981, ApJS, 46, 177
Bosma, A. 1981, AJ, 86, 1791
Bosma, A., Goss, W. M., & Allen, R. J. 1981, A&A, 93, 106
Bosma, A., van der Hulst, J. M., & Sullivan III, W. T. 1977, A&A, 57, 373
Bottema, R. 1988, A&A, 197, 105
Burbidge, E. M., & Burbidge, G. R. 1962, ApJ, 135, 366
Burbidge, E. M., & Burbidge, G. R. 1964, ApJ, 140, 1445
Burbidge, E. M., & Burbidge, G. R. 1968a, ApJ, 151, 99
Burbidge, E. M., & Burbidge, G. R. 1968b, ApJ, 154, 857
Burbidge, E. M., Burbidge, G. R., & Prendergast, K. H. 1959, ApJ, 130, 26
Burbidge, E. M., Burbidge, G. R., & Prendergast, K. H. 1960, ApJ, 132, 654
Burbidge, E. M., Burbidge, G. R., & Prendergast, K. H. 1961, ApJ, 134, 874
Burbidge, E. M., Burbidge, G. R., & Prendergast, K. H. 1963, ApJ, 138, 375
Buta, R. 1987a, ApJS, 64, 1
Buta, R. 1987b, ApJS, 64, 383
Buta, R. 1988, ApJS, 66, 233
Buta, R. 1995, ApJS, 96, 39
Buta, R., & Purcell, G. B. 1998, AJ, 115, 484
Buta, R., private comunication to 33
Carranza, G., Crillon, R., & Monnet, G. 1969, A&A, 1, 479
Chincarini, G., & Walker, M. F. 1967a, ApJ, 149, 487
Chincarini, G., & Walker, M. F. 1967b, ApJ, 147, 407
Comte, G., & Duquennoy, A. 1982, A&A, 114, 7
Comte, G., Monnet, G., & Rosado, M. 1979, A&A, 72, 73
Considère, S., & Athanassoula, E. 1982, A&A, 111, 28
Considère, S., & Athanassoula, E. 1988, A&AS, 76, 365
Corbelli, E., & Schneider, S. E. 1997, ApJ, 479, 244
Corradi, R. L. M., Boulesteix, J., Bosma, A., et al. 1991, A&A, 244, 27
Courtés, G., Petit, H., Hua, C. T., et al. 1993, A&A, 268, 419
Crocker, D. A., Baugus, P. A., & Buta, R. 1996, ApJS, 105, 353
Danver, C. G. 1942, Lund. Obs. Ann. No., 10
Dickson, R. J., & Hodge, P. W. 1981, AJ, 86, 826
de Jong, R. S., & van der Kruit, P. C. 1994, A&AS, 106, 451
de Vaucouleurs, G. 1973, ApJ, 181, 31
de Vaucouleurs, G. 1959, ApJ, 170, 728
de Vaucouleurs, G., de Vaucouleurs, A., Corwin, H. G., et al. 1991, Third Reference Catalogue of Bright Galaxies (Springer, New York) (RC3)
Deul, E. R., & van der Hulst, J. M. 1987, A&AS, 67, 509
Duval, M. F., & Monnet, G. 1985, A&AS, 61, 141
Elmegreen, D. M., & Elmegreen, B. G. 1987, ApJ, 314, 3
Evans, I. N., Koratkar, A. P., Storchi-Bergmann, T., et al. 1996, ApJSS, 105, 93
Feinstein, C. 1997, ApJS, 112, 29
Fridman, A. M., Khoruzhii, O. V., Lyakhovich, V. V., et al. 2001, A&A, 371, 538
García-Gómez, C., & Athanassoula, E. 1991, A&AS, 89, 159 (GGA)
García-Gómez, C., & Athanassoula, E. 1993, A&AS, 100, 431
Goad, J. W., De Veny, J. B., & Goad, L. E. 1979, ApJS, 39, 439
González Delgado, R. M., Pérez, E., Tadhunter, C., Vílchez, J. M., & Rodríguez Espinosa, J. M. 1997, ApJS, 108, 155
Gottesman, S. T. 1982, AJ, 87, 751
Grosbøl, P. J. 1985, A&AS, 60, 261
Grosbøl, P. J., & Patsis, P. A. 1998, A&A, 336, 840
Guhatakurta, P., van Gorkom, J. H., Kotany, C. G., & Balkowski, C. 1988, AJ, 96, 851
Hackwell, J. A., & Schweizer, F. 1983, ApJ, 265, 643
Helfer, T. T., & Blitz, L. 1995, ApJ, 450, 90
Héraudeau, Ph., & Simien, F. 1996, A&AS, 118, 111
Hodge, P. W., Gurwell, M., Goldader, J. D., & Kennicutt, R. C. Jr. 1990, ApJS, 73, 661
Hodge, P. W., Balsley, J., Wyder, T. K., & Skelton, B. P. 1999, PASP, 111, 685
Hunt, L. K., Malkan, M. A., Rush, B., et al. 1999, ApJS, 125, 349
Hutchmeier, W. K. 1975, A&A, 45, 259
Hutchmeier, W. K., & Witzel, A. 1979, A&A, 74, 138
Iye, M., Okamura, S., Hamabe, M., & Watanabe, M. 1982, ApJ, 256, 103
Kaneko, N., Morita, K., Fukui, Y., et al. 1989, ApJ, 337, 691

Kaneko, N., Satoh, T., Toyama, K., et al. 1992, AJ, 103, 422
Kaneko, N., Aoki, K., Kosugi, G., et al. 1997, AJ, 114, 94
Kennicutt, R. C. 1981, AJ, 86, 1847
Knapen, J. H. 1997, MNRAS, 286, 403
Knapen, J. H. 1998, MNRAS, 297, 255
Knapen, J. H., Arnth-Jensen, N., Cepa, J., & Beckman, J. E. 1993, AJ, 106, 56
Knapen, J. H., Cepa, J., Beckman, J. E., del Rio, S., & Pedlar, A. 1993, ApJ, 416, 563
Koribalski, R., Dahlem, M., Mebold, U., & Brinks, E. 1993, A&A, 268, 14
Laine, S., & Gottesman, S. T. 1998, MNRAS, 297, 1041
Lauberts, A. 1982, in The ESO/Uppsala Survey of the ESO(B) Atlas (Garching: European Southern Observatory)
Listz, H., & Dickey, J. M. 1995, AJ, 110, 998
Lu, N. Y. 1998, ApJ, 506, 673
Ma, J., Peng, Q.-H., & Gu, Q-S. 1998, A&AS, 130, 449
Marcelin, M., Petrosian, A. R., Amram, P., & Boulesteix, J. 1994, A&A, 282, 363
Mathewson, D. S., & Ford, V. L. 1996, ApJS, 107, 97
Maucherat, A. J., Dubout-Crillon, R., Monnet, G., & Figon, P. 1984, A&A, 133, 341
Meyssonier, N. 1984, A&AS, 58, 351
Milliard, B., & Marcelin, M. 1981, A&A, 95, 59
Monnet, G., Paturel, G., & Simien, F. 1981, A&A, 102, 119
Mulder, P. S., & van Driel, W. 1993, A&A, 272, 63
Newton, K. 1980, MNRAS, 190, 689
Okamura, S. 1978, PASJ, 30, 91
Ondrechen, M. P., van der Hulst, J. M., & Hummel, E. 1989, ApJ, 342, 39
Oosterloo, T., & Shostak, S. 1993, A&AS, 99, 379
Peletier, R. F., Knapen, J. H., Shlosman, I., et al. 1999, ApJS, 125, 363
Pellet, A., & Simien, F. 1982, A&A, 106, 214
Pence, W. D., & Blackman, C. P. 1984, MNRAS, 207, 9
Pence, W. D., Taylor, K., & Atherton, P. 1990, ApJ, 357, 415
Petit, H. 1998, A&AS, 131, 317
Petit, H., Hua, C. T., Bersier, D., & Courtés, G. 1996, A&A, 309, 446
Planesas, P., Scoville, N., & Myers, S. T. 1991, ApJ, 369, 364
Press, W. H., Teukiolsky, S. A., Vetterling, W. H., & Flannery, B. P. 1992, Numerical Recipes (Cambridge Univ. Press)
Prieto, M., Longley, D. P. T., Perez, E., et al. 1992, A&AS, 93, 557
Puerari, I., & Dottori, H. A. 1992, A&AS, 93, 469
Roberts, M. S., & Warren, J. L. 1970, A&A, 6, 165
Rodrigues, I., Dottori, H., Cepa, J., & Vilchez, J. 1998, A&AS, 128, 545
Rogstad, D. H., & Shostak, G. S. 1971, A&A, 13, 99
Rots, A. H., Bosma, A., van der Hulst, J. M., Athanassoula, E., & Crane, P. C. 1990, AJ, 100, 387
Rozas, M., Beckman, J. E., & Knapen, J. H. 1996, A&A, 307, 735
Rozas, M., Zurita, A., & Beckman, J. E. 2000a, A&A, 354, 823
Rozas, M., Zurita, A., Beckman, J. E., & Pérez, D. 2000b, A&AS, 142, 259
Rozas, M., Zurita, A., Heller, C. H., & Beckman, J. E. 1999, A&AS, 135, 145
Rubin, V. C., Burbidge, E. M., Burbidge, G. R., & Prendergast, K. H. 1964, ApJ, 140, 80
Rubin, V. C., Burbidge, E. M., Burbidge, G. R., Crampin, D. J., & Prendergast, K. H. 1965, ApJ, 141, 759
Rubin, V. C., Ford, W. K. Jr, & Thonnard, N. 1980, ApJ, 238, 471
Ryder, S. D., Buta, R. J., Toledo, H., et al. 1996, ApJ, 460, 665
Ryder, S. D., Zasov, A. V., McIntyre Walsh, W., & Sil'chenko, O. K. 1998, MNRAS, 293, 411
Sánchez-Portal, M., Díaz, A. I., Terlevich, R., et al. 2000, MNRAS, 312, 2
Schmitt, M., & Kinney, A. L. 2000, ApJSS, 128, 479
Scowen, P. A., Dufour, R. J., & Hester, J. J. 1992, AJ, 104, 92
Shane, W. W. 1975, in La dynamique des galaxies spirales, C.N.R.S. Int. Colloq. 241, Paris
Stocke, J. 1955, AJ, 60, 216
Thean, A. H. C., Mundell, C. G., Pedlar, A., & Nicholson, R. A. 1997, MNRAS, 290, 15
Tsvetanov, Z., & Perosian, A. 1995, ApJS, 101, 287
Tully, R. B. 1974, ApJS, 27, 437
van Albada, G. D. 1980, A&A, 90, 123
van Albada, G. D., & Shane, W. W. 1975, A&A, 42, 433
van der Hulst, T., & Sancisi, R. 1988, AJ, 95, 1354
van der Kruit, P. C. 1973, ApJ, 186, 807
van der Kruit, P. C. 1974, ApJ, 192, 1
van der Kruit, P. C. 1976, A&AS, 25, 527
von Linden, S., Reuter, H. P., Heidt, J., Wielebinski, R., & Pophl, M. 1996, A&A, 315, 52
Warner, P. J., Wright, M. C. H., & Baldwin, J. E. 1973, MNRAS, 163, 163
Weliachew, L., & Gottesman, S. T. 1973, A&A, 24, 59
Weiner, B. J., Williams, T. B., van Gorkom, J. H., & Sellwod, J. A. 2001, ApJ, 546, 916
Wevers, B. M. H. R., van der Kruit, P. C., & Allen, R. J. 1986, A&AS, 66, 505
Wilke, K., Möllenhoff, C., & Matthias, M. 2000, A&A, 361, 507
Wong, T., & Blitz, L. 2000, ApJ, 540, 771
Zasov, A. V., & Sil'chencko, O. K. 1987, SvA Lett., 13, 18

2.2 Deprojecting spiral galaxies using Fourier analysis. Application to the Frei sample

Barberà, C., Athanassoula, E. and García-Gómez, C., Deprojecting spiral galaxies using Fourier analysis. Application to the Frei sample. *Astronomy and Astrophysics* 415, 849-861 (2004) EDP Sciences. DOI:10.1051/0004-6361:20034186

A&A 415, 849–861 (2004)
DOI: 10.1051/0004-6361:20034186

Astronomy & Astrophysics

Deprojecting spiral galaxies using Fourier analysis. Application to the Frei sample⋆

C. Barberà[1], E. Athanassoula[2], and C. García-Gómez[1]

[1] D.E.I.M., Campus Sescelades, Avd. dels Països Catalans 26, 43007 Tarragona, Spain
[2] Observatoire de Marseille, 2 Place Le Verier, 13248 Marseille cedex 04, France

Received 12 August 2003 / Accepted 30 September 2003

Abstract. We present two methods that can be used to deproject spirals, based on Fourier analysis of their images, and discuss their potential and restrictions. Our methods perform particularly well for galaxies more inclined than 50° or for non-barred galaxies more inclined than 35°. They are fast and straightforward to use, and thus ideal for large samples of galaxies. Moreover, they are very robust for low resolutions and thus are appropriate for samples of cosmological interest. The relevant software is available from us upon request. We use these methods to determine the values of the position and inclination angles for a sample of 79 spiral galaxies contained in the Frei et al. (1996) sample. We compare our results with the values found in the literature, based on other methods. We find statistically very good agreement

Key words. galaxies: structure – galaxies: spiral

1. Introduction

Disc galaxies are observed projected on the sky. Yet for many purposes one needs to be able to deproject them. Thus in morphological studies one needs information on different sizes and their ratios, e.g. to obtain the shape of rings, the axial ratio and strength of bars, or the shape (diamond-like, elliptical, or rectangular-like) of bar isophotes. Similarly in photometrical studies one may need cuts along particular directions, like the bar major or minor axis, or one may need to compare arm with inter-arm regions located at the same distance from the center, or one may need to correct for extinction. For studies involving the Tully-Fisher relation one needs to know the inclination of the galaxy in order to obtain its velocity. Our own interest in deprojection angles stems from the fact that we started a quantitative study of the properties of spiral structure in near-by disc galaxies, and for this we first need to deproject all our images. Indeed the list of all studies for which it is necessary to know the spatial orientation of the galaxy is too long to include here.

We will study the spiral structure in disc galaxies decomposing each image by means of bidimensional Fourier transforms. The first step is to deproject the galaxy image. It is thus necessary to determine the two deprojection angles, namely the position angle (hereafter PA) and the inclination angle (hereafter IA). The PA is the angle between the line of nodes of the projected image and the north, measured towards the east, while the IA is the angle between the perpendicular to the plane of the galaxy and the line of sight. Several methods have been proposed so far to obtain these angles, the most commonly used ones being based on photometry or kinematics. A standard way is to fit ellipses to the outer isophotes. The axis ratio of the outer ellipses is a measure of the IA, while the direction of the major axis gives the PA. Another procedure is based on the gas kinematics within the disc, using two dimensional velocity fields and assuming that the emission comes from material in a thin disk in circular motion around the center. The selected PA and IA angles are those that minimize the departures from such a flow.

These are not the only methods used in the literature. Danver (1942) used a special display table to rotate the galaxy images until they were circular. Grøsbol (1985) applied a one dimensional Fourier transform to the intensity distribution in the outer parts of galaxy disks and adopted the deprojection angles that minimized the bisymmetric ($m = 2$) Fourier coefficient. Comte et al. (1979) used the distribution of HII regions in the $\ln(r) - \theta$ plane to fit straight lines to the arms, under the hypothesis that they are well described by logarithmic spirals. Two dimensional Fourier analysis has also been used to determine the deprojection angles. Considère & Athanassoula (1982) used the HII region distribution, selecting the angles that maximized the signal-to-noise ratio in the $m = 2$ component, and Considère & Athanassoula (1988), applied the same criterion to galaxy images. Iye et al. (1982) used an image of NGC 4254 and selected the angles that maximized the axisymmetric component. Finally García-Gómez & Athanassoula (1991) and García-Gómez et al. (2002) also used

Send offprint requests to: C. Barberà,
e-mail: cbarbera@etse.urv.es

⋆ Table 7 is only available in electronic form at the CDS via anonymous ftp to cdsarc.u-strasbg.fr (130.79.128.5) or via http://cdsweb.u-strasbg.fr/cgi-bin/qcat?J/A+A/415/849

HII region distributions and maximized the axisymmetric components These authors also used a second method selecting the deprojection angles that made the HII region distribution most uniform.

All methods used for the deprojection of disk galaxies suffer from some kind of systematic errors. They will all work properly in the case of perfectly axisymmetric thin disks in circular motion about their centers, which is never the case for real galaxies. Thus, when we fit ellipses to the outer isophotes, the presence of strong arms can bias the results. This bias is known as Stocke's effect (Stocke 1955). On the other hand, Athanassoula & Misiriotis (2002) show that, even for very strong bars, the isophotes in the outermost part of the disc are sufficiently circular to be used for deprojection, provided that there is no spiral structure and one can go sufficiently far out from the center of the disc. The reason for this difference is that spiral arms extend far out in the disk, while bars are confined to the inner parts. Kinematical methods can be biased by warps in the outer parts, or by non-circular motions in the central parts due to bars or other perturbations.

The two deprojection methods, which we will introduce here, are based on the Fourier analysis of galaxy images. In Sects. 2 and 3 we introduce the sample and the methods, respectively. In Sect. 4 we assess our two methods and apply them to our sample. In Sect. 5 we compare the values obtained by the different methods, i.e. our two methods and those previously used in the literature. This will allow a quantitative comparison of the performance of the different methods. In Sect. 6, we adopt the values of the PA and IA that we will use in our quantitative studies of the spiral structure in the sample of galaxies. We summarize in Sect. 7.

2. The sample

Frei et al. (1996) presented a catalog of images of 113 galaxies in different pass-bands. All galaxies are nearby, bright and well resolved and were selected to span all the Hubble classification classes. This catalog is thus ideal for statistical studies.

As we are interested in the spiral structure of disc galaxies, we selected from the Frei sample all the galaxies with Hubble types between 2 and 7. We included also the galaxies NGC 4340, NGC 4866 and NGC 5701 with Hubble types −1 and 0 and the galaxy NGC 4178 with Hubble type 8, as their disks have a regular shape and they are not too inclined. For the same reason, we discard nearly edge-on galaxies, in which structure is not visible.

We are left with a sample of 79 galaxies, the general properties of which are listed in Table 1. Column 1 gives the galaxy name, Col. 2 the Hubble type and Col. 3 this type as coded in the RC3 catalog (de Vaucouleurs 1991). Column 4 gives the arm class as defined in Elmegreen & Elmegreen (1987). Finally, Col. 5 gives the filters used when observing each of the galaxy images. Figure 1 shows the distribution of galaxy types for our sample. We note that Hubble types are not uniformly sampled, since types Sbc to Scd are clearly over-represented. Figure 2 shows the distribution of arm classes in the galaxy sample. Again the different arm classes are not uniformly sampled. In the present sample, arm class 9 is much better represented than the other arm classes.

Table 1. Properties of the galaxies in the sample.

Name	T	S	AC	Filters
NGC 2403	.SXS6..	6.0	4	g, i, r
NGC 2541	.SAS6..	6.0	1	g, i, r
NGC 2683	.SAT3..	3.0	–	B_J, R
NGC 2715	.SXT5..	5.0	–	B_J, R
NGC 2775	.SAR2..	2.0	3	B_J, R
NGC 2903	.SXT4..	4.0	4	g, i, r
NGC 2976	.SA.5P.	5.0	3	B_J, R
NGC 2985	PSAT2..	2.0	3	B_J, R
NGC 3031	.SAS2..	2.0	12	g, i, r
NGC 3079	.SBS5.	7.0	–	B_J, R
NGC 3147	.SAT4..	4.0	3	B_J, R
NGC 3184	.SXT6..	6.0	9	B_J, R
NGC 3198	.SBT5..	5.0	–	g, i, r
NGC 3319	.SBT6..	6.0	5	g, i, r
NGC 3344	RSXR4..	4.0	9	B_J, R
NGC 3351	.SBR3..	3.0	6	B_J, R
NGC 3368	.SXT2..	2.0	8	B_J, R
NGC 3486	.SXR5..	5.0	9	B_J, R
NGC 3596	.SXT5..	5.0	5	B_J, R
NGC 3623	.SXT1..	1.0	–	B_J, R
NGC 3631	.SAS5..	5.0	9	B_J, R
NGC 3672	.SAS5..	5.0	2	B_J, R
NGC 3675	.SAS3..	3.0	3	B_J, R
NGC 3726	.SXR5..	5.0	5	B_J, R
NGC 3810	.SAT5..	5.0	2	B_J, R
NGC 3877	.SAS5*.	5.0	–	B_J, R
NGC 3893	.SXT5*.	5.0	12	B_J, R
NGC 3938	.SAS5..	5.0	9	B_J, R
NGC 3953	.SBR4..	4.0	9	B_J, R
NGC 4030	.SAS4..	4.0	9	B_J, R
NGC 4088	.SXT4..	4.0	–	B_J, R
NGC 4123	.SBR5..	5.0	9	B_J, R
NGC 4136	.SXR5..	5.0	9	B_J, R
NGC 4144	.SXS6$.	6.0	–	B_J, R
NGC 4157	.SXS3$.	3.0	–	B_J, R
NGC 4178	.SBT8..	8.0	–	g, i, r
NGC 4189	.SXT6$.	6.0	2	g, i, r
NGC 4192	.SXS2..	2.0	–	g, i, r
NGC 4216	.SXS3*.	3.0	–	g, i, r
NGC 4254	.SAS5..	5.0	9	g, i, r
NGC 4258	.SXS4..	4.0	–	g, i, r

3. Deprojection methods

In this paper we introduce two methods, based on the Fourier transforms and which are closely linked to the two methods used by García-Gómez et al. (2002) for HII region distributions. Let $I(u, \theta)$ be the image of the galaxy written in polar

Table 1. continued.

Name	T	S	AC	Filters
NGC 4303	.SXT4..	4.0	9	g,i,r
NGC 4321	.SXS4..	4.0	12	g,i,r
NGC 4340	.LBR+..	−1.0	–	B_J,R
NGC 4394	RSBR3..	3.0	6	B_J,R
NGC 4414	.SAT5$.	5.0	3	g,i,r
NGC 4450	.SAS2..	4.0	12	B_J,R
NGC 4487	.SXT6..	6.0	5	B_J,R
NGC 4498	.SXS7..	6.5	4	g,i,r
NGC 4501	.SAT3..	3.0	9	g,i,r
NGC 4527	.SXS4..	4.0	–	g,i,r
NGC 4535	.SXS5..	5.0	9	g,i,r
NGC 4548	.SBT3..	3.0	5	g,i,r
NGC 4559	.SXT6..	6.0	–	g,i,r
NGC 4569	.SXT2..	2.0	–	g,i,r
NGC 4571	.SAR7..	6.5	–	g,i,r
NGC 4579	.SXT3..	3.0	9	g,i,r
NGC 4593	RSBR3..	3.0	5	B_J,R
NGC 4651	.SAT5..	5.0	9	g,i,r
NGC 4654	.SXT6..	6.0	4	g,i,r
NGC 4689	.SAT4..	4.0	3	g,i,r
NGC 4725	.SXR2P.	2.0	6	g,i,r
NGC 4826	RSAT2..	2.0	6	g,i,r
NGC 4866	.LAR+*/	−1.0	–	B_J,R
NGC 5005	.SXT4..	4.0	3	B_J,R
NGC 5033	.SAS5..	5.0	9	g,i,r
NGC 5055	.SXT4..	4.0	3	g,i,r
NGC 5248	.SXT4..	4.0	12	B_J,R
NGC 5334	.SBT5*.	5.0	2	g,i,r
NGC 5364	.SAS6..	4.0	9	B_J,R
NGC 5371	.SXT4..	4.0	9	B_J,R
NGC 5585	.SXS7..	7.0	1	B_J,R
NGC 5669	.SXT6..	6.0	5	B_J,R
NGC 5701	RSBT0..	0.0	–	B_J,R
NGC 5792	.SBT3..	3.0	–	B_J,R
NGC 5850	.SBR3..	3.0	8	B_J,R
NGC 5985	.SXR3..	3.0	9	B_J,R
NGC 6015	.SAS6..	6.0	–	B_J,R
NGC 6118	.SAS6..	6.0	–	B_J,R
NGC 6384	.SXR4..	4.0	9	B_J,R
NGC 6503	.SAS6..	6.0	–	B_J,R

coordinates (r,θ), and $u = \ln(r)$. We define the Fourier transform of this image as:

$$A(p,m) = \int_{u_{\min}}^{u_{\max}} \int_0^{2\pi} I(u,\theta)\, \exp[i(pu + m\theta)]\, \mathrm{d}\theta \mathrm{d}u. \quad (1)$$

In this equation, p corresponds to the radial frequency and m to the azimuthal frequency. Thus the $m = 1$ values correspond to one-armed components, the $m = 2$ values to two-armed components and so on. The values of $u_{\min} = \ln(r_{\min})$ and $u_{\max} = \ln(r_{\max})$ are set by the inner and outer radius of the image, or of the part that we will analyze.

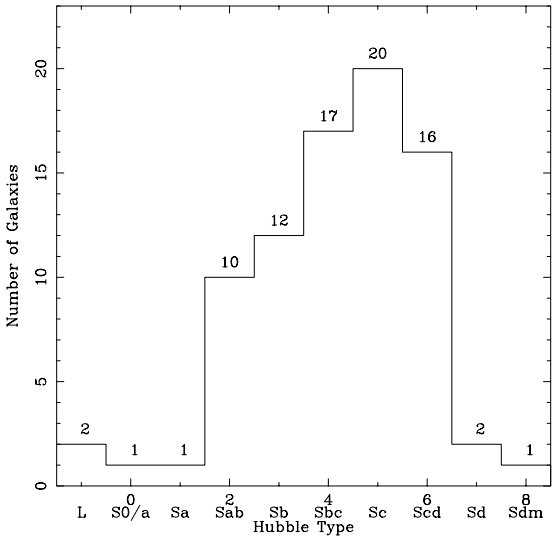

Fig. 1. Galaxy distribution as a function of galaxy type.

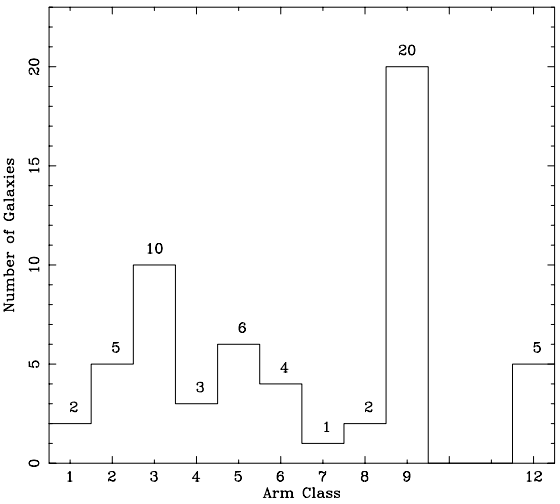

Fig. 2. Galaxy distribution as a function of arm class.

Fixing the value of m, we can calculate the power associated to this component simply as:

$$P_m = |A(p,m)| = \left| \int_{-p_{\max}}^{p_{\max}} A(p,m)\, \mathrm{d}p \right|. \quad (2)$$

The value of $p_{\max}$ is related to the resolution in Fourier space through

$$p_{\max} = \frac{1}{2\Delta u} = \frac{N-1}{2\,(u_{\max} - u_{\min})}, \quad (3)$$

where N is the number of points used in the Fourier transform in the radial dimension, usually $N = 256$ or $N = 512$.

In our first method we try to minimize the effect of the spiral structure by minimizing the ratio:

$$\mathrm{BAG1} = \frac{P_1 + P_2 + \cdots + P_6}{P_0 + P_1 + \cdots + P_6}. \quad (4)$$

This is equivalent to maximizing the contribution of the axisymmetric component. Since a badly deprojected galaxy will

look oval, and thus contribute to the $m = 2$ component as a bar, for our second method we simply minimize the ratio

$$\mathrm{BAG2} = \frac{P_2}{P_0}. \quad (5)$$

In order to check the performance of our two methods, we tested them using artificially generated, yet realistic, galaxies. In the first series of tests the artificial galaxies were simple axisymmetric exponential disks. We projected this disk using inclinations from 20° to 80°. Then, these disks were interpolated with square grids with decreasing resolution, in order to simulate the effect of lower resolution in more distant galaxies. We investigated resolutions ranging from 300×300 pixels to 40×40 pixels. For all these cases, we applied our two methods and compared their results with the true values of the deprojection angles. In all the cases our methods performed extremely well. The deprojection angles were recovered exactly, except in the cases of very low resolutions and inclinations lower than 30°, where we obtained errors of the order of ±2° in the values of PA and IA.

We repeated these experiments adding a spiral component to the disk. The artificial galaxy is then described by

$$I(r,\theta) = \mathrm{e}^{(-r/\alpha)} + A * \mathrm{e}^{(-r_0/\alpha)} \exp\left[-\left(\frac{r-r_0}{\sigma}\right)^2\right] \cos(p \ln(r) + 2\theta),$$

where r, θ correspond to the polar coordinates and α, A, r_0, σ and p are the constants of the model. In these cases we recovered again the deprojection angles with great precision, although not exactly. A typical example is given in Fig. 3. For inclinations lower than 30° both methods recovered the PA with a precision of ±4°. For inclinations higher than 30° we recovered the PA with a precision of ±2°. These error bars were doubled in the case of very low resolutions. In the case of the values of IA, all methods recovered the IA value exactly in all cases, except in the cases of very low resolutions where the precision of the values of IA was about ±2°.

These tests show beyond doubt that both our methods perform very well, obtaining very accurate values of the deprojection angles for artificially generated, yet realistic, galaxies in a variety of situations. Our methods can perform very well for very inclined, nearly edge on galaxies, with inclinations as great as 80 degrees and they are also very reliable in the more difficult cases of galaxies nearly face on. An interesting result of the test is also the good performance of our methods in the case of very low resolutions. This indicates that our methods can be used also to obtain the values of the deprojection angles in the case of very distant galaxies. Thus, our methods can be applied with confidence to samples of galaxies of cosmological interest. We will apply these methods to the galaxies of the present sample and then compare the values of the deprojection angles determined by our methods with the angles determined by the rest of the methods that can be found in the literature.

4. Deprojection of the galaxies

We applied the two methods described in the previous section to the galaxies in the present sample. For each image we proceeded as follows. First we constructed a grid covering all the possible range of values of the PA and IA in increments of 2 degrees. For each pair of angles (PA,IA) we deproject the galaxy image and we compute the Fourier transform (1) with the help of a polar grid. Using Eq. (2) we then calculate the power in each component and then the value of the ratios BAG1 and BAG2. We repeat this for every (PA,IA) pair on the grid. The optimum values are those for which we have a minimum.

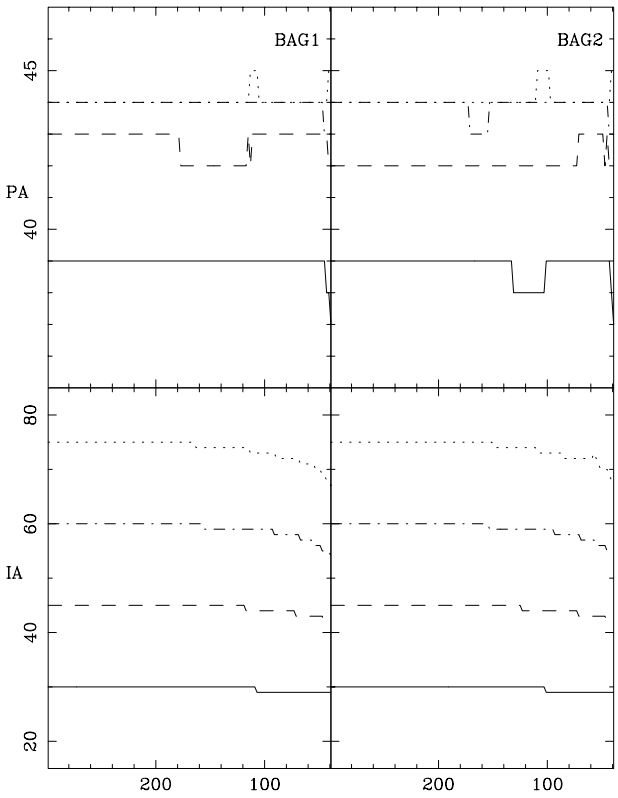

Fig. 3. Position (upper row) and inclination angle (lower row) found by our two methods. The results for BAG1 are in the left column, those for BAG2 in the right. The position angle is 45° and the inclination angle 30° (full line), 45° (dashed line), 60° (dot-dashed line) and 75° (dotted line). Note the excellent performance of all methods in all cases. For this particular example we adopted $\alpha = 30$, $A = 0.1$, $r_0 = 25$, $\sigma = 12.5$ and $p = 2$.

We illustrate the use of our methods with the help of three galaxies: NGC 6503, NGC 5055 and NGC 3631. The first has been chosen as an example of a good case, the second of an intermediate and the third of a bad case. For each case, we give, on a rectangular grid of (PA,IA) values, two grey scale plots, one for the values of BAG1 and the other for the values of BAG2. Light shades denote low values and dark shades high values. We also superpose, on the grey scale plots, isocontours. The values in the parentheses above and to the right of each panel correspond to the values of the PA and IA that give the minimum value of the ratio in each case, i.e. the values that render the image most axisymmetric. The symbols depicted in each graph show the results found in the literature, obtained with other methods. For the ellipse fitting of the outer isophotes of an image we use the symbol P, for values based on a kinematical analysis we use a K symbol followed by another letter

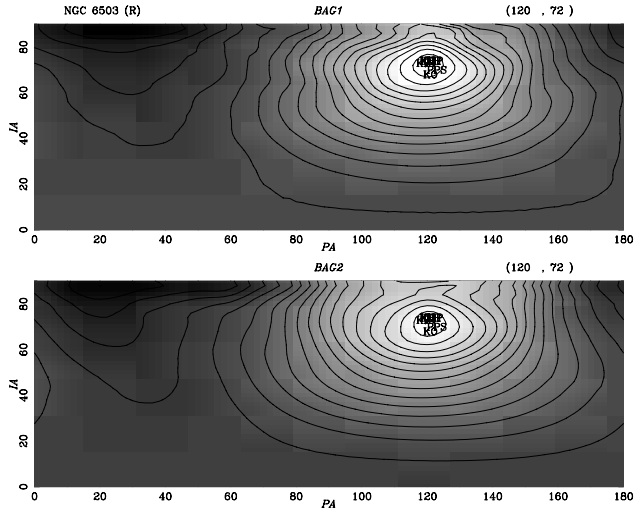

Fig. 4. Results of our methods for the galaxy NGC 6503 and the *R* filter. The upper panel corresponds to our first method and the lower panel to the second method. We give the values of the PA and IA of the minimum in parenthesis in the upper right part of each panel. Symbols are described in the text.

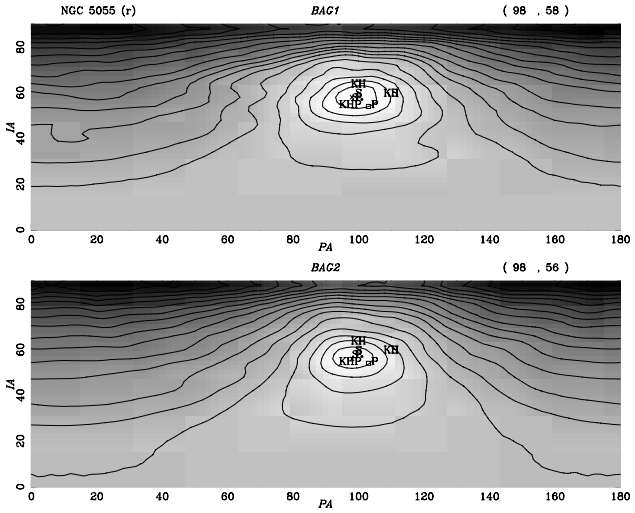

Fig. 5. Results of our methods for the galaxy NGC 5055 and the *r* filter. Layout as in Fig. 4.

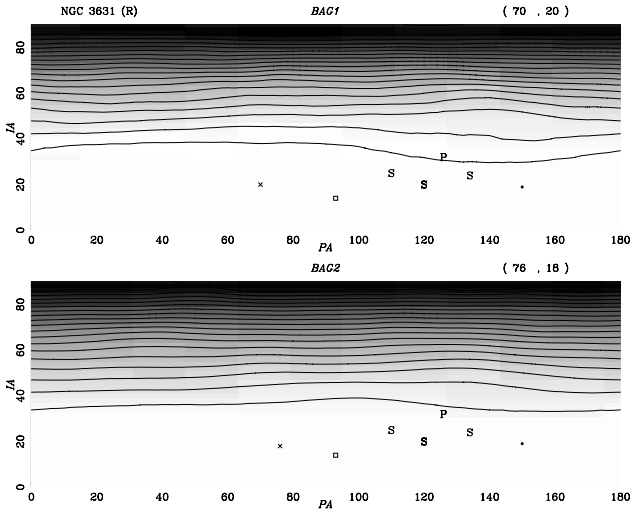

Fig. 6. Results of our two methods for the galaxy NGC 3631 in the *R* band. Layout is as in Fig. 4.

to indicate the kind of data used. Thus KH indicates HI velocity fields, KO optical velocity fields, KC is used for CO velocity fields and KS for long slit measures. For methods based on the spiral structure we use a S. The "×" mark the position of the minimum values of BAG1 or BAG2, depending on the plot. The squares correspond to the mean weighted values given in Table 8 and obtained from BAG1 (or BAG2, respectively) and all the images of this galaxy and finally, the filled circle marks the location of the adopted values for this galaxy as explained in Sect. 6. Figure 4 shows our results for NGC 6503, a good case where the position of the minimum is well constrained by both methods, which further agree well between them and also with the rest of the estimates, as given by other methods found in the literature. In Fig. 5 we show the results for the galaxy NGC 5055.

NGC 3631 is an example of a very poor case and is shown in Fig. 6. As we can see, all the methods give values of the IA that are in general agreement, while the values of the PA are not well constrained. Only the kinematical methods are capable of constraining the value of this angle for galaxies with low inclinations. In Figs. 7–10 we show the images of NGC 3351, NGC 3486, NGC 4501 and NGC 5364, deprojected with the adopted deprojection angles.

For the computation of the Fourier transforms it is necessary to avoid the very central parts of the galaxies as we work with logarithmic radial coordinates ($u = \ln(r)$) and the center will give a singularity. In general it is sufficient to eliminate a relatively small part. For example, for the Frei sample we found it sufficient to eliminate the innermost part of the image, which is within a radius equal to 10% of its extent. There are two cases, however, where it is necessary to discard a larger region. The first case corresponds to galaxies with noticeable bulges. These, being nearly spherical, look round on the plane of the sky. When deprojecting the galaxy, the bulge will be stretched to an elongated shape, thus giving strong spurious signals in the $m = 2$ components that will bias results towards (PA,IA) = (0,0). Thus for this kind of galaxies it is necessary to avoid the bulge-dominated region and use mainly the disc in calculating the Fourier transform. For the Frei sample we found that, for such galaxies, we had to avoid the inner region within a radius equal to 20% of the extent of the image. For a few cases with great bulges like NGC 3031, it is necessary to go even to 30%. Another galaxy type where is necessary to discard a more considerable region in the central parts of the image are the strongly barred galaxies, like NGC 3351 or NGC 4548. If we keep this inner structure, our methods try to render the bar circular and not the external disc. As the bars are normally of larger dimensions than the bulge, for these cases it is necessary to eliminate a region enclosing the whole bar and, in cases with an inner ring, also that ring. In some cases this includes a region within a radius equal to 50% of the extent of the image. In these

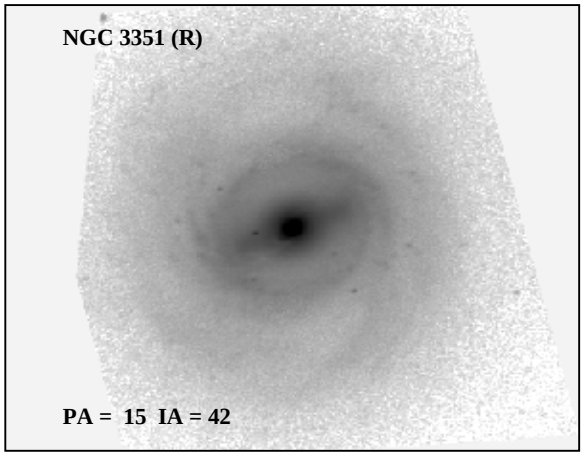

Fig. 7. Deprojected image of NGC 3351 in the *R* filter.

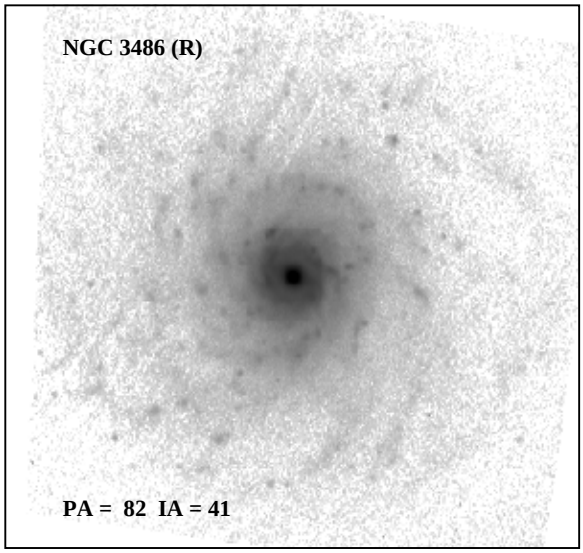

Fig. 8. Deprojected image of NGC 3486 in the *R* filter.

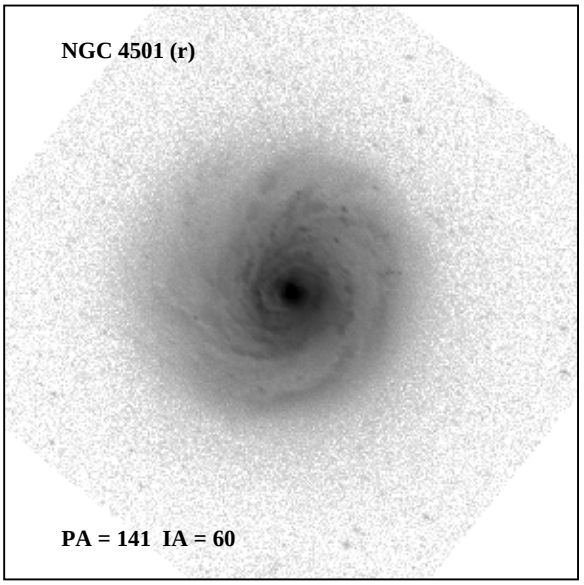

Fig. 9. Deprojected image of NGC 4501 in the *r* filter.

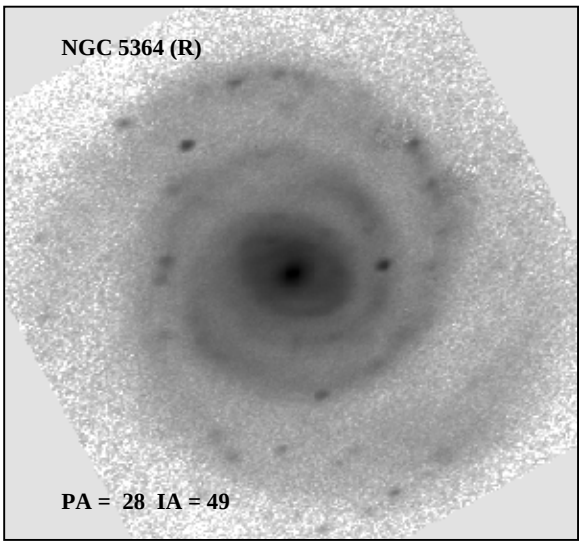

Fig. 10. Deprojected image of NGC 5364 in the *R* filter.

cases, however, we are left with the less bright and noisier parts of the galaxy image and we can expect larger uncertainties.

It is crucial to consider how well our two methods constrain the deprojection angles they find. Indeed if the minimum in figures like 4, 5 or 6 is very shallow, then any small perturbation, due to e.g. local structure on the images, may cause substantial changes in the values of PA and IA at which the minimum occurs, and thus large uncertainties ΔPA and ΔIA. In order to quantify this effect we proceed as follows. We first find the minimum and maximum of all BAG1 and BAG2 values on the grid, and divide the range they delimit in 20 equal parts. We then calculate the number of pair values of PA and IA within the lower most 5% of this range and calculate the ratio, N_5, of the number of pair values in this bin over the total number of pair values. This value is a measure of the size of the well surrounding the minima. For well constrained values N_5 will be small and the larger it gets the greater is the uncertainty in the determined values. We can thus use N_5 as a measure of how well constrained the values are.

Let us now compare the relative performance of our two methods. In Fig. 11 we plot the correlation between the N_5 values determined using the BAG1 method against the values determined by the BAG2 method. The solid line corresponds to the best fitting straight line with a correlation coefficient of 0.92 and a slope of 0.95, while the dashed line indicates a one to one correlation. For this plot we use all the galaxies in the sample, combining the *r* and *R* pass-bands. It shows that the performance of the two methods is comparable, BAG2 giving somewhat better constrained values.

We next consider whether there is any dependency of the uncertainty on the color used to obtain the galaxy image. In Fig. 12 we give the correlations between the N_5 values

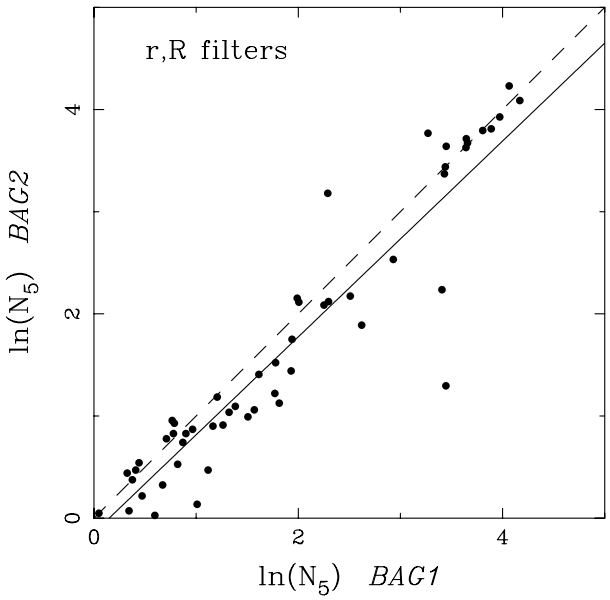

Fig. 11. Correlation between the N_5 values determined by applying our methods to the *r* and *R* pass-bands. The solid line corresponds to the best fitting line, while the dashed line indicates a one to one correlation.

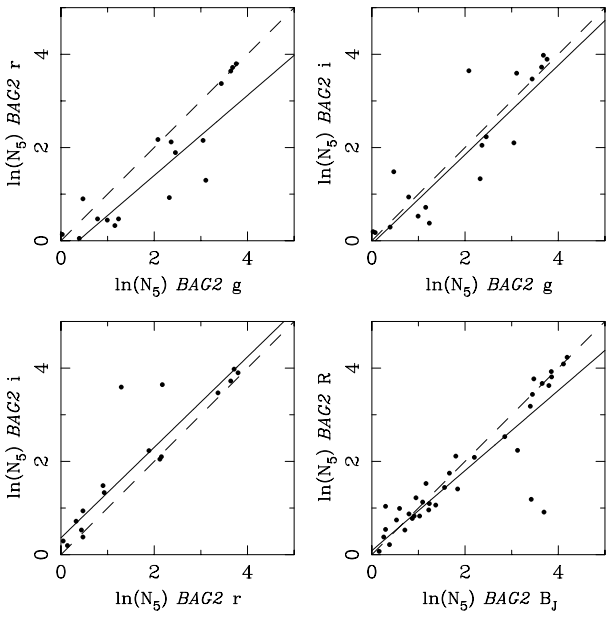

Fig. 12. Correlations for the N_5 values determined using the galaxy images in different pass-bands using the BAG2 method. The lines are as in Fig. 11.

obtained for the galaxy images in different pass-bands using the BAG2 method. It shows that there is a good correlation between the values obtained using different colors. The solid line indicates the best fitting straight line, while the dashed line is a one to one correlation. The values of the correlation coefficients range between 0.85 and 0.94, the lowest values corresponding to the correlation between the *g* and *r* filters in the upper left panel. The slopes of the lines take values between 0.85, for the

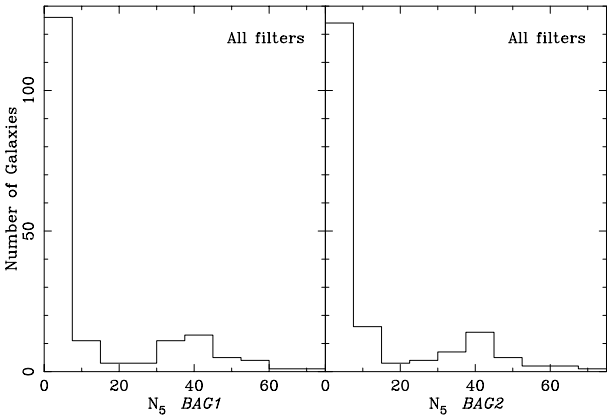

Fig. 13. Distribution of the number of galaxies as a function of the N_5 values for our two methods. The left panel corresponds to method BAG1, and the right panel to method BAG2.

$B_J - R$ correlation, and 0.97, for the $r - i$ correlation. These plots show that the passband used in the galaxy image is not an important source of uncertainty in the determination of the deprojection angles. There is tendency for *R* to fare better than B_J, and for *r* to fare better than *i*, which in turn fares better than *g*, but the effect is small. The correlations for the values obtained using the BAG1 method are similar.

In Fig. 13 we show histograms of the distribution of the number of galaxies as a function of the N_5 value. The left panel corresponds to the values of the BAG1 method, while the right panel corresponds to the values of the BAG2 method. Based on the results of Fig. 12 we have pooled together in these plots all the images in the different pass-bands. As can be seen, for the great majority of images we obtain low values of the N_5 ratio, indicating that the deprojection values are well constrained. In both cases, however, the distribution seems to be bimodal, and there are a few galaxies for which we obtain large values of N_5, indicating that there are large uncertainties in these cases. Let us now consider the source of these large uncertainties.

The main source of uncertainty is in fact the orientation of the galaxy on the plane of the sky. For nearly face-on galaxies it is difficult to determine the IA and, particularly, the PA. Thus, for these galaxies we may expect greater uncertainties. This is shown in Fig. 14 where we plot the N_5 values as a function of the inclination angle, pooling together all the images in the *r* and *R* pass-bands. The lower panel corresponds to the BAG1 method and the upper panel to the BAG2 method. This figure shows that the deprojection angles are very well constrained by our methods for *all* galaxies with inclinations greater than 45 degrees. On the other hand, uncertainties may appear for galaxies with a lower value of the inclination angle. Such uncertainties are indeed expected for galaxies with inclination angles less than 35 degrees. Indeed, in such cases, methods based on images are not sensitive to the PA angle and one has to turn to kinematic methods. There are, however, galaxies with inclination angle between 35 and 55 degrees which have large uncertainties, and we want to examine the source of these uncertainties further.

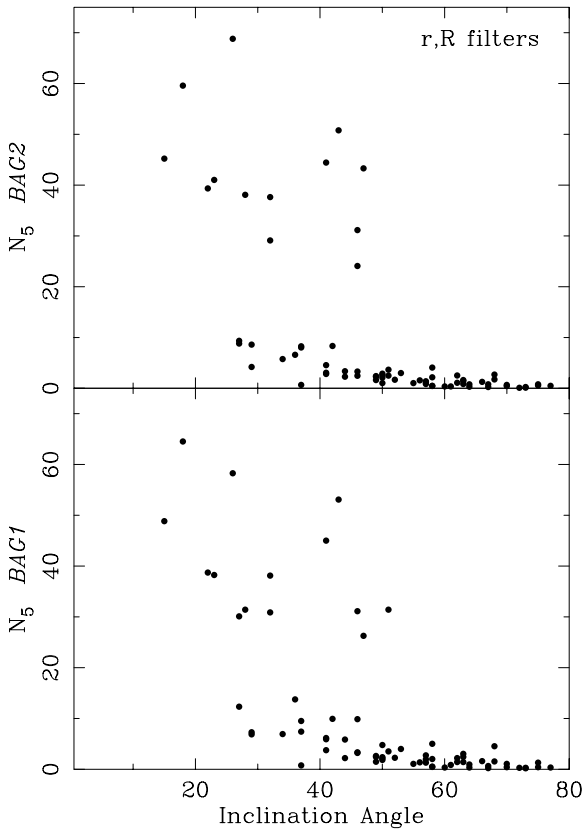

Fig. 14. Effect of the inclination on the uncertainties of the deprojection angles determined by our two methods. The lower panel corresponds to method BAG1 and the upper panel to method BAG2.

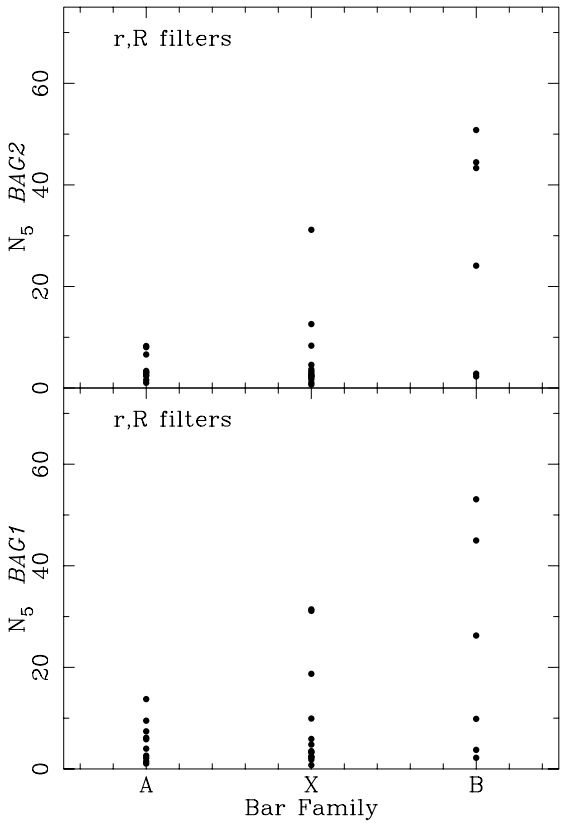

Fig. 15. Effect of the bar family type on the uncertainties of the deprojection angles determined by our two methods. The lower panel corresponds to the BAG1 method and the upper panel to the BAG2 method.

We find a systematic trend with family (i.e. with the existence of a bar). In Fig. 15 we plot N_5 as a function of bar strength using our two methods and restricting ourselves to galaxies with inclinations between 35 and 55 degrees. We note a systematic increase of N_5 with bar strength. Thus, the bar strength is a significant source of uncertainty for both our methods. This is due to the fact that for barred galaxies we use a smaller fraction of the image, thus making our methods less precise and less immune to "noise" or structure in the galaxy. To show this we took a non-barred galaxy, NGC 3486, and calculated N_5 discarding the innermost 50% of the image as for the case of strongly barred galaxies. We found a considerable increase of N_5, thus proving that it is the reduction of the fraction of the image that we use in the Fourier transform that introduces this uncertainty. Hubble type and Arm class could in principle also affect the uncertainties of our two methods. To test this we constrain ourselves to galaxies with inclination angles between 35 and 55 degrees and plot the values of the N_5 ratios as a function of Hubble type and Arm class. We did not find any significant trend, thus indicating that our methods are not affected by the Hubble type (i.e. the relative bulge size of the galaxy) or Arm class (i.e. the presence of strong arms). The former must be due to the fact that the central region carved out because of the bulge is smaller than that carved out because of the bar, thus leaving sufficient disc area for the Fourier transforms.

5. Comparison of the deprojection methods

In this section we will compare the values of the deprojection angles determined by the different methods. In making the comparisons we grouped the methods in groups which are as homogeneous as possible. We thus group together all the values determined by the kinematics, as all authors use similar methods for data reduction. We also group together all values obtained by means of ellipse fitting to the outer isophotes. We use also the values of the RC3 (de Vaucouleurs et al. 1991) catalog as a single group, as they constitute a large and rather homogeneous sample. The same can be said for the values determined by Grøsbol (1985) and Danver (1942). We will also consider another group formed by all the previous determinations of the deprojection angles obtained from the different criteria on the power spectra obtained by bidimensional Fourier transforms on the HII region distribution of the galaxies. This gives us a total of six groups.

For comparing any two methods we fitted a straight line to all pairs of values, using a maximum likelihood algorithm (Press et al. 1992), which minimizes the χ^2 merit function

$$\chi^2(a,b) = \sum_{i=1}^{N} \frac{(y_i - a - bx_i)^2}{\sigma_{yi}^2 + b^2\sigma_{xi}^2}, \quad (6)$$

where σ_{xi}^2 and σ_{yi}^2 are a measure of the errors for the ith value. In the correlations including the PA, we assign weights according the IA, since galaxies with low inclination have ill-defined position angles. These weights are taken from a linear function of the IA, such that this weight is zero for a face on galaxy (IA = 0) and one for a galaxy with IA = 30 degrees. For IA $\geq$ 30 this weight is taken as unity. The σ_{xi} and σ_{yi} are taken as the inverse of the weights, i.e. $\sigma_i = 1/w_i$. For the correlations with the IA we use unweighted values, i.e. $\sigma_{xi} = \sigma_{yi} = 1$.

Errors in the determination of the deprojection angles will introduce a scatter in the plot and lower the correlation coefficient as well as increase the mean of the orthogonal distances. We can use the parameters of these lines and the goodness of fit coefficients to measure quantitatively the relative performance of the different methods. For each straight line we obtain the value of the zero point (a) and of the slope (b), as well as two measures of the goodness of the correlation. These are the weighted mean of the perpendicular distances of the points to the straight line and the weighted correlation coefficient, defined as

$$\rho = \frac{\sum_{i=1}^{N} w_i(x_i - \overline{x})(y_i - \overline{y})}{\sqrt{\sum_{i=1}^{N} w_i(x_i - \overline{x}))^2 \sum_{i=1}^{N} w_i(y_i - \overline{y}))^2}}, \quad (7)$$

where the means are defined as

$$\overline{x} = \frac{\sum_{i=1}^{N} w_i x_i}{\sum_{i=1}^{N} w_i}, \qquad \overline{y} = \frac{\sum_{i=1}^{N} w_i y_i}{\sum_{i=1}^{N} w_i}. \quad (8)$$

In Figs. 16–18 we show examples of correlations between methods. In Fig. 16 we show the correlations between the values derived for the PA (left panel) and the IA (right panel) for our two methods. As we can see, there is an excellent agreement between them, with a weighted correlation coefficient of 0.97 for the PA values and 0.97 for the IA values. In Fig. 17 we show the correlations between our first method and the values derived from the kinematics. In this case, the correlation coefficients are 0.91 for the PA values and 0.86 for the IA values, showing again a good agreement between these two methods. Finally, in Fig. 18 we show the correlations between our second method and the values given in the RC3 catalogue (1991). The correlation coefficients are in this case 0.96 and 0.87, again showing a good agreement. All the rest of the correlations have a similar shape and similar correlation coefficients.

The results of all the correlations are shown in Tables 2 to 6. Table 2 shows the mean weighted orthogonal distances to the regression lines. The values above and to the right of the main diagonal correspond to the correlation of the PA values, while the values below and to the left of the main diagonal correspond to the correlations of the cos(IA) values. We use the cos(IA) instead of the IA values because the former are uniformly distributed in the sky. Table 3 shows the weighted

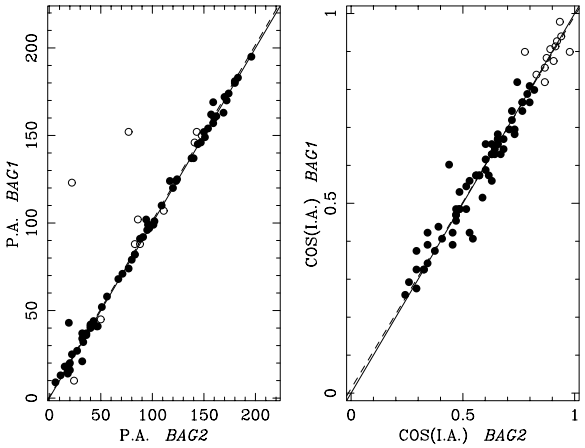

Fig. 16. Comparison off the PA values found by our two methods (left panel) and of the corresponding IA values (right panel). Galaxies with inclination less than 35 degrees are plotted with open symbols and the remaining ones with full symbols. The solid line gives the least squares fitting straight line, calculated as explained in the text, and the dashed one the diagonal.

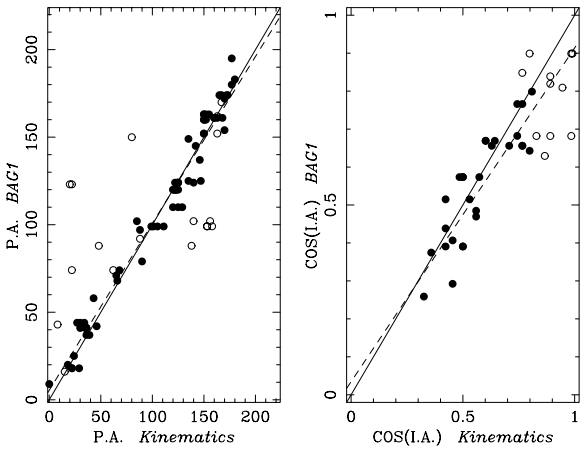

Fig. 17. Comparing the deprojected angles obtained with BAG1 with those obtained from the kinematics. The layout is as in Fig. 16.

correlation coefficients of the linear fits and Tables 4 and 5 the zero points and slopes of the straight lines respectively. Finally, Table 6 gives the number of points used in each correlation. Note that for a given pair of methods these numbers do not need to be equal for the PA and IA correlations, as some authors give only one of these values.

Both the figures and tables show that the PA values are better determined in a statistical sense than the IA values, in good agreement with what was already found by García-Gómez & Athanassoula (1991) and García-Gómez et al. (2002). The mean correlation coefficient for the PA values is 0.86, while the mean correlation coefficient for the IA is 0.81. But this effect is only marginal.

We can not single out any particular method as being better than the rest, since all the correlations give both for the PA and IA zero points near zero and slopes near 1, thus indicating that none of the methods gives a systematic bias in the

Table 2. Weighted mean orthogonal distances for the PA correlations (upper triangle) and the cos(IA) ones (lower triangle). All values are divided by their range interval and multiplied by 100 for the sake of comparison.

	BAG1	BAG2	RC3	G	D	K	P	S
BAG1		1.79	3.53	5.68	5.24	5.10	8.24	6.10
BAG2	2.06		3.32	5.49	5.31	5.48	7.21	7.00
RC3	4.68	4.45		3.03	2.33	4.44	7.57	6.69
G	4.02	3.97	3.83		5.15	6.92	10.16	6.90
D	4.71	4.55	4.05	5.43		2.60	16.60	4.32
K	5.34	5.69	4.57	5.72	5.29		9.41	2.89
P	4.68	5.13	6.14	5.59	6.43	7.95		12.99
S	4.93	4.57	4.76	4.40	5.88	5.34	6.96	

Table 3. Weighted correlation coefficients for the PA correlations (upper triangle) and the cos(IA) ones (lower triangle).

	BAG1	BAG2	RC3	G	D	K	P	S
BAG1		0.97	0.95	0.91	0.84	0.91	0.74	0.88
BAG2	0.97		0.96	0.92	0.85	0.92	0.79	0.88
RC3	0.87	0.90		0.98	0.99	0.90	0.77	0.88
G	0.83	0.83	0.78		0.93	0.84	0.72	0.86
D	0.89	0.91	0.90	0.76		0.98	0.38	0.93
K	0.86	0.87	0.85	0.74	0.88		0.70	0.98
P	0.78	0.78	0.74	0.55	0.69	0.55		0.47
S	0.91	0.91	0.83	0.80	0.85	0.88	0.63	

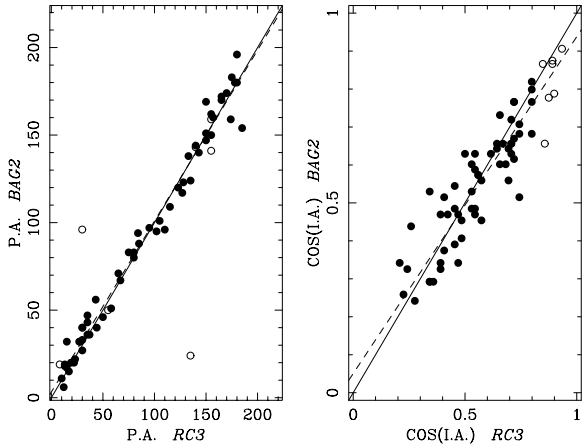

Fig. 18. Comparing the deprojected angles obtained with BAG2 with those obtained from the RC3 catalogue. The layout is as in Fig. 16.

determination of the values. We can also check the dispersion in each method either by computing the mean of the correlation coefficients of a method over the rest, or by using the mean distance. None of the methods has means which are strongly discrepant with the rest of the mean values. The lowest mean of the correlation coefficient and the highest mean distance is obtained for the values determined using the ellipse fitting to the outer isophotes, but this could be due to the fact that this is the most heterogeneous set of data. Our two methods give mean correlation coefficients with the rest of the methods of 0.89 for BAG1 and 0.9 for BAG2 in the case of PA and of 0.87 and 0.88 for the BAG1 and BAG2 method respectively in the case of IA. This indicates that our methods are well suited for the derivation of the deprojection angles. In general, we can conclude that all the methods for deriving the deprojection angles are well suited from a statistical point of view.

6. Final adopted values

For each galaxy we need to adopt a pair of deprojection angles that will be used for the subsequent analysis of the spiral structure and which is based in all the information obtained for that galaxy combining the results of different methods. The results of our analysis are shown in Table 7, which will be only published in electronic form at the CDS. In Col. 1 we give the galaxy name, then for each galaxy we give in Cols. 2–3 the results of method BAG1 for each of the filters. Columns 4–5 give the results of method BAG2. Column 6 give the filter used to obtain the image. Columns 7–8 give respectively the PA and IA measured for this galaxy using other methods that were found in the literature. Column 9 gives a weight for these values. These were obtained deprojecting the galaxy image in the *r* or *R* pass-bands and are just a measure of the degree of roundness of this particular image using these particular values of the deprojection angles. Column 10 gives a code for the deprojection method used to obtain these values. For photometric techniques we use a P, for kinematics we use a K symbol followed by another letter to indicate the kind of kinematics used. Thus, KH indicates HI velocity fields, KO optical velocity fields, KC is used for CO velocity fields and KS for long slit measures. For methods based on the spiral structure we use a S. In Col. 11 we give a code number to point to the reference from which these values were obtained, which is resolved at the end of the table. In Cols. 12–13 we give the mean PA and IA of the values obtained by method BAG1 using all the available

Table 4. Zero points of the best fitting straight line for the PA correlations (upper triangle) and the cos(IA) ones (lower triangle).

	BAG1	BAG2	RC3	G	D	K	P	S
BAG1		0.55	2.94	8.27	−5.95	5.68	10.45	−3.56
BAG2	0.01		3.26	5.42	−2.82	3.59	7.89	−8.37
RC3	0.06	0.05		1.48	−4.43	−8.10	−2.82	−22.80
G	−0.05	−0.02	0.05		−8.32	−4.51	7.13	−24.10
D	0.12	0.09	0.08	0.22		4.16	21.44	−0.99
K	0.03	0.03	−0.02	0.25	−0.04		1.91	−5.24
P	0.14	0.13	0.03	0.29	−0.33	−0.07		−17.18
S	0.02	0.04	0.05	0.17	−0.06	0.01	0.12	

Table 5. Slopes of the best fitting straight line for the PA correlations (upper triangle) and the cos(IA) ones (lower triangle).

	BAG1	BAG2	RC3	G	D	K	P	S
BAG1		1.01	0.98	0.94	1.04	0.95	0.97	1.00
BAG2	0.98		0.98	0.94	1.02	0.95	1.00	1.00
RC3	0.87	0.89		1.01	1.03	1.02	1.08	1.11
G	1.07	1.03	0.98		1.03	0.98	1.03	1.16
D	0.77	0.81	0.87	0.61		0.97	0.94	1.00
K	0.88	0.89	1.03	0.61	1.06		1.09	1.04
P	0.81	0.83	1.03	0.60	1.64	1.23		1.03
S	0.96	0.94	0.92	0.72	1.18	0.99	0.76	

filters for this galaxy. These mean values are the values that we will use for this galaxy and method BAG1. Column 14 gives a weight for these values as in Col. 9. Columns 15–17 give the same values as Cols. 12–14, but for method BAG2. Finally in Col. 18 we give the adopted PA value for this galaxy computed as the weighted mean of all the available values and in Col. 19 the uncertainty in this value of the PA, computed as the weighted dispersion. Columns 20–21 give the same values for the adopted IA. In Table 3 we give only the adopted values and their uncertainties for each galaxy. In Col. 1 we give the galaxy name, in Cols. 2–3 the adopted PA and its uncertainty ΔPA and in Cols. 4–5 the adopted IA and its uncertainty ΔIA.

Table 6. Number of galaxies for the PA correlations (upper triangle) and the cos(IA) ones (lower triangle).

	BAG1	BAG2	RC3	G	D	K	P	S
BAG1		76	66	48	29	89	124	48
BAG2	76		65	47	28	88	123	47
RC3	66	65		38	25	76	117	36
G	48	47	38		18	46	94	30
D	29	28	25	18		53	46	24
K	39	38	31	30	22		107	145
P	122	121	115	92	46	73		92
S	48	47	36	30	24	35	92	

7. Summary

In this paper we introduce two new methods to obtain the deprojection angles of disc galaxies. These are based on two dimensional Fourier transforms of galaxy images. We also introduce a way of assessing the accuracy of these estimates. The methods perform particularly well for galaxies with inclinations greater than 55 degrees. For less inclined galaxies, the major source of uncertainty is the bar strength. For non-barred galaxies our methods perform well up to inclinations of 30 degrees. The tests of our methods show as well that they can be used for low resolution images, thus making them appropiate for samples of galaxies of cosmological interest. A statistical comparison with the values of the deprojection angles determined using other methods shows good agreement between the various methods, thus enhancing confidence in statistical results. When deriving the values for a particular galaxy, however, it is best to apply more than one method to obtain the values of the PA and IA, since different methods introduce different biases. It can thus be that for a particular galaxy two methods, because of their different biases, give rather different results, specially for the case of PA in nearly face-on galaxies. These biases do not make it possible to determine the deprojection parameters of a galaxy with a precision better than around five degrees. Finally, using a combination of the values obtained by our two methods and the rest of values found in the literature, we give a list of adopted deprojection angles with a measure of their respective uncertainty

Appendix A: Deprojection software

In order to facilitate the use of the two methods presented in this paper we make available upon request the software necessary for the PA and IA calculation. For those wishing to write their own software we give here some technical information on the methods.

We found it more straightforward to do the interpolation on the plane of the sky. For this we first define on the plane of the galaxy an appropriate polar grid, which we project on

Table 8. Adopted values of the deprojection angles for the galaxies in the sample.

Name	PA	ΔPA	IA	ΔIA
NGC 2403	124	3	57	3
NGC 2541	170	2	57	7
NGC 2683	41	2	73	3
NGC 2715	19	3	68	4
NGC 2775	158	3	37	3
NGC 2903	20	4	61	3
NGC 2976	142	3	63	4
NGC 2985	178	6	37	3
NGC 3031	153	4	56	3
NGC 3147	150	5	32	4
NGC 3184	84	59	18	11
NGC 3198	39	3	70	3
NGC 3319	38	1	62	3
NGC 3344	156	1	24	6
NGC 3351	15	4	42	5
NGC 3368	157	6	50	1
NGC 3486	82	9	41	6
NGC 3596	155	8	27	2
NGC 3623	175	–	75	–
NGC 3631	152	–	20	6
NGC 3672	9	3	67	3
NGC 3675	0	1	66	1
NGC 3726	13	2	52	3
NGC 3810	25	6	44	2
NGC 3877	36	1	77	1
NGC 3893	171	5	50	1
NGC 3938	22	1	12	7
NGC 3953	14	2	58	4
NGC 4030	29	5	41	2
NGC 4088	52	6	68	2
NGC 4123	137	7	47	4
NGC 4136	92	3	29	8
NGC 4178	32	1	72	2
NGC 4189	81	9	44	5
NGC 4192	152	2	75	1
NGC 4216	19	1	73	5
NGC 4254	60	3	29	5
NGC 4258	160	4	64	3
NGC 4303	137	2	27	1
NGC 4321	153	4	28	3
NGC 4340	98	2	46	4
NGC 4394	111	5	23	2
NGC 4414	161	3	55	3
NGC 4450	174	5	50	3
NGC 4487	77	7	51	3
NGC 4498	136	2	58	2
NGC 4501	141	2	60	2
NGC 4527	67	1	70	2

the plane off the sky. We calculate the values on the nodes of this 2D grid, using four points Lagrange interpolation using the Cartesian grid of the fits file. For deprojection purposes and depending on the resolution of the galaxy images we used grids with 256×256 or 512×512 nodes.

Table 8. continued.

Name	PA	ΔPA	IA	ΔIA
NGC 4535	5	7	46	3
NGC 4548	146	4	41	2
NGC 4559	147	3	67	1
NGC 4569	23	1	63	2
NGC 4571	44	4	32	3
NGC 4579	94	3	37	1
NGC 4593	104	3	44	1
NGC 4651	78	4	49	2
NGC 4654	122	3	57	4
NGC 4689	163	3	35	3
NGC 4725	38	5	51	3
NGC 4826	111	2	53	4
NGC 5005	68	3	64	2
NGC 5033	173	2	62	2
NGC 5055	100	1	57	2
NGC 5248	103	6	46	7
NGC 5334	14	4	41	2
NGC 5364	28	4	49	3
NGC 5371	17	5	46	6
NGC 5585	37	6	50	2
NGC 5669	50	5	47	3
NGC 5701	88	–	24	1
NGC 5792	84	–	75	–
NGC 5850	156	12	34	5
NGC 5985	16	3	58	2
NGC 6015	28	4	62	3
NGC 6118	55	3	63	1
NGC 6384	32	5	48	3
NGC 6503	121	2	73	2

Acknowledgements. We would like to thank A. Bosma for useful discussions. In preparing this paper we made extensive use of the CDS Strasbourg database. CGG and CB acknowledge financial support by the Dirección de Investigación científica y Técnica under contract AYA2001-0762. We also thank the Picasso program of bilateral exchanges under contract HF2001-023. This paper was finished while E.A. was in I.N.A.O.E. She thanks the I.N.A.O.E. staff for their kind hospitality and ECOS-Nord/ANUIES for a travel grant that made this trip possible.

References

Allsopp, N. J. 1979, MNRAS, 188, 765
Athanassoula, E., & Misiriotis, A. 2002, MNRAS, 330, 35
Arsenault, R., Boulesteix, J., Georgelin, Y., & Roy, J.-R. 1988, A&A, 200, 29
Benedict, G. F. 1976, AJ, 81, 799
Begeman, K. G. 1987, Ph.D. Thesis
Blackman, C. P. 1979, MNRAS, 188, 93
Boselli, A., & Gavazzi, G. 2002, A&A, 386, 124
Boselli, A., Lequeux, J., Contursi, A., et al. 1997, A&A, 324, 13
Braine, J., Combes, F., & van Driel, W. 1993, A&A, 280, 451
Brandt, J. C., Kalinowski, J. K., & Roosen, R. G. 1972, ApJS, 24, 421
Braun, R., Walterbos, R. A. M., Kennicutt, R. C., & Tacconi, L. J. 1994, ApJ, 420, 558
Bottema, R. 1988, A&A, 197, 105
Boroson, T. A. 1981, ApJS, 46, 177
Boroson, T. A., Strom, K. M., & Strom, S. E. 1983, ApJ, 274, 39

Bosma, A., Goss, W. M., & Allen, R. J. 1981, A&A, 93, 106
Boggess, N. W. 1959, PASP, 71, 524
Burbidge, E. M., Burbidge, G. R., & Prendergast, K. H. 1963, ApJ, 138, 375
Buta, R. 1988, ApJS, 66, 233
Chincarini, G., & Walker, M. F. 1967, ApJ, 149, 487
Comte, G., Monnet, G., & Rosado, M. 1979, A&A, 72, 73
Considère, S., & Athanassoula, E. 1982, A&A, 111, 82
Considère, S., & Athanassoula, E. 1988, A&AS, 76, 365
Corradi, R. L. M., Boulesteix, J., Bosma, A., et al. 1991, A&A, 244, 27
Côté, S., Carignan, C., & Sancisi, R. 1991, AJ, 102, 904
Danver, C. G. 1942, Lund. Obs. Ann., No. 10
de Jong, R. S., & van der Kruit, P. C. 1994, A&AS, 106, 451
de Vaucouleurs, G., & Caulet, A. 1982, ApJS, 49, 51
de Vaucouleurs, G., de Vaucouleurs, A., Corwin, H. G., et al. 1991, Third Reference Catalogue of Bright Galaxies (New York: Springer) (RC3)
Elmegreen, D. M., & Elmegreen, B. G. 1987, ApJ, 314, 3
Foster, P. A., & Nelson, A. H. 1985, MNRAS, 215, 555
Fraternalli, F., van Moorsel, G., Sancisi, R., & Oosterlo, T. 2002, AJ, 123, 3124
Frei, Z., Guhathakurta, P., Gunn, J., & Tyson, J. A. 1996, AJ, 111, 174
García-Gómez, C., & Athanassoula, E. 1991, A&AS, 89, 159
García-Gómez, C., Athanassoula, E., & Barberá, C. 2002, A&A, 389, 68
García-Ruiz, I., Sancisi, R., & Kuijken, K. 2002, A&A, 394, 769
Garrido, O., Marcelin, M., Amram, P., & Boulesteix, J. 2002, A&A, 387, 821
Gottesman, S. T., & Weliachew, L. 1975, ApJ, 195, 23
Grosbøl, P. J. 1985, A&AS, 60, 261
Guhatakurta, P., van Gorkom, J. H., Kotany, C. G., & Balkowski, C. 1988, AJ, 96, 851
Haynes, M. P., Giovanelli, R., Chamaraux, P., et al. 1999, AJ, 117, 2093
Héraudeau, Ph., & Simien, F. 1996, A&AS, 118, 111
Higdon, J. L., Buta, R. J., & Purcell, G. B. 1998, AJ, 115, 80
Hunt, L. K., Malkan, M. A., Rush, B., et al. 1999, ApJSS, 125, 349
Irwin, J. A., & Seaquist, E. R. 1991, ApJ, 371, 111
Iye, M., Okamura, S., Hamabe, M., & Watanabe, M. 1982, ApJ, 256, 103
Jogee, S., Knapen, J. H., Laine, S., et al. 2002, ApJ, 570, L55
Kent, S. 1984, ApJS, 56, 105
Kent, S. 1986, AJ, 91, 130
Kent, S. 1987, AJ, 93, 81
Kent, S. 1988, AJ, 96, 514
Kornreich, D. A., Hayes, M. P., Lovelace, R. V. E., & van Zee, L. 2000, AJ, 120, 139
Knapen, J. H. 1997, MNRAS, 286, 403
Knapen, J. H., Cepa, J., Beckman, J. E., del Rio, S., & Pedlar, A. 1993, ApJ, 416, 563
Koopmann, R. A., Kenney, J. D. P., Young, J. 2001, ApJS, 135, 125
Laurikainen, E., & Salo, H. 2000, A&AS, 141, 103
Marcelin, M., Boulesteix, J., & Georgelin, Y. 1983, A&A, 1128, 140
Mathewson, D. S., & Ford, V. L. 1996, ApJS, 107, 97
Meyssonier, N. 1984, A&AS, 58, 351
Michard, R. 1985, A&AS, 59, 205
Miller, B., & Hodge, P. W. 1991, BAAS, 23, 966
Mölllenhoff, C., & Heidt, J. 2001, A&A, 368, 16
Moore, E. M., & Gottesman, S. T. 1998, MNRAS, 294, 353
Moriondo, G., Giovanardi, C., & Hunt, L. K. 1988, A&AS, 130, 81
Münch, G. 1959, PASP, 71, 101
Oosterloo, T., & Shostak, S. 1993, A&AS, 99, 379
Phookun, B., Vogel, S. N., & Mundy, L. G. 1993, ApJ, 418, 113
Press, W. H., Teukolsky, S. A., Vetterling, W. H., & Flannery, B. P. 1992, Numerical Recipes (Cambridge Univ. Press)
Prieto, M., Longley, D. P. T., Perez, E., et al. 1992, A&AS, 93, 557
Prieto, M., Gottesman, S. T., Aguerri, J. A. L., & Varela, A. M. 1997, AJ, 114, 1413
Puerari, I., & Dottori, H. A. 1992, A&AS, 93, 469
Rhee, M.-H., & van Albada, T. S. 1996, A&AS, 115, 407
Rots, A. H. 1975, A&A, 45, 43
Rots, A. H. 1980, A&AS, 41, 189
Sakamoto, K. 1996, ApJ, 471, 173
Sánchez-Portal, M., Díaz, A. I., Terlevich, R., et al. 2000, MNRAS, 312, 2
Schmitt, M., & Kinney, A. L. 2000, ApJSS, 128, 479
Shostak, G. S., Willis, A. G., & Crane, P. C. 1981, A&A, 96, 393
Sicking, F. J. 1997, Ph.D. Thesis, Univ. Groningen
Sofue, Y., Tomita, A., Honma, M., & Tutui, Y. 1999, PASJ, 51, 737
Stil, J. M., & Israel, F. P. 2002, A&A, 389, 42
Stocke, J. 1955, AJ, 60, 216
Swaters, R. A., & Balcells, M. 2002, A&A, 390, 863
Terndrup, D. M., Davies, R. L., Frogel, J. A., DePoy, D. L., & Wells, L. A. 1994, ApJ, 432, 518
Thean, A. H. C., Mundell, C. G., Pedlar, A., & Nicholson, R. A. 1997, MNRAS, 290, 15
Thornley, M. D., & Mundy, L. G. 1997, ApJ, 484, 202
Thornley, M. D., & Mundy, L. G. 1997, ApJ, 490, 682
Tully, B., Verheijen, M. A. W., Pierce, M. J., Huang, J. S., & Wainscoat, R. J. 1996, AJ, 112, 247
Vallejo, O., Braine, J., & Baudry, A. 2002, A&A, 387, 429
van Albada, G. D. 1980, A&A, 90, 123
van Albada, G. D., & Shane, W. W. 1975, A&A, 42, 433
van der Kruit, P. C. 1973, ApJ, 186, 807
van der Kruit, P. C. 1974, ApJ, 192, 1
van der Kruit, P. C., & Shostak, G. S. 1982, A&A, 105, 351
van Driel, W., & Buta, R. J. 1991, A&A, 245, 7
van Moorsel, G. A. 1983, A&AS, 54, 1
van Moorsel, G. A., & Wells, D. C. 1985, AJ, 90, 1038
Verdes-Montenegro, L., Bosma, A., & Athanassoula, E. 1997, A&A, 321, 754
Verdes-Montenegro, L., Bosma, A., & Athanassoula, E. 2000, A&A, 356, 827
Walterbros, R. A. M., Braun, R., & Kennicutt, R. C. Jr. 1994, AJ, 107, 184
Weiner, B. J., Williams, T. B., van Gorkom, J. H., & Sellwod, J. A. 2001, ApJ, 546, 916
Wevers, B. M. H. R., Appleton, P. N., Davies, R. D., & Hart, L. 1984, A&A, 140, 125
Wevers, B. M. H. R., van der Kruit, P. C., & Allen, R. J. 1986, A&AS, 66, 505
Zasov, A. V., & Sil'chencko, O. K. 1987, SvA Lett., 13, 186

2.3 Deprojecting spiral galaxies using Fourier analysis. Application to the Ohio sample

García-Gómez, C., **Barberà, C.**, Athanassoula, E., Bosma, A. and Whyte, L., Deprojecting spiral galaxies using Fourier analysis. Application to the Ohio sample. *Astronomy and Astrophysics* 421, 595-601 (2004) EDP Sciences. DOI:10.1051/0004-6361:20035735

A&A 421, 595–601 (2004)
DOI: 10.1051/0004-6361:20035735

Astronomy & Astrophysics

Deprojecting spiral galaxies using Fourier analysis. Application to the Ohio sample⋆

C. García-Gómez[1], C. Barberà[1], E. Athanassoula[2], A. Bosma[2], and L. Whyte[3]

[1] DEIM, Campus Sescelades, Avd. dels Països Catalans 26, 43007 Tarragona, Spain
[2] Observatoire de Marseille, 2 place Le Verrier, 13248 Marseille Cedex 04, France
[3] School of Physics and Astronomy, University of Nottingham, Nottingham NG7 2RD, UK

Received 24 November 2003 / Accepted 7 April 2004

Abstract. We use two new methods developed recently (Barberà et al. 2004, A&A, 415, 849), as well as information obtained from the literature, to calculate the orientation parameters of the spiral galaxies in the Ohio State University Bright Galaxy Survey. We compare the results of these methods with data from the literature, and find in general good agreement. We provide a homogeneous set of mean orientation parameters which can be used to approximately deproject the disks of the galaxies and facilitate a number of statistical studies of galaxy properties.

Key words. galaxies: structure – galaxies: spiral

1. Introduction

The accurate determination of the deprojection angles of a spiral galaxy is a necessary first step before one can study quantitatively its morphology, photometry or kinematics. These angles are the position angle (hereafter PA), which is the angle between the line of nodes of the projected image and the north, measured towards the east, and the inclination angle (hereafter IA), which is the angle between the perpendicular to the plane of the galaxy and the line of sight.

In this paper we use the two methods based on the Fourier transform of galactic images developed recently (Barberà et al. 2004, hereafter BAG) and combine them with information obtained from different sources in the literature to obtain accurate values of the deprojection angles of the Ohio State University Bright Spiral Galaxy Survey (hereafter OSU) sample of bright galaxies. We will use this information in subsequent papers to deproject the galaxy images so as to be able to study the spiral structure in disc galaxies by decomposing each image with the help of bidimensional Fourier transforms.

The OSU survey has been described thoroughly in Eskridge et al. (2002) and will not be discussed further here. The Early Data Release (20 June 2002) is a magnitude limited sample containing 205 disc galaxies with Hubble types $T \geq 0$, apparent magnitudes $M_B \leq 12$ and diameters $D \leq 6\farcm5$. As in the preceding paper (BAG), we have concentrated on the galaxies with Hubble types $2 \leq T \leq 7$ for which the Fourier methods can be usefully applied. This brings our sample to a total of 158 galaxies which, when combined with the disc galaxies of the Frei et al. (1996) sample, will constitute a sample of about 200 galaxies with different Hubble types and with information in different colour bands on which we will base our subsequent studies on spiral structure in spiral galaxies.

2. Deprojection methods

The determination of the deprojection angles of spiral galaxies can be made using different methods, usually based either on the photometry, or on the kinematics. In the photometric methods ellipses are fitted to the outer isophotes of the images. The axis ratio of the outer ellipses is given as a measure of the IA, while the direction of the major axis of the ellipse gives the PA. The observation of the gas kinematics within the disc, with the determination of two dimensional velocity fields, is another commonly used method. It is necessary to make the assumption that the emission comes from material in a thin disc in circular motion around the center. The selected PA and IA angles are those which minimize the departures from such a flow. This method is the most reliable one for the determination of the PA of galaxies near face on.

Several other methods can be found in the literature. For instance, Danver (1942) used a special display table to rotate the galaxy images until they looked approximately circular. Grøsbol (1985) used a one dimensional Fourier transform of the intensity distribution in the outer parts of galaxy discs and adopted the deprojection angles that minimized the bisymmetric ($m = 2$) Fourier coefficient. Comte et al. (1979)

Send offprint requests to: C. García-Gómez,
e-mail: cgarcia@etse.urv.es

⋆ Table 1 is only available in electronic form at the CDS via anonymous ftp to cdsarc.u-strasbg.fr (130.79.128.5) or via http://cdsweb.u-strasbg.fr/cgi-bin/qcat?J/A+A/421/595

used the distribution of HII regions in the $\ln(r) - \theta$ plane to fit straight lines to the arms, under the hypothesis that they are well described by logarithmic spirals. Two dimensional Fourier analysis, similar to the methods presented in BAG, has also been used previously to determine the deprojection angles. Considère & Athanassoula (1982) used the HII region distribution, selecting the angles that maximized the signal-to-noise ratio in the $m = 2$ component, and Considère & Athanassoula (1988), applied the same criterion to galaxy images. Iye et al. (1982) used an image of NGC 4254 and selected the angles that maximize the axisymmetric component. Finally, García-Gómez & Athanassoula (1991) and García-Gómez et al. (2002) also used HII region distributions and maximized the axisymmetric components. These authors also used a second method selecting the deprojection angles that make the HII region distribution most uniform with azimuth.

In BAG we introduced two new methods, again based on the Fourier transforms, which are closely related to the two methods used by García-Gómez et al. (2002) for HII region distributions. Let $I(u, \theta)$ be the image of the galaxy written in polar coordinates (r, θ), and $u = \ln(r)$. We define the Fourier transform of this image as:

$$A(p, m) = \int_{u_{\min}}^{u_{\max}} \int_{0}^{2\pi} I(u, \theta)\ \exp[\mathrm{i}(pu + m\theta)]\, \mathrm{d}\theta \mathrm{d}u. \quad (1)$$

In this equation, p corresponds to the radial frequency and m to the azimuthal frequency. Thus the $m = 1$ values correspond to an asymmetry, the $m = 2$ values to a bisymmetric component, and so on. The values of $u_{\min} = \ln(r_{\min})$ and $u_{\max} = \ln(r_{\max})$ are set by the inner and outer radius of the image, or of the part that we will analyze.

Fixing the value of m, we can calculate the power associated to this component simply as:

$$P_m = |A(p, m)| = \left| \int_{-p_{\max}}^{p_{\max}} A(p, m)\, \mathrm{d}p \right|. \quad (2)$$

The value of $p_{\max}$ is related to the resolution in Fourier space through

$$p_{\max} = \frac{1}{2\Delta u} = \frac{N - 1}{2(u_{\max} - u_{\min})}, \quad (3)$$

where N is the number of points used in the Fourier transform in the radial dimension, usually $N = 256$ or $N = 512$.

In our first method we try to minimize the effect of all non-axisymmetric structure by minimizing the ratio:

$$BAG1 = \frac{P_1 + P_2 + \cdots + P_6}{P_0 + P_1 + \cdots + P_6}. \quad (4)$$

This is equivalent to maximizing the contribution of the axisymmetric component. Experience shows that components of order larger than 6 are too noisy to be of use. Since a badly deprojected galaxy will look oval, and thus contribute to the $m = 2$ component as a bar, for our second method we simply minimize the ratio

$$BAG2 = \frac{P_2}{P_0}. \quad (5)$$

None of the methods proposed so far are free from systematic errors. They are designed to work properly in the case of perfectly axisymmetric thin discs in circular motion about their centers, which is rarely the case for real disc galaxies. For instance, when we try to fit ellipses to the outer isophotes, the presence of strong arms, or (pseudo-) rings can influence the value of the PA, and hence also the IA. This particular bias is known as Stock's effect (1955). On the other hand, warps in the outer parts of the discs, or non-circular motions in the central parts due to bars or other perturbations, can bias the results of the kinematical methods. The methods based on the Fourier analysis of the images are also not free of systematic biases, but their results are as reliable as the kinematical methods, as shown in BAG. Thus, the more reliable way of determining the deprojection angles is to compile the information of different sources and to combine the results in order to minimize the different biases. This is the procedure we followed for the spiral galaxies in the Frei et al. (1996) sample and we will also follow it for the present sample.

3. Application to the OSU sample of galaxies

For each galaxy in the sample we proceed as follows to determine the deprojection angles. First we make a thorough search in the literature of all the determinations of the deprojection angles using different methods. Then we apply the BAG1 and BAG2 methods to each of the images of the galaxies in the sample. The values obtained for each method and each image are averaged to give the results of each of our two methods. We then use the literature values and the values determined by our two methods to deproject the broad band B image of each galaxy. We do not use the H band image, since, sometimes at least, it goes to less depth than the B band image, and since for some galaxies the field of view is too limited. According to the shape of the deprojected image we give a weight to the pair of determined deprojection angles. If the deprojected image is neatly round we give a weight of 3; we diminish the weight as the deprojected image deviates from circular shape. This allows us to spot some systematic errors, as e.g. cases where the photometry does not extend to sufficiently large radii, and thus minimize their effects on the finally adopted value. These weights, together with other information on the quality of the individual studies, considerations on how appropiate a particular method is for the galaxy at hand etc., are taken into account when adopting the final (PA, IA) values.

We checked our results by visual inspection of all the deprojected images. We found that for 35 out of the 158 galaxies (22%) a correction to the value obtained by the weighted average of all results was necessary. Three categories of galaxies were particularly affected : 1) galaxies with strong outer spiral structure or outer (pseudo-) rings, like the galaxies NGC 1350, NGC 5247 and NGC 7479; 2) highly inclined galaxies with a strong bulge, like NGC 3169 and NGC 4856; and 3) galaxies seen very face-on, like NGC 3938 and NGC 4303, for which the determination of the position angle is difficult. For the galaxies in groups 1) and 2), normally a typical correction of $5°-10°$ was necessary, while for very face-on galaxies our methods can give values for the PA quite different from the

values determined using other methods. Where adequate, we preferred the determination based on HI kinematics, but in other cases we adopted the criterion that the outer disk isophote has to be circular. This percentage of correction bodes ill for a full automation of the deprojection process in case of very large samples, as becomes possible e.g. with the Sloan Digital Sky Survey.

The results of our analysis are shown in Table 1, which will be published in the electronic version only. In Col. 1 we give the galaxy name, then for each galaxy we give in Cols. 2 and 3 the results of method *BAG*1 for each of the colour bands. Columns 4 and 5 give the results of method *BAG*2. In both cases the colour bands are listed in the sequence B, H. Column 6 gives the colour band used to obtain the image. Columns 7 and 8 give respectively the PA and IA measured for this galaxy using other methods that were found in the literature. Column 9 gives a weight for these values. These were obtained deprojecting the galaxy image in the *B* band, and are just a measure of the degree of roundness of this particular image using these particular values of the deprojection angles. Column 10 gives a code for the deprojection method used to obtain these values. For photometric techniques we use a P, for kinematics we use a K symbol followed by another letter to indicate the kind of kinematics used. Thus, KH indicates HI velocity fields, KO optical two-dimensional velocity fields, KC is used for CO velocity fields and KS for long slit measures. The symbol KP indicates a combination of the information coming from both kinematic and photometric analyses. For methods based on the spiral structure we use a S. In Col. 11 we give a code number to point to the reference from which these values were obtained, which is resolved at the end of the table. In Cols. 12 and 13 we give the mean PA and IA of the values obtained by method *BAG*1 using all the available filters for this galaxy. These mean values are the values that we will use for this galaxy and method *BAG*1. Column 14 gives a weight for these values as in Col. 9. Columns 15–17 give the same values as Cols. 12–14, but for method *BAG*2. Finally, in Col. 18 we give the adopted PA value for this galaxy computed as the weighted mean of all the available values and in Col. 19 the uncertainty in this value of the PA, computed as the weighted dispersion. Columns 20 and 21 give the same values for the adopted IA. In Table 2 we give only the adopted values and their uncertainties for each galaxy. In Col. 1 we give the galaxy name, in Cols. 2 and 3 the adopted PA and its uncertainty ΔPA and in Cols. 4 and 5 the adopted IA and its uncertainty ΔIA.

4. Comparison with data in the literature

Some of the galaxies are present both in the Frei et al. (1996) and the Ohio (2002) samples. We have made a consistency check between the values determined by the BAG methods using different images in different passbands for these galaxies, obtained with different instrumentation.

In order to compare the values obtained using the two samples we fit a straight line to all pairs of values, using a

Table 2. Adopted values of the deprojection angles for the galaxies in the sample.

Name	PA	Δ PA	IA	Δ IA
IC 4444	55	2	34	5
IC 5325	14	13	31	2
NGC 150	119	2	61	3
NGC 157	38	4	46	3
NGC 210	163	5	51	3
NGC 278	39	7	22	4
NGC 289	132	8	41	5
NGC 488	9	4	39	2
NGC 578	107	4	57	4
NGC 613	118	5	44	2
NGC 685	97	–	35	6
NGC 779	160	–	73	2
NGC 864	32	12	43	3
NGC 908	77	2	63	1
NGC 1003	95	1	71	1
NGC 1042	112	–	35	–
NGC 1058	145	–	15	8
NGC 1073	164	–	19	–
NGC 1084	38	6	53	4
NGC 1087	1	2	52	2
NGC 1187	135	6	40	6
NGC 1241	143	3	55	1
NGC 1300	87	–	35	–
NGC 1302	180	1	17	–
NGC 1309	75	6	26	1
NGC 1317	78	–	29	–
NGC 1350	6	6	59	1
NGC 1371	133	2	45	1
NGC 1385	174	5	51	3
NGC 1421	6	7	81	5
NGC 1493	71	2	21	–
NGC 1559	63	1	57	3
NGC 1617	106	1	62	1
NGC 1637	31	–	40	–
NGC 1703	177	–	30	–
NGC 1792	137	2	62	2
NGC 1832	17	11	46	3
NGC 1964	29	3	67	1
NGC 2090	12	2	65	–
NGC 2196	50	8	39	2
NGC 2280	163	–	67	–
NGC 2559	6	–	63	1
NGC 2775	158	3	38	3
NGC 2964	94	2	54	3
NGC 3059	0	–	0	–
NGC 3169	50	3	53	4
NGC 3223	128	4	48	3
NGC 3261	77	14	40	1
NGC 3275	30	–	20	–

Table 2. continued.

Name	PA	ΔPA	IA	ΔIA
NGC 3319	39	2	61	4
NGC 3338	96	3	55	5
NGC 3423	31	14	34	2
NGC 3504	155	–	19	3
NGC 3507	92	11	28	5
NGC 3511	73	2	69	0
NGC 3513	123	9	36	7
NGC 3583	125	2	51	2
NGC 3596	146	8	29	3
NGC 3646	50	2	60	3
NGC 3675	180	–	63	–
NGC 3681	108	3	11	16
NGC 3684	130	5	47	3
NGC 3686	18	6	39	3
NGC 3705	122	–	65	–
NGC 3726	14	2	53	3
NGC 3810	25	5	45	2
NGC 3877	36	1	77	1
NGC 3887	9	7	42	4
NGC 3893	169	5	51	2
NGC 3938	21	1	11	6
NGC 3949	119	2	52	2
NGC 4030	32	6	40	2
NGC 4051	132	2	43	5
NGC 4062	99	2	66	2
NGC 4100	167	2	72	1
NGC 4123	132	7	48	5
NGC 4136	97	8	31	7
NGC 4145	101	8	55	–
NGC 4151	21	1	21	1
NGC 4178	33	2	72	2
NGC 4212	74	1	52	3
NGC 4254	59	3	29	5
NGC 4303	137	1	27	–
NGC 4314	79	14	26	2
NGC 4388	90	2	74	4
NGC 4394	111	4	25	3
NGC 4414	160	4	54	4
NGC 4448	93	1	67	1
NGC 4450	175	5	51	4
NGC 4457	82	–	31	–
NGC 4487	76	6	52	3
NGC 4504	143	2	51	2
NGC 4527	68	2	70	2
NGC 4548	141	5	35	11
NGC 4571	42	8	32	3
NGC 4579	94	4	37	2
NGC 4580	159	5	43	4

Table 2. continued.

Name	PA	ΔPA	IA	ΔIA
NGC 4593	98	16	46	2
NGC 4618	23	10	38	4
NGC 4643	58	11	37	4
NGC 4651	78	5	48	2
NGC 4654	122	3	57	4
NGC 4665	115	3	29	2
NGC 4666	41	–	74	1
NGC 4689	162	5	36	4
NGC 4698	168	–	67	–
NGC 4699	45	2	43	3
NGC 4772	145	1	65	2
NGC 4775	93	–	18	–
NGC 4781	117	4	62	2
NGC 4818	0	–	72	–
NGC 4900	0	–	18	–
NGC 4902	102	21	23	7
NGC 4930	55	9	40	4
NGC 4939	8	5	59	3
NGC 4941	17	1	59	2
NGC 4995	96	3	47	2
NGC 5005	65	–	63	–
NGC 5054	159	2	54	1
NGC 5085	39	9	38	7
NGC 5101	140	–	32	–
NGC 5121	27	5	35	2
NGC 5161	78	1	66	1
NGC 5247	22	14	24	5
NGC 5334	15	3	43	5
NGC 5371	8	–	46	5
NGC 5427	72	6	32	6
NGC 5448	108	4	66	3
NGC 5483	21	5	26	3
NGC 5643	108	2	23	0
NGC 5676	46	1	61	1
NGC 5701	45	–	20	–
NGC 5713	12	2	30	2
NGC 5850	160	11	34	4
NGC 5921	137	10	36	3
NGC 5962	109	4	45	2
NGC 6215	78	–	34	–
NGC 6221	178	6	50	7
NGC 6300	115	6	50	1
NGC 6384	32	4	48	2
NGC 6753	29	4	34	3
NGC 6782	45	–	26	2
NGC 6902	155	1	45	3
NGC 6907	45	1	32	3
NGC 7083	5	1	58	4

Table 2. continued.

Name	PA	ΔPA	IA	ΔIA
NGC 7184	62	1	73	2
NGC 7205	69	3	60	1
NGC 7213	30	7	15	2
NGC 7217	86	5	29	4
NGC 7412	45	–	42	–
NGC 7418	137	2	40	3
NGC 7479	35	7	44	4
NGC 7552	175	7	38	5
NGC 7582	157	–	65	–
NGC 7606	146	–	68	–
NGC 7713	172	3	68	–
NGC 7723	41	8	47	1
NGC 7741	166	4	43	5

maximum likelihood algorithm (Press et al. 1992), which minimizes the χ^2 merit function

$$\chi^2(a,b) = \sum_{i=1}^{N} \frac{(y_i - a - bx_i)^2}{\sigma_{yi}^2 + b^2\sigma_{xi}^2}, \quad (6)$$

where σ_{xi}^2 and σ_{yi}^2 are a measure of the errors for the ith value.

In the correlations including the PA, we assign weights according to the IA, since galaxies with low inclination have ill-defined position angles. These weights are taken from a linear function of the IA, such that this weight is zero for a face on galaxy (IA = 0) and unity for a galaxy with IA ≥ 30 degrees. For IA ≥ 30 this weight is taken as unity. The σ_{xi} and σ_{yi} appearing in Eq. (6) are defined as the inverse of the weights, i.e $\sigma_i = 1/w_i$. For the correlations with the IA we use unweighted values, i.e. $\sigma_{xi} = \sigma_{yi} = 1$.

The comparison (not shown here) between the values of the BAG1 method derived for the galaxies in the Frei sample and those in the Ohio sample is excellent, the correlation coefficient of the PA values is 0.97, and for the case of the cos (IA) values is 0.98. In the case of the BAG2 method the correlation coefficient is 0.96 for the PA values and 0.94 for the cos (IA) values. These values indicate that our methods give comparable values when used on images taken from different samples and with different passbands. Thus, this is a further indication of the robustness of our two methods, which, added to the relative comparison with the other methods presented in BAG, shows that our methods can be used with confidence.

We also compared the results for our methods with data from the RC3, and with kinematic data available in the literature. We show in Figs. 1 and 2 the comparison with BAG2. Results for BAG1 are similar and thus will not be shown here. In Fig. 1, the correlation coefficient is 0.96 for the PA values, and 0.87 for the cos (IA) values. The three outlying points above the correlation in the left panel of Fig. 1 correspond to three late spirals with a very open spiral structure while in the inner parts there is a late type bar.

As for the comparison with the kinematic data, in Fig. 2, the correlation coefficient is 0.84 for the PA values, and 0.85 for the cos (IA) values. There is thus a good correlation, but not an excellent one. Excluding the galaxies for which the inclination is less than IA = 30 degrees, the correlation improves significantly. The correlation coefficients now become 0.96 and 0.88 for the PA and the cos (IA), respectively. This reflects the fact that for galaxies not far from face-on only the kinematics can provide a good estimate for the deprojection angles. It also argues that our methods fare very well for all galaxies which are not nearly face-on.

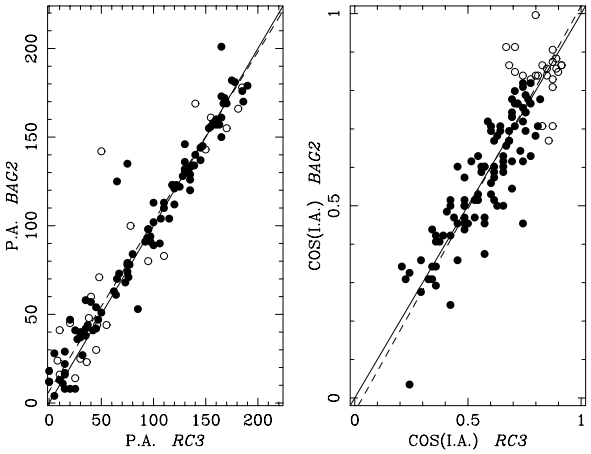

Fig. 1. Comparison of the deprojected angles obtained with *BAG*2 with RC3 values, for the galaxies present in the Ohio sample. Left panel corresponds to the correlation for the PA values, while the right panel shows the correlation for the cos (IA) values. Galaxies with inclination less than 30 degrees are plotted with open symbols and the remaining ones with full symbols. The solid line gives the least squares fitting straight line, calculated as explained in the text, and the dashed one the diagonal.

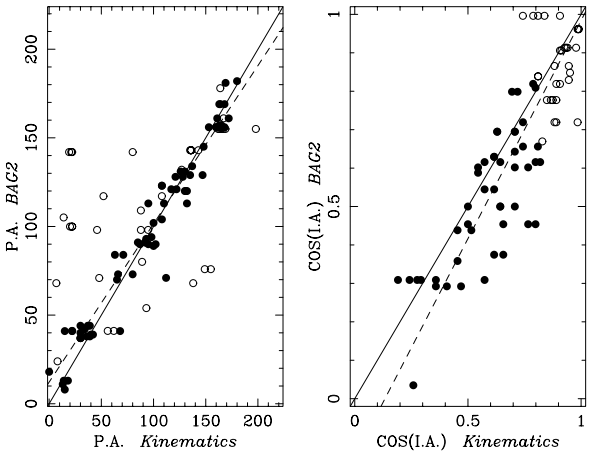

Fig. 2. Comparing the deprojected angles obtained with *BAG*2 for the galaxies in the Ohio sample with data obtained from kinematics in the literature. The layout is as in Fig. 1.

5. Summary

In this paper we calculate the deprojection angles of the spiral galaxies in the Ohio State University Bright Galaxy Sample. These values are determined using all the information compiled

in the literature, plus the results of two methods based on the Fourier analysis of galaxy images developed recently by some of the authors (BAG). We thus provide a homogeneous set of values for the deprojection angles, a necessary first step for a number of statistical studies of disc galaxy properties.

We have also compared the results of BAG1 and BAG2 with data from RC3 and with estimates from large scale kinematics found in the literature, and find that our methods perform very well, except for cases where the galaxy is nearly face-on, where only the estimates from kinematics are reliable.

Our methods, as well as most of the other ones, rely on two assumptions, which, if found to be considerably wrong could introduce a significant bias. The first assumption is that the galactic discs are thin. Although corrections for thickness are possible, as e.g. advocated in the RC3, they are rather cumbersome, have to rely on statistical evaluations and can also introduce some bias. The second assumption is that discs are not oval. The question of noncircular disks is not an easy one to settle on a statistical basis, as indicated by recent work by Ryden (2004). If discs are indeed found to be oval, then the result of *all* deprojection methods will be flawed and several results on galactic discs will need to be revised. This will also have considerable implications on the density distribution in galactic halos. Discussing them, or divising new methods which can find the orientation parameters for such disk galaxies is beyond the scope of this paper.

From the discussion in the previous sections we can conclude that our two methods fare at least as well as other deprojection methods, but that the best approach is to compile results from different methods and use them all to obtain the values of the orientation parameters. Of course this is lengthy and will be difficult to do for large samples, such as the ones that can be obtained from the Sloan Digital Sky Survey.

Acknowledgements. We thank the referee, R. Buta for his helpful suggestions which improved considerably the present paper. We thank also Guiseppe Aronica for his help in the initial stages of the image cleaning. In preparing this paper we made extensive use of the CDS Strasbourg database. C.G.G. and C.B. acknowledge financial support by the Dirección de Investigación cintífica y Técnica under contract AYA2001-0762. We also thank the Picasso program of bilateral exchanges under contract HF2001-023, and support from the European Union under contract HPMT-CT-2001-00338.

References

Aguerri, J. A. L., Varela, A. M., Prieto, M., & Muñoz-Tuñón, C. 2000, AJ, 119, 1638
Allsopp, N. J. 1979, MNRAS, 188, 765
Alonso-Herrero, A., Simpson, Ch., Ward, M. J., & Wilson, A. S. 1998, ApJ, 495, 196
Barberà, C., Athanassoula, E., & García-Gómez, C. 2004, A&A, 415, 849
Baumgart, C. W., & Peterson, C. J. 1986, PASP, 98, 56
Becker, R., Mebold, U., Reif, K., & van Woerden, H. 1988, A&A, 203, 21
Bertola, F., Corsini, E. M.,Vega Beltrán, J. C., et al. 1999, ApJ, 519, 127
Blackman, C. P. 1979a, MNRAS, 186, 701
Blackman, C. P. 1979b, MNRAS, 186, 717
Blackman, C. P. 1979c, MNRAS, 188, 93
Blackman, C. P. 1980a, MNRAS, 190, 459
Blackman, C. P. 1980b, MNRAS, 191, 123
Blackman, C. P. 1981, MNRAS, 195, 451
Blackman, C. P. 1982, MNRAS, 198, 517
Blackman, C. P. 1983, MNRAS, 202, 379
Boroson, T. A. 1981, ApJS, 46, 177
Boroson, T. A., Strom, K. M., & Strom, S. E. 1983, ApJ, 274, 39
Bosma, A., Ekers, R. D., & Lequeux, J. 1977, A&A, 57, 97
Boselli, A., Lequeux, J., Contursi, A., et al. 1997, A&A, 324, 13
Broeils, A. H., & van Woerden, H. 1994, A&AS, 107, 129
Burbidge, E. M., & Burbidge, G. R. 1968, ApJ, 154, 857
Burbidge, E. M., Burbidge, G. R., & Prendergast, K. H. 1960, ApJ, 132, 654
Burbidge, E. M., Burbidge, G. R., & Prendergast, K. H. 1961, ApJ, 134, 874
Burbidge, E. M., Burbidge, G. R., & Prendergast, K. H. 1963, ApJ, 138, 375
Buta, R. 1987, ApJS, 64, 383
Buta, R., van Driel, W., Braine, J., et al. 1995, ApJ, 450, 593
Comte, G., Monnet, G., & Rosado, M. 1979, A&A, 72, 73
Considère, S., & Athanassoula, E. 1982, A&A, 111, 82
Considère, S., & Athanassoula, E. 1988, A&AS, 76, 365
Crocker, D. A., Baugus, P. D., & Buta, R. 1996, ApJS, 105, 353
Dahlem, M. 1992, A&A, 264, 483
Danver, C. G. 1942, Lund. Obs. Ann., No. 10
de Jong, R. S., & van der Kruit, P. C. 1994, A&AS, 106, 451
de Vaucouleurs, G., de Vaucouleurs, A., Corwin, H. G., et al. 1991, Third Reference Catalogue of Bright Galaxies (New York: Springer) (RC3)
Duval, M. F. 1983, IAUS, 100, 237
Duval, M. F., & Monnet, G. 1985, A&AS, 61, 141
England, M. N. 1989, ApJ, 344, 669
England, M. N., Gottesman, S. T., & Hunter, J. H. Jr. 1990, ApJ, 348, 456
Erwin, P., & Sparke, L. S. 2003, ApJS, 146, 299
Eskridge, P. B., Frogel, J. A., Pogge, R. W., et al. 2002, ApJS, 143, 73
Foster, P. A., & Nelson, A. H. 1985, MNRAS, 215, 555
Frei, Z., Guhathakurta, P., Gunn, J., & Tyson, J. A. 1996, AJ, 111, 174
Fridman, A. M., Khorizhii, O. V., Lyakhovich, V. V., et al. 2001, A&A, 371, 538
Gallimore, J. F., Baum, S. A., O'Dea, C. P., Pedlar, A., & Brinks, E. 1999, ApJ, 524, 684
García-Gómez, C., & Athanassoula, E. 1991, A&AS, 89, 159
García-Gómez, C., Athanassoula, E., & Barberá, C. 2002, A&A, 389, 68
Garrido, O., Marcelin, M., Amram, P., & Boulesteix, J. 2002, A&A, 387, 821
Grosbøl, P. J. 1980, in Photometry and Kinematics of Galaxies, 101
Grosbøl, P. J. 1985, A&AS, 60, 261
Grosbøl, P. J., & Patsis, P. A. 1998, A&A, 336, 840
Guhatakurta, P., van Gorkom, J. H., Kotany, C. G., & Balkowski, C. 1988, AJ, 96, 851
Haynes, M. P., Giovanelli, R., Chamaraux, P., et al. 1999, AJ, 117, 2093
Haynes, M. P., Jore, K. P., Barrett, E. A., Broelis, A. H., & Murray, B. M. 2000, AJ, 120, 703
Héraudeau, Ph., & Simien, F. 1996, A&AS, 118, 111
Higdon, J. L., Buta, R. J., & Purcell, G. B. 1998, AJ, 115, 80
Hunt, L. K., Malkan, M. A., Rush, B., et al. 1999, ApJS, 125, 349
Iye, M., Okamura, S., Hamabe, M., & Watanabe, M. 1982, ApJ, 256, 103
Irwin, J. A., English, J., & Sorathia, B. 1999, AJ, 117, 2102

Jarrett, T. H., Chester, T., Cutri, R., Schneider, S. E., & Huchra, J. P. 2003, AJ, 125, 525
Kaneko, N., Aoki, K., Kosugi, G., et al. 1997, AJ, 114, 94
Kenney, J. D. P., Carlstrom, J. E., & Young, J. S. 1993, ApJ, 418, 687
Kent, S. 1986, AJ, 91, 130
Kent, S. 1988, AJ, 96, 514
Kornreich, D. A., Hayes, M. P., Lovelace, R. V. E., & van Zee, L. 2000, AJ, 120, 139
Koopmann, R. A., Kenney, J. D. P., & Young, J. 2001, ApJS, 135, 125
Laine, S., & Gottesman, S. T. 1998, MNRAS, 297, 1052
Lindblad, P. A. B., Kristen, H., Joersaeter, S., & Hoegbom, J. 1997, A&A, 317, 36
Lu, N. Y. 1998, ApJ, 506, 673
Ma, J., Peng, Q.-H., & Gu, Q.-S. 1998, A&AS, 130, 449
Ma, J. 2001, ChJAA, 1, 395
Mathewson, D. S., & Ford, V. L. 1996, ApJS, 107, 97
Miller, B., & Hodge, P. W. 1991, BAAS, 23, 966
Moiseev, A. V. 2000, A&A, 363, 843
Möllenhoff, C., & Heidt, J. 2001, A&A, 368, 16
Moore, E. M., & Gottesman, S. T. 1998, MNRAS, 294, 353
Moriondo, G., Giovanardi, C., & Hunt, L. K. 1988, A&AS, 130, 81
Odewahn, S. C. 1991, AJ, 101, 829
Ohta, K., Hamabe, M., & Wakamatsu, K. 1990, ApJ, 357, 71
Okamura, S. 1978, PASJ, 30, 91
Oosterloo, T., & Shostak, S. 1993, A&AS, 99, 379
Pedlar, A., Howley, P., Axon, D. J., & Unger, S. W. 1992, MNRAS, 259, 369
Peletier, R. F., Knapen, J. H., Shlosman, I., et al. 1990, ApJS, 125, 409
Peletier, R. F., & Willner, S. P. 1991, ApJ, 382, 382
Pellet, A., & Simien, F. 1982, A&A, 106, 214
Pence, W. D., & Blackman, C. P. 1984a, MNRAS, 207, 9
Pence, W. D., & Blackman, C. P. 1984b, MNRAS, 210, 547
Peterson, C. J., & Huntley, J. M. 1980, ApJ, 242, 913
Phookun, B., Vogel, S. N., & Mundy, L. G. 1993, ApJ, 418, 113
Press, W. H., Teukolsky, S. A., Vetterling, W. H., & Flannery, B. P. 1992, Numerical Recipes (Cambridge Univ. Press.)
Prieto, M., Longley, D. P. T., Pérez, E., et al. 1992, A&AS, 93, 557
Prieto, M., Gottesman, S. T., Aguerri, J. A. L., & Varela, A. M. 1997, AJ, 114, 1413
Rhee, M.-H., & van Albada, T. S. 1996, A&AS, 115, 407
Rots, A. H. 1980, A&AS, 41, 189
Rubin, V. C., Burbidge, E. M., Burbidge, G. R., & Prendergast, K. H. 1964, ApJ, 140, 80
Rubin, V., Waterman, A. H., & Kenney, J. D. P. 1999, AJ, 118, 236
Ryden, B. S. ApJ, 601, 214
Ryder, S. D., Buta, R. J., Toledo, H., et al. 1996, ApJ, 460, 665
Ryder, S. D., Zasov, A. V., Sil'chenki, O. K., McIntyre, V. J., & Walsh, W. 1988, MNRAS, 293, 338
Sánchez-Portal, M., Díaz, A. I., Terlevich, R., et al. 2000, MNRAS, 312, 2
Schmitt, M., & Kinney, A. L. 2000, ApJS, 128, 479
Sperandio, M., Chincarini, G., Rampazzo, R., & de Souza, R. 1995, A&AS, 110, 279
Sofue, Y., Tomita, A., Honma, M., & Tutui, Y. 1999, PASJ, 51, 737
Stock, J. 1955, AJ, 60, 216
Swaters, R. A., & Balcells, M. 2002, A&A, 390, 863
Terndrup, D. M., Davies, R. L., Frogel, J. A., DePoy, D. L., & Wells, L. A. 1994, ApJ, 432, 518
Tully, B., Verheijen, M. A. W., Pierce, M. J., Huang, J. S., & Wainscoat, R. J. 1996, AJ, 112, 247
van der Kruit, P. C., & Shostak, G. S. 1982, A&A, 105, 351
van Moorsel, G. A., & Wells, D. C. 1985, AJ, 90, 1038
Verheijen, M. A. W., & Sancisi, R. 2001, A&A, 370, 765
Vollmer, B., Cayate, V., Boselli, A., Balkowski, C., & Duschl, W. J. 1999, A&A, 349, 411
Walsh, W., Staveley-Smith, L., & Oosterloo, T. 1997, AJ, 113, 1591
Warmels, R. H. 1998a, A&AS, 72, 427
Warmels, R. H. 1998b, A&AS, 73, 453
Weiner, B. J., Williams, T. B., van Gorkom, J. H., & Sellwood, J. A. 2001, ApJ, 546, 916
Wevers, B. M. H. R., van der Kruit, P. C., & Allen, R. J. 1986, A&AS, 66, 505
Zasov, A. V., & Kyazumov, G. A. 1981, Sov. Astron. Lett., 7, 73

2.4 Measuring bar strength using Fourier analysis of galaxy images

García-Gómez, C., Athanassoula, E., **Barberà, C.** and Bosma, A., Measuring bar strength using Fourier analysis of galaxy images. *Astronomy and Astrophysics* 601, A132 (2017) EDP Sciences. DOI:10.1051/0004-6361/201628830

A&A 601, A132 (2017)
DOI: 10.1051/0004-6361/201628830

Astronomy & Astrophysics

Measuring bar strength using Fourier analysis of galaxy images

C. Garcia-Gómez[1], E. Athanassoula[2], C. Barberà[1], and A. Bosma[2]

[1] DEIM, Campus Sescelades, Avd. dels Països Catalans 26, 43007 Tarragona, Spain
e-mail: carlos.barbera@urv.cat
[2] LAM (Laboratoire d'Astrophysique de Marseille), CNRS, Aix Marseille Université, UMR 7326, 13388 Marseille, France

Received 1 May 2016 / Accepted 13 February 2017

ABSTRACT

We present two methods for bar strength measurement on disc galaxies based on a two-dimensional Fourier analysis of their images. Our methods are able to recover the whole spiral structure of disc galaxies and are very robust when comparing the results from images obtained with different filters. In particular, these methods are capable of detecting small bars regardless of the filter used to obtain the galaxy image. Our relative measurements of bar strength show a good agreement with different bar indicators used in the literature. We use our methods to determine the general morphologies indicated in the Third Reference Catalog of Bright Galaxies (RC3 catalogue) classified as non-barred (SA), mildly barred (SAB), or barred (SB) galaxies. Our numerical indicators are in good agreement with the three galaxy populations estimated visually.

Key words. galaxies: structure – galaxies: spiral

1. Introduction

Most disc galaxies show bar components when studied in the near-infrared (NIR; Eskridge et al. 2000; Knapen et al. 2000; Grosbol et al. 2004; Marinova & Jogee 2007; Menéndez-Delmestre et al. 2007). The strength of the detected bar, however, varies within a very wide range, from very strong and long bars to small short bars or more massive ovals.

Intuitively, the difference between a weak and strong bar is clear, but there is no unique definition of bar strength. Thus, a bar is called strong if it includes a large portion of light (or mass) of a galaxy, but sometimes longitude and thickness of the bar is also considered. But, is a very thin short bar stronger or weaker than a long massive oval? The answer is not unique and depends on the definition used.

Different attempts to measure the bar strength can be found in the literature. Elmegreen & Elmegreen (1985) and Regan & Elmegreen (1997) used the ratio between the peak surface brightness in the bar to the minimum surface brightness in the interbar region. Martin (1995), Martinet & Friedli (1997), and Chapelon et al. (1999) used the axis ratio and bar length. Rozas et al. (1998) used the ratio of the flux inside the bar to the flux outside excluding the bulge. Aguerri et al. (1998) and Aguerri et al. (2000) used the ratio between the amplitudes of the Fourier $m = 2$ and $m = 0$ components. Seigar & James (1998) used a parameter called the "equivalent angle" defined as the angle subtended at the centre of the galaxy by a sector of the underlying disc and bulge that emits as much light as the bar component within the same radial limits. Abraham & Merrifield (2000) introduced the parameter

$$f_{\rm bar} = \frac{2}{\pi}\left[\arctan\left(\frac{b}{a}\right)_{\rm bar}^{-1/2} - \arctan\left(\frac{b}{a}\right)_{\rm bar}^{+1/2}\right], \quad (1)$$

where $(b/a)_{\rm bar}$ is the intrinsic axial ratio of the bar that is obtained from the deprojected image or calculated from its apparent axial ratio and inclination of the galaxy (e.g. Abraham et al. 1999). This parameter is closely related to a morphologist's subjective notion of bar strength and maps the bar strength into a closed interval from zero to unity. A non-barred galaxy has a value of $f_{\rm bar} = 0$, while an ideal galaxy with a bar of infinite strength has a value of $f_{\rm bar} = 1$. Galaxies with a value of $f_{\rm bar} > 0.11$ correspond to systems in which $(b/a)^2 < 0.5$ and should be classified as barred, as shown in Abraham et al. (1999). This parameter was used by Whyte et al. (2002) to study the bar distribution in the Ohio State University Bright Spiral Galaxy Survey (hereafter OSU) sample of bright galaxies Eskridge et al. (2000) and showed some evidence of a bi-modality in the distribution that would suggest that barred and unbarred galaxies are not the extreme of a single distribution. Aguerri (1999) used the parameter $\epsilon_b = 10(1-b/a)$ as a measure of the bar strength and showed that there is a strong correlation between bar strength and star formation activity; Shlosman et al. (2000) also used this parameter to show that in active galaxies there is a deficiency of "thin bars" (i.e. bars with high ellipticity). Marinova & Jogee (2007) have recently used this parameter to study the distribution of barred galaxies in the OSU sample. Using this parameter, these authors do not find evidence of a bimodal distribution, and note that bar fraction and bar strength do not seem to depend on Hubble type. They also note that a significant portion of unbarred galaxies in the Third Reference Catalog of Bright Galaxies (RC3 catalogue) by de Vaucouleurs et al. (1991) turn out to be barred when studied in H band images. This higher portion of barred galaxies in the infrared had already been referred to by Eskridge et al. (2000) on visual inspection.

Using numerical simulations of the dynamics of disc galaxies, Combes & Sanders (1981) introduced the bar torque as measured by the $Q_{\rm b}$ parameter, which is a measure of the relative amplitude of the second harmonic over the axisymmetric force. Buta & Block (2001) and Laurikainen & Salo (2002) used this bar torque $Q_{\rm b}$ as a measure of bar strength. This parameter is defined as the maximum value of the ratio of the tangential force to the mean axisymmetric radial force, i.e. it is a

A&A 601, A132 (2017)

local criterion. When using images in the K band, Block et al. (2001) noted that this parameter correlates only weakly with the optical bar type as listed in the Revised Shapley Ames by Sandage & Tammann (1981) and de Vaucouleurs (RC3) catalogues. This could be because some bars with strong bulges have their azimuthal forces diluted by the average radial force exerted by strong bulges. Block et al. (2002), Laurikainen et al. (2004), and Buta et al. (2004) have calculated this parameter for the galaxy images of the OSU sample. This parameter correlates well with deprojected bar ellipticities, even though the calculation of this parameter requires some model assumptions on the vertical density distribution of the discs (Laurikainen & Salo 2002). Such a correlation is to be expected as the shape of the bar is related to the shape of the orbits supporting it and these should depend on the global force field. Buta et al. (2004) also showed that the Q_b parameter correlates well with the f_{bar} parameter derived by Whyte et al. (2002) for the OSU sample.

Nevertheless, the Q_b parameter can be influenced by the torques exerted by spiral arms. Buta et al. (2003) introduced a method that separates the influence of the spiral arms from that of the bar. This methodology was based on the previous analysis of some barred galaxies by Ohta et al. (1990). This method uses the assumption that the distribution of the Fourier amplitudes as a function of radius are symmetric for each component. The main component is thus identified in the even harmonics and subtracted from the galaxy image, so that the bar strength can be calculated separately from that of the arm. In this case, however, strong symmetric arms can couple nonlinearly with the bar component and a direct substraction of the arm component can give an unreliable value of Q_b. Buta et al. (2005) applied this method to the galaxy images in the OSU sample and found that the distribution of bar strengths declines smoothly with increasing Q_b, where more than 40% of the sample have $Q_b \leq 0.1$. The Q_b parameter can also be influenced by the existence of a classical bulge. For this reason, Durbala et al. (2009) first subtract this bulge contribution from the image before calculating the numerical value of the Q_b parameter.

Finally, Speltincx et al. (2008) applied this parameter to the OSU sample to compare the bar strengths in the B and H filters and concluded that the ratio of bar strengths in the two filters is on average $Q_{B/H} = 1.25$ and that this is mainly due to the reduced bulge dilution of the radial forces in the B band. They showed also that this parameter could be used with confidence to quantify bar strength at high redshifts.

Other bar strength definitions can be obtained from reasonable combinations of the bar strength attributes, i.e. its length, axial ratio, and mass. In some simplifying cases, only one of these attributes is used, which leads to clear-cut measuring systems, which, nevertheless, do not take into account all the bar properties. This is not, however, necessarily a disadvantage, since the right mix of attributes in any strength formula is unknown. In fact, there is no right or best strength criterion. Some criteria are more adequate than others for a given application, while other criteria may be more suitable for another particular case. Here we introduce and test some new criteria for the bar strength, all of which take the global (as opposed to local) strength of the bar into account. They are all based on the Fourier analysis of galaxy images and are introduced in the following sections.

This paper is organised as follows: Sect. 2 gives a general introduction to the two-dimensional Fourier analysis technique and, as an example, applies it to a disc galaxy with a well-developed global bi-symmetric pattern. In Sect. 3 we present the sample and the new measures of bar strength. Section 4 applies this technique to model barred galaxies and to some representative examples of galaxies. Section 5 compares these measures between them and discusses the effect of wavelength on the bar strength. In Sect. 6 we compare our values to those previously used and in Sect. 7 we make a global comparison of the values measured by our indicators with the classification as non-barred (SA), mildly barred (SAB), or barred (SB) galaxies according to the RC3 catalogue. We conclude in Sect. 8.

2. Fourier analysis technique

The two-dimensional fast Fourier transform (FFT) method, which analyses the spiral structure of disc galaxies, was first introduced by Considère & Athanassoula (1982) for the HII region distribution and, independently, by Iye et al. (1982) for a photometric image of the galaxy NGC 4254. Considère & Athanassoula (1988) used it for a sample of images of bright spiral galaxies. It was later fully developed by García-Gómez & Athanassoula (1991), who introduced the possibility of dealing with the whole complexity of Fourier spectra, separating all the signals present in each spectrum. In this paper, we apply this method to galaxy images and, in this section, start by summarizing the main points. More information can be found in Barberà et al. (2004), and García-Gómez et al. (1991).

We use the galaxy images in the bright galaxy sample of Frei et al. (1996) and in the OSU sample. As we are only interested in the relative intensities, we use the uncalibrated images, first removing foreground stars and subtracting the sky background. We then centre the images on the pixel with the highest density. The next step is to deproject the galaxy image $I_p(r,\theta)$ using the position angles (hereafter PA) and inclination angles (hereafter IA) of each galaxy to obtain the light distribution of the galaxy on its equatorial plane $I(r,\theta)$. The step of deprojecting galaxy images is a crucial phase of the whole process because a bad deprojection contributes to the Fourier spectra with spurious signals. The deprojection of the galaxy images has been treated in detail separately for the Frei and OSU sample in the papers by Barberà et al. (2004), and García-Gómez et al. (1991), respectively, but we briefly describe the process for the sake of completeness. Basically, the Fourier deprojection method aims to minimise the relative power of the component associated with an oval distortion. Any oval component gives a strong signal in the bysymmetric component (i.e. a symmetry after a rotation of π degrees). If we choose a bad pair of deprojecting angles (PA, IA) the galaxy disc looks oval and, hence, we get a stronger bi-symmetric signal in the Fourier spectrum. Thus, we can obtain a good guess of the deprojection angles by comparing the power in this component over the rest of the components of the spectrum.

Given the deprojected image of the galaxy $I(u,\theta)$, where $u = \ln(r)$, we calculate the two-dimensional Fourier transform defined as

$$A(p,m) = \int_{u_{\min}}^{u_{\max}} \int_0^{2\pi} I(u,\theta) e^{i(pu+m\theta)}\, d\theta du. \quad (2)$$

The Fourier transform is a very convenient tool for the analysis of the spiral structure as we decompose the galaxy image using the orthogonal basis of logarithmic spirals. Spiral arms are known to follow this function approximately (Danver 1942; Kennicutt 1981; Ma 2001). In Eq. (2), p corresponds to the radial frequency and m to the azimuthal frequency. While p is a real variable, m only takes integer values. The spectra obtained with $m = 1$ correspond to one-armed spirals, or asymmetries

within the galaxy image. The $m = 2$ spectra correspond to bi-symmetric signals, i.e. signals with a periodicity of π radians. These signals are associated with the common two-armed spirals, which look the same after a rotation by π radians around the galaxy centre, or to a bar. Similarly, the $m = 3$ spectrum are associated with signals corresponding to three-armed spirals and so on for the spectrum of $m = 4$ and higher azimuthal frequencies. The radial frequency p is related to the pitch angle i of the spiral arm via the relation

$$p = -\frac{m}{\tan(i)}. \tag{3}$$

In order to obtain a good resolution in the frequency space, we fix the range of radial frequencies, $(-p_{\max}, p_{\max})$, by setting $p_{\max} = 128$ and with a rate of sampling of $\delta p = 0.125$, giving a total of $N = 2^{11}$ samples in the Fourier transform, which is very adequate for our purposes. The value of δu is fixed to the value of the maximum radial frequency through the expression

$$\delta u = \frac{2\pi}{N\delta p} = \frac{\pi}{p_{\max}}. \tag{4}$$

Then, the range of radial frequencies is linked to the range of u values $(-u_{\max}, u_{\max})$ by the relation

$$u_{\max} = \frac{N\,\delta u}{2} = \frac{\pi N}{2p_{\max}}. \tag{5}$$

In order to avoid aliasing (Gibbs phenomenon) we taper the values in the central part of the galaxy by the function

$$F = \begin{cases} \sin^2(\frac{\pi}{2}\frac{r}{r_{\min}}): & r < r_{\min} \\ 1: & r \geq r_{\min}. \end{cases} \tag{6}$$

Here the length $r_{\min}$ depends on the structure of the galaxy and is obtained for each galaxy image separately after visual inspection. This $r_{\min}$ was selected as a fraction of the radius at 25th magnitude ($R25$) of each galaxy. When this selection was made we calculated the galaxy spectra and ensured that the spectra of all m values were not dominated by the signal of the central bulge. Bulges are not perfectly round and symmetric and, if the value of the $r_{\min}$ is selected too small, bulge residuals dominate all the spectra through higher harmonics. Thus, an asymmetric bulge gives strong signals in the $m = 1$, while a symmetric bulge entirely dominates the $m = 2$ component. These signals also dominate the corresponding associated higher harmonics. If such very bright structures are not tapered out, they can dominate the Fourier transform and hide the contribution of the remaining spiral components. This procedure is described in Fig. 1, where we show the effect of the selection of the value of $r_{\min}$ on the spectra of the galaxy NGC 4303. When using a value that is 20% lower than the value actually selected, the $m = 1$ spectrum is dominated by a strong signal in the central part, centred around values of $p = 0$. On the other hand, when using the selected value of $r_{\min}$ the spectra are dominated by the signals in the $m = 2$ spectrum, i.e. the central oval of this galaxy and the arms. This signal does not change appreciably when using a value of $r_{\min}$ 20% higher than the value actually used.

Following the above described procedure, we obtain a series of spectra for each galaxy image: one for each value of the azimuthal frequency m. Each of these spectra is combination of signals corresponding to spirals with the same multiplicity but with different pitch angles, each associated with different values of the radial frequency p.

In Fig. 2, we show the modulus of the $m = 2$ Fourier spectrum of the galaxy NGC 4535 obtained from an r band image,

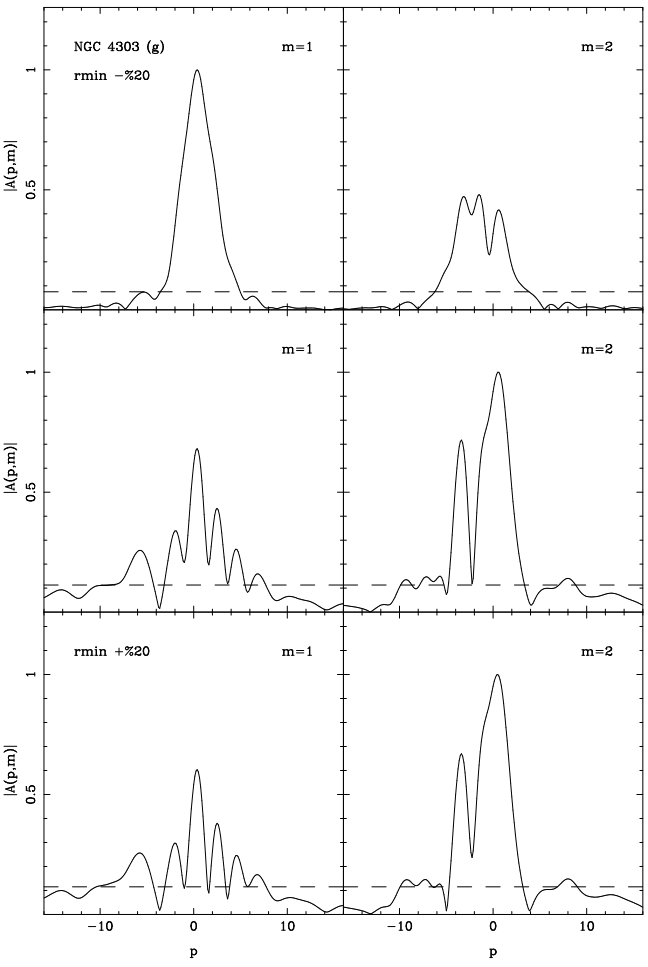

Fig. 1. *Upper panel*: modulus of the $m = 1$ and $m = 2$ Fourier spectra obtained from a g band image of the galaxy NGC 4303 using a $r_{\min}$ value lower by a 20%. *Middle panel*: same spectra obtained the right value of $r_{\min}$. *Lower panel*: spectra obtained using a value of $r_{\min}$ 20% higher.

and we plot normalised amplitudes for the spectra. We are only interested in the relative amplitudes of the signals and this means that the galaxy images do not need to be calibrated when comparing the signals of each galaxy. As can be seen in Fig. 2, the different spectra of each galaxy can be very complex. This means that many different signals contribute to each spectrum and, in order to recover the galaxy image properly, we need to unravel this complexity. We do so by fitting the modulus of each spectrum by a sum of Gaussians as follows:

$$|A(p,m)| = \sum_{j=1}^{N_g} C_j \exp\left(-\frac{(p-p_j)^2}{2\sigma_j^2}\right). \tag{7}$$

In this relation, p_j represents the central frequency of the Gaussian, σ_j its dispersion, and C_j its amplitude. The number of Gaussians used in each fit, N_g, depends on the complexity of the spectrum and thus varies from spectrum to spectrum and from galaxy to galaxy. In the upper panel of Fig. 2 we show, as a typical case, the result of this fitting process to the $m = 2$ spectrum of the image in the r band of the galaxy NGC 4535. We have used a total of five Gaussians for this particular fit and the fit obtained is excellent; the difference between the modulus

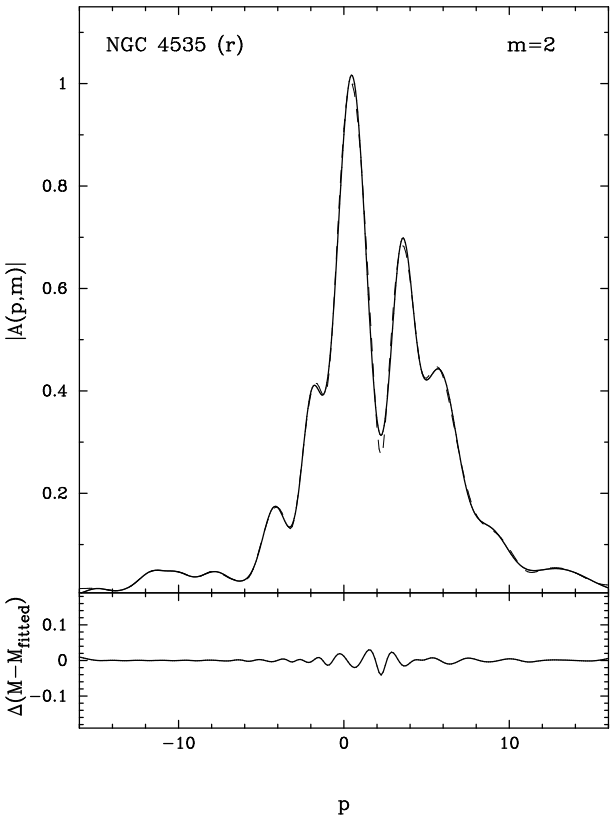

Fig. 2. *Upper panel*: modulus of the $m = 2$ Fourier spectrum obtained from an r band image of the galaxy NGC 4535. This modulus has considerable substructure, due to the presence of many components. We superimpose using a dotted line the Gaussian fit, obtained as described in the text. *Lower panel*: difference between the value of the $m = 2$ modulus and the Gaussian fit. This fit, whose quality is typical for our sample, reproduces very well the $m = 2$ modulus, in spite of the latter's complexity.

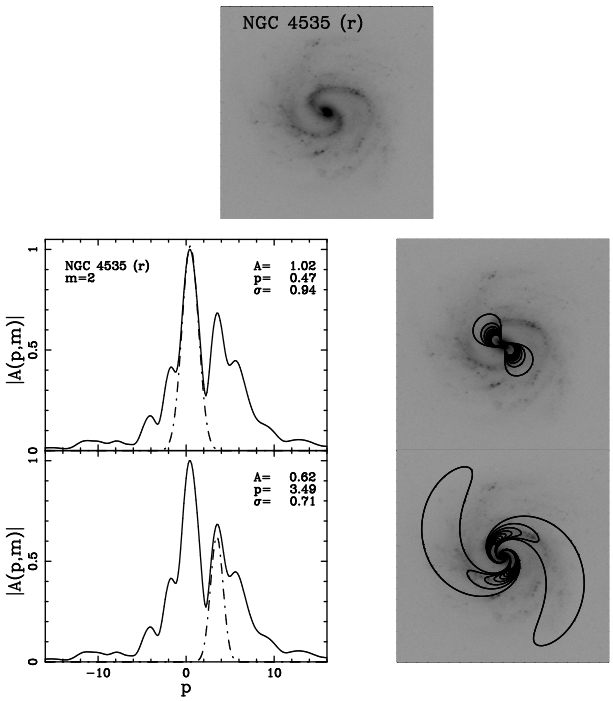

Fig. 3. Principal $m = 2$ components for NGC 4535. The *upper panel* shows the deprojected galaxy viewed in the r band. The *second and third rows* of panels concern the bar and the main spiral components, respectively. In the *left* we give the modules of the selected components (dot-dashed lines) and the total $m = 2$ modulus (solid line). In the *right-hand panels* we superpose the density of the component on the galaxy image. It is clear that these two components alone give a reasonable but not perfect reproduction of the main features of the galaxy. For a more detailed comparison, more components should be used.

and the fit is hardly visible over most of the range of the radial frequencies p. The small difference between the modulus of the spectrum and the Gaussian fit can be measured in the lower panel of Fig. 2, where we show the differences between the two values as a function of radial frequency. The fits for other values of the azimuthal frequencies or for other images of different galaxies are of similar quality and do not depend on the passband used.

Since we assume that each of these Gaussians corresponds to a different signal and that all signals add up to constitute a particular spectrum, we can recover their contribution to the galaxy image by simply Fourier transforming back each of the signals separately. The spectrum of a component must be a complex function as is the case for the spectrum of any m component of the galaxy image, i.e.

$$A(p, m) = \mid A(p, m) \mid \mathrm{e}^{i\phi(p,m)}. \tag{8}$$

For each of the fitted Gaussian components, given a fixed value of m, we keep the same complex phase as in the transformed spectrum. Then the fitted spectra in the complex domain, can be expressed by

$$A(p, m) = \sum_{j=1}^{N_g} C_j \exp\left(\frac{(p - p_j)^2}{2\sigma_j^2}\right) \mathrm{e}^{i\phi(p,m)}. \tag{9}$$

Thus, the density of each component can be recovered through the following inverse Fourier transform:

$$D_{jm}(u, \theta) = \frac{1}{4\pi^2 \mathrm{e}^{2u}} \int_{-\infty}^{\infty} C_j \exp\left(\frac{-(p - p_j)^2}{2\sigma_j^2}\right) \mathrm{e}^{\mathrm{i}\phi(p,m)} \mathrm{e}^{-\mathrm{i}(pu+m\theta)} \, \mathrm{d}p, \tag{10}$$

where $D_{jm}(u, \theta)$ is the density distribution corresponding to the jth Gaussian component of the azimuthal frequency m. In the second and third rows of panels in Fig. 3 we show the result of the inverse transformation of the two highest components in the $m = 2$ spectrum of the r band image of the galaxy NGC 4535. The major peak corresponds to the bar component, while the second highest peak gives a two-armed structure. It can be noted, from this figure, that this component gives a general outline of the main two-armed spiral, but this is far from perfect. This is because the two-armed spiral seen in this particular image is the result of the superposition of all the components in this spectrum. This shows that to recover the details of a galaxy image, it is necessary to use a decomposition of the spectra including all the main signals. This procedure can be used to recover and analyse all the details of the spiral structure of a galaxy image. In this paper we concentrate exclusively in the bar signals and we leave the detailed analysis of the spiral structure for a forthcoming paper.

3. Samples and bar strength measures

3.1. The samples

In this paper we work with two galaxy samples: the Frei sample (Frei et al. 1996) and the Ohio State University Bright Spiral Galaxy Survey (OSU; Eskridge et al. 2002). From these samples we only kept galaxies that are less inclined than 65°, do not have very luminous foreground stars projected on the image, and without strong irregularities. Thus we get 25 spiral galaxies in the g, r, and i passbands and 35 galaxies observed in the B_J and R passbands from the Frei sample. For their deprojection we use the values found in Barberà et al. (2004).

The OSU provides deep, photometrically non-calibrated images of a complete magnitude limited sample of nearly 200 bright, nearby, well-resolved spirals. This survey selects galaxies with Hubble type S0/a or later with a magnitude in the blue $B < 12$ and a diameter $D < 6$ arcmin. For a number of these all colours $BVRJHK$ are available, while for a few some bands are still missing. From the OSU Early Data Release, we have taken only those galaxies with galaxy type $2 \leq t \leq 7$, which are less inclined than 65° and for which we have position and inclination angles calculated with the same method as for the Frei sample (García-Gómez & Athanassoula 1991). This gives a total of 128 galaxies for which we analyse the B and H images. All of these galaxies have already been classified as SA, SAB, and SB in the RC3 catalogue. Thus, in this paper, we use this standard classification for the barred galaxies of our sample.

We analysed all the images following the procedure outlined in Sect. 2. We also obtained the relevant spectra and decomposed the modulus of each single spectrum in its Gaussian components. Then, we were able to obtain all the spiral components in each of the m Fourier spectra for all the galaxy images. This gives a wealth of information on the spiral structure for each galaxy. In Table 1 we show all the components in the $m = 1, 2$, and 3 spectra that are within the 25% of the maximum signal for all the example galaxies in this paper. We computed all the components in the following m spectra: $m = 1, 2, 3, 4, 6, 8$ for all the galaxies; we plan to use this information to analyse the spiral structure of disc galaxies in a forthcoming paper. In Table 1, Col. 1 gives the NGC galaxy name, Col. 2 the filter used in the image, Col. 3 the corresponding m Fourier spectra, and in Cols. 4–6, we give the parameters of the Gaussian components, namely their centre, peaks, and dispersion. The bar components are showed in boldface, as their discussion is the main objective of this paper.

3.2. Measures of the bar strength

We understand intuitively that stronger bars have more prominent bar components (i.e. bar Gaussians in the spectra). We have several ways of quantifying this fact using the measurements obtained with the FFT transform technique. We can choose to use the amplitude of the fitted Gaussian, its integrated modulus, or its power to characterise the bar strength. We use uncalibrated galaxy images and some caution must be taken when comparing the signals from different galaxies.

We examine the $m = 2$ spectrum of each galaxy image to see whether there is a bar component or not. Such a component would necessarily have a peak within the range $-1.0 \leq p \leq 1.0$. The bar component, however, does not need to be the strongest signal in the $m = 2$ spectrum. So, we define the bar component as the highest signal within this particular range. We designate its amplitude or central peak by C_B and its radial frequency by p_B while its dispersion is defined by σ_B.

For each bar signal we then define the value of the bar modulus, hereafter B_M,

$$B_M = C_B \int_{-p_{max}}^{p_{max}} \exp\left(-\frac{(p-p_B)^2}{2\sigma_B^2}\right) dp, \tag{11}$$

and similarly, we define the bar power as the value

$$B_P = C_B^2 \int_{-p_{max}}^{p_{max}} \exp\left(-\frac{(p-p_B)^2}{\sigma_B^2}\right)^2 dp. \tag{12}$$

Either of these two values, B_M or B_P, can be used to characterise the bar signal.

To avoid problems with non-calibrated images. All images are normalised to their maximum brightness, this is, the intensity value of the brightest pixel after cleaning up the images from all foreground stars and bad pixels. For all the galaxies in our sample this centring process is critical. If the images were not centred in this brightest pixel, we obtained a spurious contribution to the $m = 1$ component clearly visible in the spectrum.

In this way, the B_M and B_P values can be used to compare bars in different galaxies. With this normalisation, these values are a relative measure of the importance of the bar signal within each galaxy. These parameters can also be further normalised to other galaxy properties, as are the power or the modulus in the $m = 0$ or $m = 2$ spectrum, or we can also use the sum of all the spectra combined. The $m = 0$ component corresponds to the underlying galaxy disc. The normalisation provide measures of the bar that can be helpful to understand the bar strength in relation to other galaxy components and can also be used to relate the bar signals from different galaxies. We have to be careful with these normalisations, however, as a poorly defined disc in a galaxy image can considerably bias the value of some parameters for a particular galaxy when using their $m = 0$ component in the normalisations.

Thus, the bar modulus can be normalised to the total modulus of the axisymmetric component ($m = 0$, B_{M0}), the total modulus in the bi-symmetric component ($m = 2$, B_{M2}), or to the total modulus of all the components combined ($B_{M\Sigma}$), to obtain the bar parameters defined as in the following expressions:

$$B_{M0} = \frac{C_B \int_{-p_{max}}^{p_{max}} \exp\left(-\frac{(p-p_B)^2}{2\sigma_B^2}\right) dp}{\int_{-p_{max}}^{p_{max}} |A(p,0)|\, dp} \tag{13}$$

$$B_{M2} = \frac{C_B \int_{-p_{max}}^{p_{max}} \exp\left(-\frac{(p-p_B)^2}{2\sigma_B^2}\right) dp}{\int_{-p_{max}}^{p_{max}} |A(p,2)|\, dp} \tag{14}$$

$$B_{M\Sigma} = \frac{C_B \int_{-p_{max}}^{p_{max}} \exp\left(-\frac{(p-p_B)^2}{2\sigma_B^2}\right) dp}{\sum \int_{-p_{max}}^{p_{max}} |A(p,m)|\, dp} \tag{15}$$

and similarly the expressions:

$$B_{P0} = \frac{C_B \int_{-p_{max}}^{p_{max}} \exp\left(-\frac{(p-p_B)^2}{2\sigma_B^2}\right) dp}{\int_{-p_{max}}^{p_{max}} |A(p,0)|^2\, dp} \tag{16}$$

$$B_{P2} = \frac{C_B \int_{-p_{max}}^{p_{max}} \exp\left(-\frac{(p-p_B)^2}{2\sigma_B^2}\right) dp}{\int_{-p_{max}}^{p_{max}} |A(p,2)|^2\, dp} \tag{17}$$

$$B_{P\Sigma} = \frac{C_B \int_{-p_{max}}^{p_{max}} \exp\left(-\frac{(p-p_B)^2}{2\sigma_B^2}\right) dp}{\sum \int_{-p_{max}}^{p_{max}} |A(p,m)|^2\, dp} \tag{18}$$

A&A 601, A132 (2017)

Table 1. Parameters of the Gaussian components of the Fourier decomposition for the galaxies used in the text.

NGC	Filter	m	Centre	Peak	Disp
0210	*B*	1	1.570	0.375	1.184
		2	**0.661**	**0.992**	**1.278**
			–2.287	0.384	1.022
0210	*H*	1	0.172	0.495	1.334
		2	**0.426**	**0.980**	**1.394**
			–2.140	0.355	1.063
1073	*B*	1	1.030	0.367	1.087
			–2.378	0.264	1.481
		2	**0.005**	**1.004**	**1.227**
1073	*H*	2	**0.010**	**1.013**	**1.325**
4303	*B*	1	–1.316	0.925	1.102
			1.368	0.701	0.694
			0.112	0.400	0.629
			–3.603	0.377	0.623
			3.184	0.302	0.577
		2	**0.802**	**0.521**	**0.733**
			–3.607	0.385	0.684
			–1.501	0.341	0.416
4303	*H*	1	–0.045	0.981	1.491
		2	**0.692**	**0.613**	**0.906**
			–2.120	0.248	0.487
4303	*g*	1	0.161	0.972	0.926
			2.416	0.612	0.831
			–2.064	0.451	0.776
			4.417	0.310	0.581
		2	**0.766**	**0.792**	**1.033**
			–3.553	0.774	0.753
			–1.463	0.428	0.413
			–5.695	0.292	0.758
		3	–1.533	0.276	0.736
			–3.418	0.254	0.516
			–5.479	0.245	0.568
4303	*i*	1	–1.211	0.588	1.125
			0.460	0.375	1.212
			1.477	0.374	0.771
			–3.719	0.321	0.805
			3.536	0.306	0.708
		2	**0.425**	**0.986**	**1.188**
4303	*r*	1	–0.376	0.968	1.595
			2.052	0.437	0.936
			4.042	0.325	0.669
			–3.622	0.253	0.822
		2	**-0.068**	**0.641**	**0.960**
			–3.477	0.292	0.705
4535	*g*	1	–0.538	0.449	1.036
		2	**0.488**	**1.010**	**0.969**
			3.312	0.627	0.719
			–2.309	0.456	0.681
			–4.125	0.305	0.789
			5.811	0.289	0.541
4535	*i*	1	–0.329	0.967	1.120
			1.789	0.385	0.922
			–2.385	0.261	0.742
		2	**0.468**	**0.998**	**0.914**
			3.356	0.423	0.686
			–2.190	0.287	0.696
4535	*r*	1	–0.270	0.498	1.899
			0.997	0.473	1.204
		2	**0.626**	**0.899**	**0.928**
			3.417	0.511	0.664
			–2.076	0.345	0.563
			5.880	0.225	0.594
5247	*B*	1	0.256	1.012	1.289
			–2.746	0.489	0.848
			5.443	0.270	1.168
		2	**-2.991**	**0.949**	**0.863**
			–1.061	0.761	0.629
			0.999	0.384	0.799
			2.599	0.292	0.786
		3	–2.275	0.547	1.045
5247	*H*	1	–0.392	0.991	1.157
		2	**-0.875**	**0.497**	**0.640**
			–3.454	0.469	0.708
			2.509	0.262	1.231

for the case of the power of the components. We note that $\sum$ means that $m = 0, 1, 2, 3, 4, 6, 8$. We normally exclude the $m = 5$ component, which is usually a flat component, from our analysis.

4. Application to model bars and to a few fiducial barred galaxies

4.1. Application to model bars

In order to better understand our results, we first applied our method to model galaxies, composed simply by adding an exponential disc and a Ferrer two-dimensional bar. The density distribution of the latter is given by the expression

$$\rho(x,y) = \begin{cases} (1-d(x,y))^n: & d(x,y) < 1 \\ 0: & d(x,y) \geq 1 \end{cases} \quad (19)$$

where

$$d(x,y) = \left(\frac{x}{a}\right)^2 + \left(\frac{y}{b}\right)^2, \quad (20)$$

a and b are the major and minor axes of the bar and n is the concentration index describing how fast the density decreases with

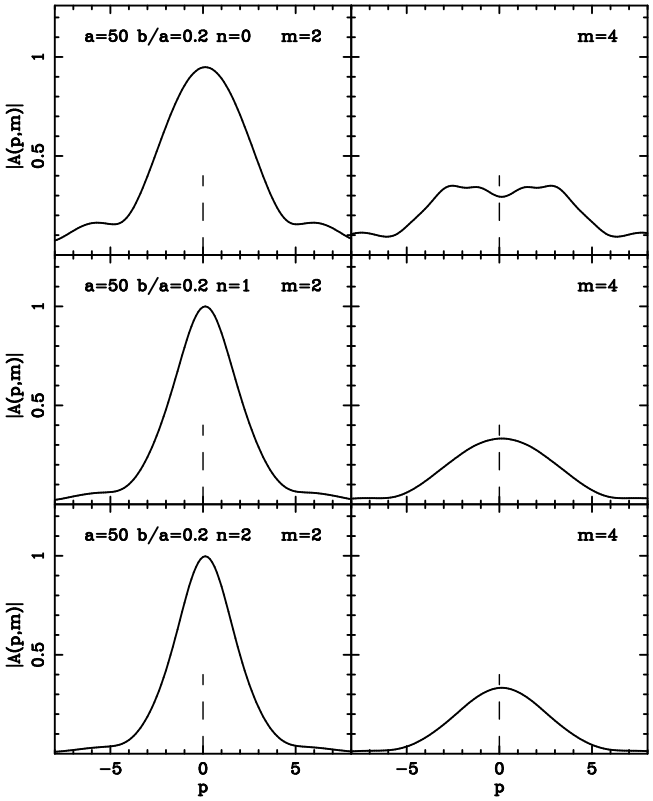

Fig. 4. Spectra from the idealised barred galaxy images with different concentration indexes and an axis ratio of 0.2. The results for the $m = 2$ components are given in the *left-hand panels* and for the $m = 4$ in the *right-hand panels*. A dashed vertical line is placed at $p = 0$. The numerical values of a, b, and n are given in the upper left corner of *the left panels*. The three signals are normalised to the maximum of the three values.

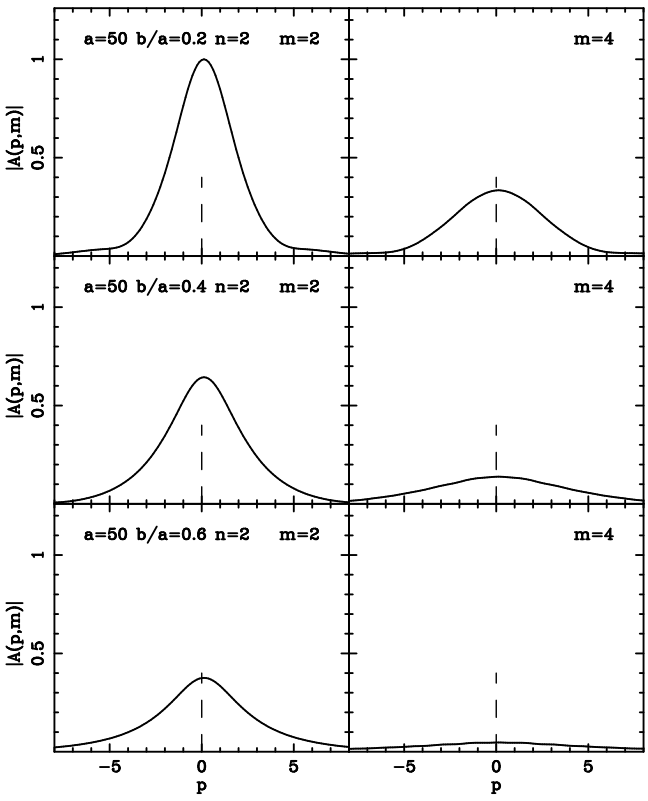

Fig. 5. Spectra from the idealised barred galaxy images with different bar axis ratio and an $n = 2$ concentration index. The results for the $m = 2$ components are given in the *left-hand panels* and the $m = 4$ in the *right-hand panels*. A dashed vertical line is placed at $p = 0$. The three signals are normalised to the maximum of the three values.

increasing distance from the centre. We always use an exponential disc with a scale length of 20 units, while we change at will the values of the axes ratio a/b and the concentration index n.

Figures 4 and 5 show the $m = 2$ and $m = 4$ spectra of different idealised bars embedded within an exponential disc. In Fig. 4 we show the effect of different values of the concentration index n on the shape of the bar signal. The signals are normalised to the maximum fiducial value of the three units to facilitate the comparison. We can see that higher values of n give bar signals having narrower profiles, but similar strengths. The secondary maxima that appear at both sides of the bar signal are entirely artificial because the combined intensity of the artificial bar and disc has a jump at the ends of the bar. In all cases, however, the modulus of the main components in the $m = 2$ spectrum has a bell shape and is centred at $p = 0$. The effect of increasing the bar axial ratio while keeping the bar concentration index constant is shown in Fig. 5. We can see in this figure that round bars give rounder signals, i.e. with larger dispersion and more extended wings. Also, as the bar becomes rounder, the relative importance of the signals is lower. This kind of signal can be easily lost when combined with strong arms. Thus, the clean separation of signals is an important step in the study of the spiral structure of galaxies. Strong bars, on the other hand, are better represented by model bars with a concentration index that is larger or equal to $n = 2$ and axis ratios with values $(b/a) < 0.5$.

Of course, these cases are very idealised. Owing to various irregularities or asymmetries, galactic bars do not necessarily give signals that are symmetric with respect to their maximum. The modulus of the spectrum then requires more components to be properly described. This was the case for NGC 4535, in Fig. 3, where the main spiral was not entirely logarithmic and more than the single maximum component was necessary to give a proper description of the $m = 2$ spectrum. Moreover, spirals often start off from the end of the bar, so the location of the maximum may be somewhat offset from $p = 0$. The Gaussian corresponding to the bar component is hereafter called the bar Gaussian, for brevity.

4.2. Application to a few fiducial barred galaxies

In this paper we focus on the detection and classification of bar structures in galaxy discs. The standard galaxy classification of barred galaxies used by de Vaucouleurs (1963) distinguishes three families of disc galaxies: SA, SB, and SAB. Galaxies in the SA family have no bars, SB galaxies have a clear bar component, while SAB galaxies are intermediate. In practice, this means that the SAB family is a mixed bag. It contains galaxies with fat ovals, galaxies with short bars, or simply unclear cases. In the more recent RC3 catalogue by de Vaucouleurs et al. (1991), this galaxy classification is maintained and it will be followed in this paper. In this section we apply our technique to four disc galaxies with different morphologies for the bar structures that have been classified accordingly in the RC3 catalogue. This allow us to check whether our method based on the analysis of the Fourier spectra can be used to identify bars and measure bar strengths in

A&A 601, A132 (2017)

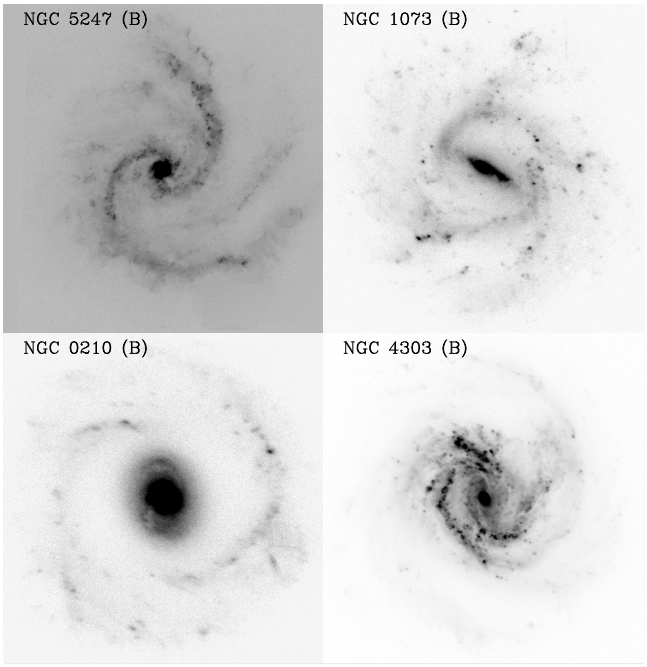

Fig. 6. Blue images of the four analysed galaxies: NGC 5247 (*upper left*), NGC 1073 (*upper right*), NGC 210 (*lower left*) and NGC 4303 (*lower right*).

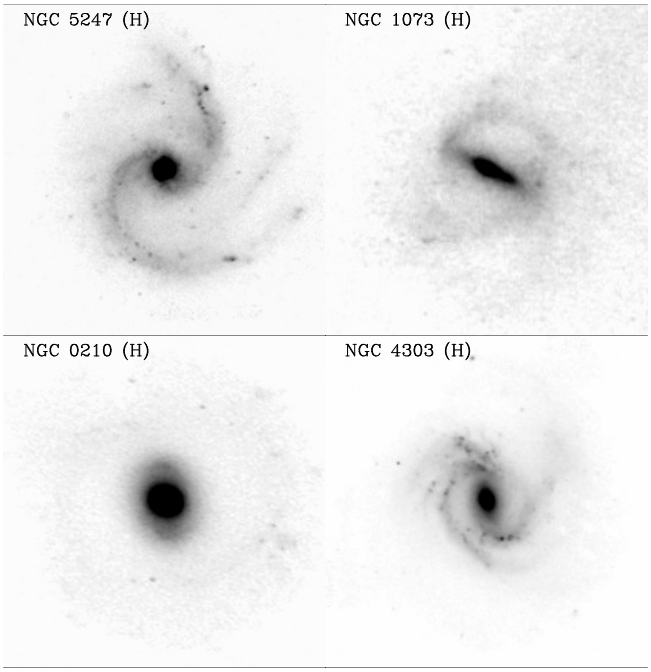

Fig. 7. Near-infrared images of the four galaxies: NGC 5247 (*upper left*), NGC 1073 (*upper right*), NGC 210 (*lower left*) and NGC 4303 (*lower right*).

disc galaxies. We show images in the blue passband of these four galaxies in Fig. 6.

A visual examination of NGC 5427 does not reveal any bar and, thus, this galaxy has been classified as SA in the RC3 catalogue. On the contrary, NGC 1073 is classified as SB in the RC3 catalogue and shows a clear strong bar structure. We have also included the galaxies NGC 210 and NGC 4303, both of which are classified as SAB in the RC3 catalogue, showing different types of bar or oval structures. Indeed, NGC 210 has a clear oval structure, while NGC 4303 has a short bar. The features in the spectra of the B passband are also clearly visible in the spectra from the H filter for the same galaxies. In Fig. 7 we show the galaxy images in the H passband. Although the spiral arms are now dimmer and smoother than in the B band, the main galaxy structures are still clearly visible.

In Fig. 8 we show, in the first column, the $m = 2$ spectra for these four galaxies as calculated from the B passband images while in the second column we show the same spectra obtained using H passband images. As we can see, the spectra of all these galaxies are very complex. Only the $m = 2$ spectrum of the strongly barred SB galaxy NGC 1073 shows a strong signal centred at $p = 0$. Even in this case, the spectrum is not perfectly symmetric, however. In the case of NGC 5247, we have a very broad $m = 2$ spectrum, which is the result of the combination of the central structure and the asymmetric multiple strong arms, which give signals for different values of the radial frequency p. In the case of the strongly barred galaxy NGC 1073 the spectrum shows indeed a strong signal, approximately centred on $p = 0$. This galaxy also shows an asymmetrical two-armed spiral, which appears in the spectrum as a very small peak on the right side of the main peak, as well as some other minor components. All of these contribute to the $m = 2$ spectrum and their blending finally gives a strong signal that is not perfectly centred on $p = 0$. This blending is clearly seen in the $m = 2$ spectrum of NGC 210, whose image shows a strong oval and rather dim spiral arms. The $m = 2$ spectrum of this galaxy shows an asymmetric strong peak that is not centred at $p = 0$, resulting from the blending of the oval signal with the signal from the dim spiral arms. NGC 4303, whose image shows stronger arms and a more complex structure, also has a broad spectrum that is the combination of all these components. As in the case of the B passband, the H image of NGC 5247 shows the broken arms, which give two strong signals with no apparent bar. For the case of NGC 1073 the strong bar signal is biased by the dim bar signal of the arms giving an asymmetric composed signal. Finally, the combined signals of the bar structure and the arms give also complex signals in the $m = 2$ spectra for the galaxies NGC 210 and NGC 4303. Comparing these two sets of spectra we can see that while the shape of the spectra can be somewhat different using two different passbands, when decomposing the spectra and obtaining all the signals separately, there are no great differences in the relevant components detected in all the passbands. We can conclude that in general the spiral or bar features of a galaxy are common to B and H passband, as is the case for these examples. This result suggests that the passband used by the Fourier technique for the detection of bar and spiral components is not a decisive factor and that the bar or spiral components can be normally detected in all the passbands.

Finally, we can study the performance of our method, when using images with lower resolution coming from deep samples of cosmological interest. For this analysis we select the strongly barred galaxy NGC 1073 because in this particular case our method gives a well-centred strong signal in the $m = 2$ spectrum corresponding to the bar, while the dimmer two-spiral structure is also represented by a smaller signal. We start with the NGC 1073 galaxy image from the OSU galaxy sample using the B passband. We degraded the resolution of the image successively by a factor 2 and recalculated its $m = 2$ spectrum for each image. Next we can study the effect of the reduction of the

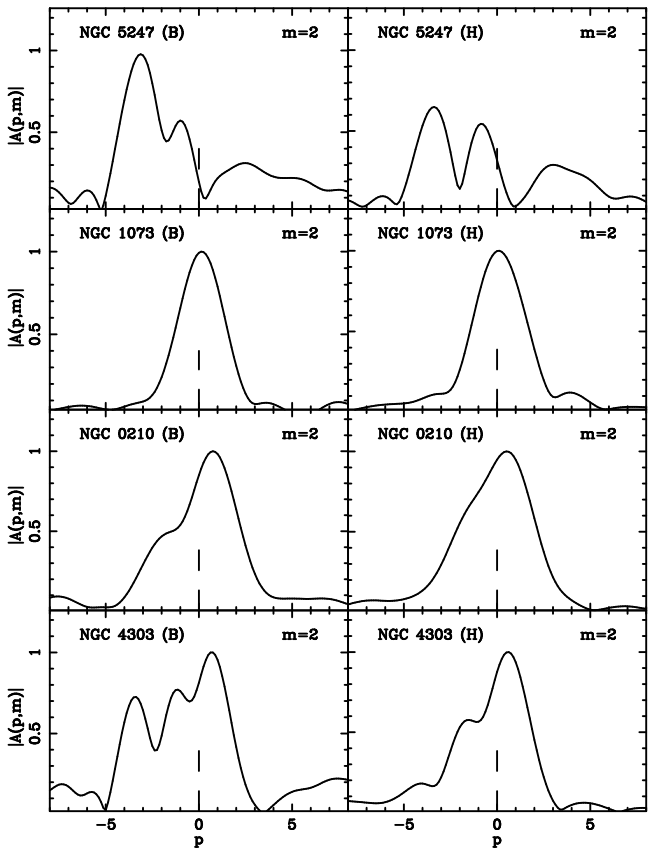

Fig. 8. Spectra from the *B* and *H* band images of the four galaxies shown in Figs. 6 and 7. *From top to bottom*, NGC 5247, NGC 1073, NGC 210, and NGC 4303 are shown. We can compare the results for the $m = 2$ components in both passbands. In the *left panels* we have the spectra for the *B* passband, while in the *right panels* the $m = 2$ spectrum for each galaxy in the *H* passband. A dashed vertical line shows the location of $p = 0$.

image resolution on the signal of the bar and spiral component. The initial image has a resolution of 640×640 pixels, while we degrade down the resolution successively until we reached a final resolution of 20×20 pixels, i.e. a reduction in resolution by a factor 32. We show the result of this analysis in Fig. 9. The left column shows the successively degraded images of NGC 1073, starting from the initial image with 640×640 pixels. In the right column, we plot the signal of its corresponding $m = 2$ spectrum. We show only three additional images with resolutions reduced by factors 4, 16, and 32. Lowering the resolution is equivalent to placing this same galaxy at longer distances by the same factors. Comparing the original signal of the $m = 2$ spectrum with the spectra of the lower resolution images, we can observe that our method is able to recover both the strong bar signal and the lower signal corresponding to the dimmer two arm structure, even at such lower resolutions. Thus, we can be confident that our method will be also useful with samples of cosmological interest with galaxies located much father away. This opens the possibility of studying the evolution in time of the spiral structure of galaxies via larger and deeper samples. The main problem with such studies, however, will be the requirement to use images with a well-defined disc, which is an essential step to obtaining a reliable deprojection of the image.

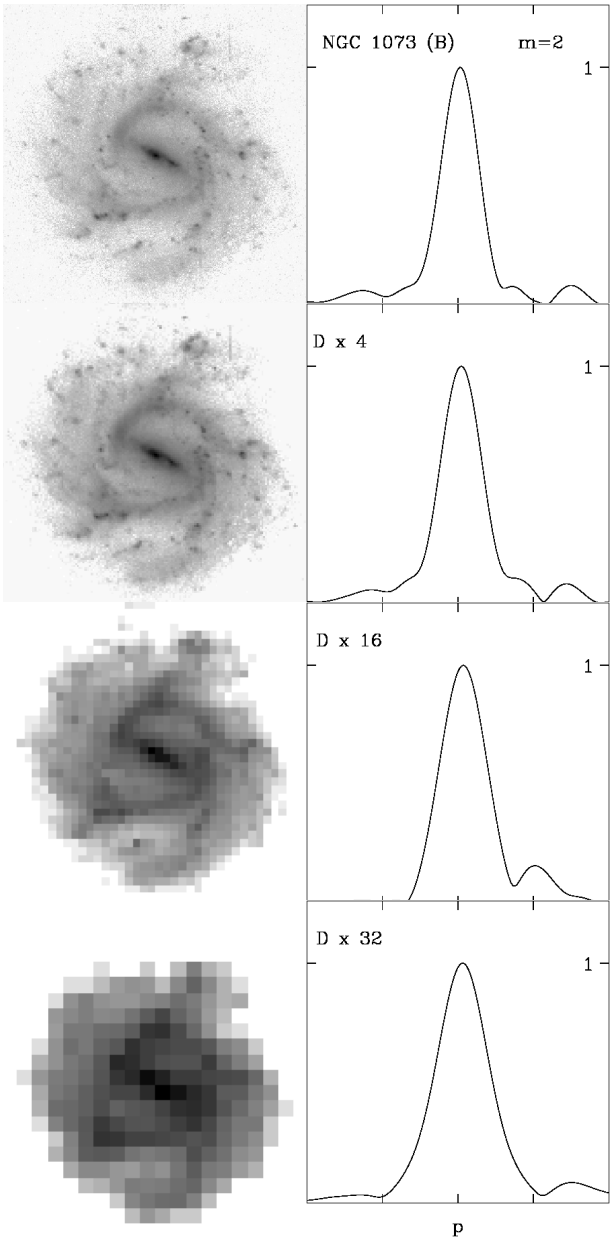

Fig. 9. Starting with the initial image in the *B* passband for NGC 1073, in each row, results of the degraded resolution in the *left column* and the resulting $m = 2$ spectrum of this degraded image by reducing resolution factors of 4, 16, and 32. We can recover the main features of the $m = 2$ spectrum even at very low resolutions.

5. Bar indicators as a function of passband

For each galaxy, we have at least two images in different passbands. One of these is located in the blue region and the other in the red or NIR region. Thus, in the case of the Frei sample we use the *g* or *B* passbands for the blue and we use the *r* or *R* passbands for the red or NIR. In the case of the OSU sample, we use the *B* filter for the blue region, while we use the *H* filter for the red or NIR. For all the images for which we detected a signal, we can compare the strength in the two passbands. This procedure can show whether bars are in fact more prominent in the red or NIR than in the blue region as has been claimed by some authors. We used all of our bar indicators to compare the

A&A 601, A132 (2017)

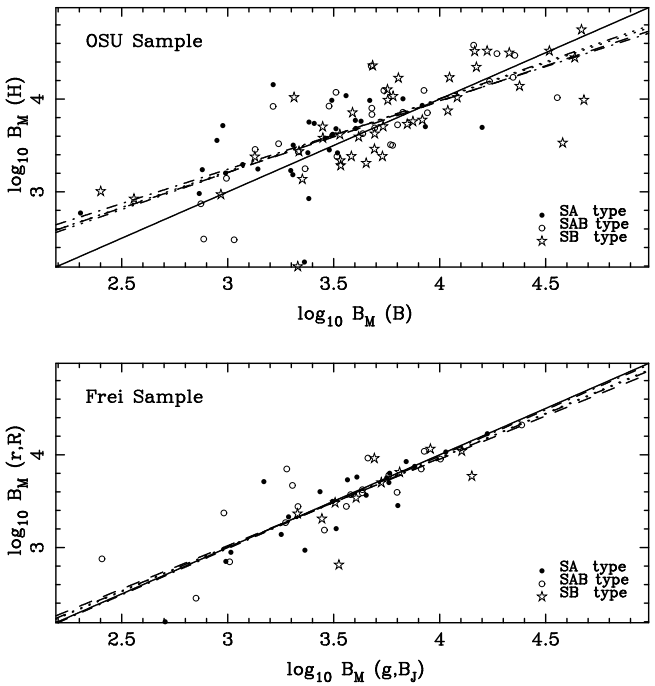

Fig. 10. Correlation between the values of the $\log_{10} B_M$ parameter for the blue and red filters. The bold line is the diagonal, while the dashed line is the standard least squares bisector line. The dot-dashed, dotted, and dot-dot-dot-dashed line correspond to the robust optimal M-regression line, the robust mean biponderate regression line, and the robust winsorised regression line, respectively. The SA galaxies are represented as filled circles, the SAB galaxies as open circles, and the SB galaxies as open stars. The upper panel gives results for the OSU sample and the lower panel for the Frei sample.

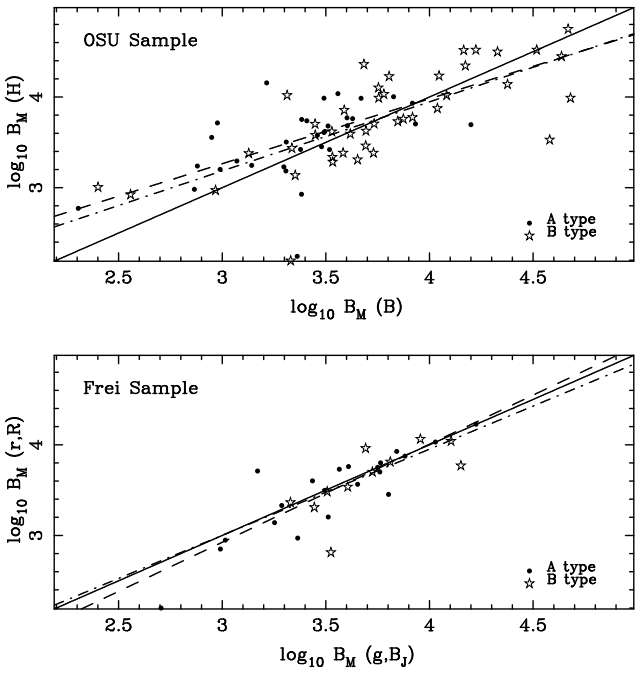

Fig. 11. Correlation between the values of the $\log_{10} B_M$ parameter for the blue and red passbands for the SA and SB galaxies separately. The layout is the same as in Fig. 10. The solid line corresponds to the diagonal, while we show only the optimal M-regression line for SA (dash-dotted line) and SB (dashed) galaxies separately.

strength of the bar signal in different passbands and all of these indicators give comparable results. We discuss here only some of these indicators for the sake of brevity.

In Fig. 10 we show the linear regression of the parameter $\log_{10} B_M$ for the blue and red passbands for both samples. For the linear regression we can compute the standard regression line and we can also perform robust regressions, which are less biased by the presence of outliers. Here we include the optimal M-regression line, the mean biponderate regression line and the winsorised regression line, as suggested by Huber (1981). The figure shows that all the linear correlations give similar results, and we can conclude that our samples are not strongly biased by outlier galaxies. We can also perform a significance test using a bootstrap technique on the values of the slope for the standard regression line and for the optimal M-regression line. In the case of the Ohio sample, the 95% confidence interval for the slope of the standard regression line is $[0.61, 0.93]$, while the same interval for the optimal M-regression line is $[0.63, 0.93]$. Both intervals exclude the value $a = 1$ for the slope of the regression line and we can conclude that bars in the B passband give stronger values for our indicators than the same values in the H passband for the Ohio sample galaxies. The same confidence intervals for the Frei sample give values of $[0.71, 1.17]$ and $[0.77, 1.19]$. Here, both intervals include the value $a = 1$ for the slope and, in this case, there is no significant difference between the values of the bar indicators in the blue passband and red passband. Thus, our results suggest that bars in the far-infrared (H passband) appear dimmer with respect to the background galaxy than the same bars in the blue or red passbands. We obtained similar results using the B_P indicator instead of the B_M indicators and, in this case, the 95% confidence intervals for the standard regression line in the Ohio sample is $[0.61, 0.91]$ and the same interval for the optimal M-regression line is $[0.63, 0.97]$. In the case of the Frei sample both intervals are $[0.74, 1.16]$ and $[0.80, 1.22]$, respectively.

The fact that the values of the slopes are very near unity in all the cases indicates, moreover, that for the galaxies with a signal detected in both passbands, there is no evidence of a significant difference between bar strength in different passbands. However, not all galaxy images in our sample showed a bar signal using our definition. All the galaxy images from the Frei sample showed bar signals in both passbands. For the galaxy images selected in the Ohio sample, however, only three galaxies from the 128 selected, namely NGC 4051, NGC 4580, and NGC 4699, failed to show a bar signal in any of the passbands at all, while 16 galaxies failed to show a bar signal at least in one of the two passbands. Five of them did not show a bar in the H image and the rest of 11 galaxies only showed a bar signal in the B band. We have to emphasise, however, that in these cases, we could have detected a bar signal if we had used a larger interval for the definition of the bar signal. In fact the interval selected, $(-1 \leq p \leq 1)$ (see Sect. 3.2), is somewhat arbitrary. If we relax this condition, we can detect a bar signal in both passbands.

Some authors (Laurikainen & Salo 2002; Marinova & Jogee 2007) have suggested that bars can be more easily detected in the infrared passbands than in the blue region of the spectrum. We used our bar indicators to compare the difference between SA and SB galaxies for the different passbands in our sample to check this result. The results are compared using the robust optimal M-regression line separately for the SA and SB galaxies in Fig. 11, where we compare the values of the $\log_{10} B_M$ parameter for the blue and red filters. There is no apparent difference between SA and SB galaxies, and a bootstrap analysis of the

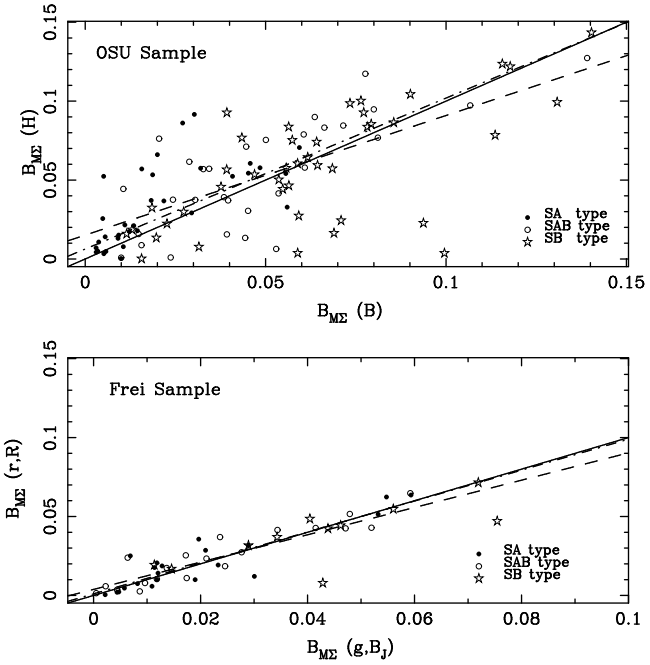

Fig. 12. Correlation of the values of the $B_{M\sum}$ parameter for the blue and red passbands for the two samples. The layout is as in Fig. 10, but here we only show the standard linear regression line (dash-dotted line) and the robust optimal M-regression line (dashed line).

slopes at a 95% confidence level confirms this result. The interval for SA galaxies in the Ohio sample is $[0.22, 0.97]$, while for SB galaxies this interval is $[0.50, 1.10]$. In the case of the Frei sample, the interval for SA galaxies is $[0.91, 1.42]$, while the interval for SB galaxies is $[0.46, 1.55]$. Thus, our data does not show any significant difference between SA and SB galaxies when using our bar indicators. We can conclude that when we use the Fourier technique there are no apparent differences in the bars detected for a particular galaxy using different passbands. These results are only valid for the set of passbands used in the galaxy samples selected for our analysis. It would be useful to extend the comparison of the bar strength to other passbands, such as the UV, using this technique to ascertain if there is some particular passband where the bars are more prominent.

In order to compare the bar signals we can also use the normalised values of our parameters described in Sect. 3.2. These normalised values, however, must be used with caution. For a particular galaxy with very well-defined arms or a poorly defined disc, the normalisation process can give a very biased indicator value. However, the results using the rest of the indicators are very similar to the results already shown in this section. In Fig.12 we show the correlations for one of the normalised parameters, namely the $B_{M\sum}$ parameter. Here we only show the standard linear regression line (dash-dotted line) and the robust optimal M-regression line (dashed line). The 95% confidence intervals for the slope do not show a significant difference between the bar indicators in the blue and red passbands. In the case of the Ohio sample these intervals are $[0.57, 0.90]$ for the standard regression line and $[0.80, 1.02]$ optimal M-regression line. In the case of the Frei sample these intervals are $[0.67, 1.02]$ and $[0.85, 1.00]$, respectively.

Using the normalised indicators, however, it is true that the values of the bar components for non-barred galaxies, as classified in the RC3 catalogue, are higher in the infrared than in the blue passbands. This is apparent in Fig.12. This would be in agreement with the claim that disc galaxies appear to be more barred in the infrared than in the visible passband. On the other hand, galaxies classified in the RC3 catalogue as barred, appear to have higher values of the indicators in the blue passband than in the red. The regression lines fail to give any significant difference between SA and SB galaxies. We will explore this result further in Sect. 7 using the distribution of the values of the normalised indicators.

6. Comparison between different bar indicators

We can find two ways of measuring the bar strength in the literature. The first is a measure of the maximum relative non-axisymmetric torque strengths (hereafter Q_b) introduced by Combes & Sanders (1981). This parameter was used by Block et al. (2002), Buta et al. (2004, 2005), and more recently by Speltincx et al. (2008). The second method, used by Whyte et al. (2002) and Marinova & Jogee (2007), is to give a measure of the bar ellipticity. These authors have concentrated their efforts in the OSU sample.

The problem of detecting a bar component has been addressed by different authors who have suggested indicators based on particular properties of the bar component. In this section we want to compare the performance of these indicators on the galaxies in the OSU sample, which has been used for different groups to measure bar strengths. We compare the relative efficiency of our bar indicators, namely B_M and B_P, with the $f_{\rm bar}$ indicator used by Whyte et al. (2002), the bar torque Q_b used by Block et al. (2001), Buta et al. (2004), and Speltincx et al. (2008) and, finally, the ellipticity $\epsilon_{\rm bar}$ used by Marinova & Jogee (2007).

As the bar indicators measure different bar properties, they are not directly comparable and a linear correlation does not seem to be an appropriate way to compare the results of the different groups of authors. Instead of the classical Pearson linear correlation coefficient, the Spearman and Kendall correlation coefficients seem to be more suitable for this study. These non-parametric coefficients are more appropriate for the case of samples that are drawn for unknown distributions; see Press et al. (1994).

Given a set of values x_i, we define the rank among these samples as R_i. If we have a second sample y_i drawn from a different probability distribution, we define the rank within this sample as S_i, then the Spearman rank correlation coefficient r_s is defined by

$$r_s = \frac{\sum_i \left(R_i - \bar{R}\right)\left(S_i - \bar{S}\right)}{\sqrt{\sum_i \left(R_i - \bar{R}\right)^2}\sqrt{\sum_i \left(S_i - \bar{S}\right)^2}}, \tag{21}$$

where $\bar{R}$ and $\bar{S}$ are the mean values of each sample. The values of this parameter must be within the range $-1 \le r_s \le 1$, and the closer the value of $|r_s|$ to 1 the better the correlation. The significance of these values against the null hypothesis of zero values can be tested by computing the parameter

$$t = r_s \sqrt{\frac{N-2}{1-r_s^2}}, \tag{22}$$

which is distributed approximately as a t-Student distribution with $N-2$ degrees of freedom. This approximation does not depend on the unknown original distribution of the data values,

which makes this method very appropriate to our purpose because the probability distribution of the values of the bar indicators is not known.

On the other hand, the Kendall τ coefficient uses only the relative ordering of ranks. Given N data points (x_i, y_i), we consider all the possible $N(N-1)/2$ pairs of data points. A concordant pair occurs if the relative ordering of the x_i values is the same as the relative ordering of the y_i values, while a discordant pair occurs on the contrary. In the case of ties, the pair is not considered as concordant or discordant and the pair is taken as an "extra y pair" if the tie is in the x values or an "extra x pair" if the tie is in the y values. If N_c is the number of concordant pairs, N_d the number of discordant pairs, E_x the number of extra x pairs, and E_y the number of extra y pairs, the Kendall τ coefficient is defined as

$$\tau = \frac{N_c - N_d}{\sqrt{N_c + N_d + E_y}\sqrt{N_c + N_d + E_x}}. \quad (23)$$

This value lies in the range $[-1, 1]$, taking extreme values only in the case of complete rank agreement or complete rank reversal, respectively. The approximate distribution or the τ coefficient in the null hypothesis of no correlation is approximately normally distributed with zero mean value and a variance of

$$\mathrm{Var}(\tau) = \frac{4N + 10}{9N(N-1)}. \quad (24)$$

We use all these parameters with a significance level of $\alpha = 0.95$ to compare all the measurements of bar strength. In the upper diagonal of Table 2, first we show the number of galaxies in common within the OSU sample, and then the values of the Pearson correlation coefficient, Spearman correlation test, and Kendall τ coefficient for each pair of authors. We also include the correlations between the values of our two indicators, B_M (first row) and B_P, and the comparison between the indicators used for the rest of the research groups. We include in the comparison only two of our bar indicators as we obtain comparable results using the rest of our bar indicators. In the cases where both B and H images were used, we combine all the values to strengthen the correlation. In the lower diagonal, we show the respective p values of the three correlation coefficients for this particular sample. The p values lower than $\alpha = 0.95$ indicate a significant correlation up to this level of significance. The p value is defined as the probability of obtaining a certain value for the coefficient in the case of null hypothesis of no correlation.

The values in Table 2 show that the bar indicators used in different works but using similar criteria to define the bar are in good agreement. The values obtained from the correlation tests are not close to the unity, nevertheless, this fact does not indicate that the correlations are not significant. As the values compared come from different bar indicators and are estimated using completely different methodology, a tight linear correlation between them is not to be expected. The values of these rank correlations are in all cases significant, i.e. they are significantly different from the zero value as is indicated by the low p values. The agreement is better for the cases where the values of the bar strength came from a similar methodology as is the case in Block et al. (2001), Buta et al. (2004), and Speltincx et al. (2008). Our bar indicators have significant positive correlations with these indicators, except for the case of the values quoted in Block et al. (2001). The correlation between the values of our bar indicators and the values from these authors, while given positive correlations, cannot be considered significant at the confidence level of 95%. Likewise, our values are not well correlated with the ellipticities of the bar as quoted in Marinova & Jogee (2007). This is not surprising, we have seen in Sect. 4 that our method is sensitive to the bar shape, in the sense that the rounder the bars, the lower the power in the $m = 2$ spectrum. We have good agreement, however, with the f_{bar} indicator used by Whyte et al. (2002). We can conclude that there is, in general, a reasonable agreement between the different bar indicators used in the literature.

Table 2. Comparison of the correlation coefficients between the different bar indicators for the galaxies in common.

	B_M	B_P	Block	Buta	Spelt.	Mari.	Whyte
		329	81	98	133	110	130
B_M		0.99	0.12	0.34	0.37	0.12	0.45
		0.99	0.17	0.25	0.24	0.08	0.45
		0.92	0.12	0.35	0.36	0.11	0.32
			81	98	133	110	130
B_P	0.00		0.15	0.36	0.39	0.18	0.48
	0.00		0.20	0.36	0.37	0.15	0.47
	0.00		0.15	0.25	0.26	0.09	0.34
				75	52	46	66
Block	0.28	0.18		0.83	0.79	0.66	0.75
	0.09	0.05		0.79	0.56	0.69	0.74
	0.11	0.07		0.69	0.72	0.54	0.57
					68	63	67
Buta	0.00	0.00	0.00		0.80	0.60	0.82
	0.00	0.00	0.00		0.76	0.59	0.80
	0.00	0.00	0.00		0.58	0.44	0.61
						106	84
Spelt	0.00	0.00	0.00	0.00		0.47	0.62
	0.00	0.00	0.00	0.00		0.55	0.70
	0.00	0.00	0.00	0.00		0.40	0.53
							73
Mari.	0.21	0.06	0.00	0.00	0.00		0.61
	0.26	0.12	0.00	0.00	0.00		0.60
	0.26	0.12	0.00	0.00	0.00		0.46
Whyte	0.00	0.00	0.00	0.00	0.00	0.00	
	0.00	0.00	0.00	0.00	0.00	0.00	
	0.00	0.00	0.00	0.00	0.00	0.00	

Notes. In the upper diagonal we find the number of galaxies in common and the values of the Pearson, Spearman, and Kendall correlation coefficients. In the lower diagonal we find the respective p values of the correlations. Values of 0.00 indicate p values lower than 10^{-5}.

7. Distribution of the bar indicators

In this section we use the values of our bar indicators as a measure of the general morphologies of galaxies indicated in the RC3 catalogue. In this catalogue the galaxies have been divided visually in three populations, namely SA, SAB, and SB, according to the visual strength of the bar, if present. In a SA galaxy no bar is present as seen by visual inspection, SB galaxies show a clear bar, while SAB galaxies are a mixed class were we can find small bars, ovals, and unclear cases. Our bar indicators give a numerical value for the bar strength and we would like to check whether our indicators reproduce the general properties of

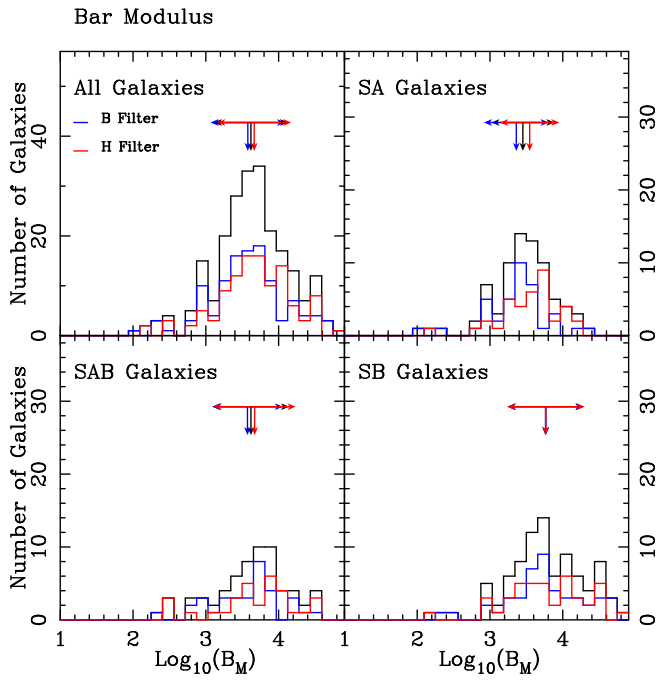

Fig. 13. Number of galaxies as a function of their bar modulus in the OSU sample. The *upper left panel* includes all galaxies, while the three others include only the SA, SAB, and SB families. In each panel the solid line corresponds to the values obtained for all the images irrespective of the filter used. We also separate the values for the galaxies studied using the *B* filter (blue) and *H* filter (red). The scales for the ordinate are not the same for all panels. The vertical arrows indicate the mean value for each population, while the length of the horizontal arrows indicate the value of the sigma of the distribution.

galaxies as derived from visual inspection. Our indicators should be able to recover the three galaxy populations in a general way. Thus, we can expect that barred galaxies from the SB type should have higher values of the bar indicators, SA galaxies should get lower values, while mixed class SAB should also produce a set of mixed values.

Figure 13 gives histograms of the number of galaxies as a function of their bar modulus in the OSU sample. The top left panel includes all the galaxies. The solid line corresponds to the distribution obtained using all the galaxy images, irrespective of the filter used. The distributions in blue correspond to the galaxy images obtained with the blue *B* filter, while the distributions in red correspond to the galaxy images obtained with the infrared *H* filter. We used the same codification for the other panels of the figure, where we separated the galaxies according to their classification in the RC3 catalogue in SA (non-barred), SAB (intermediate), or SB (barred) galaxies. The vertical arrows indicate the position of the mean of each population, while the horizontal arrows show the length of the standard deviation within each sample.

Using these distributions we can perform a series of statistical tests to ascertain if there are any differences between the galaxy populations. We start with the top left panel to see whether we can find any differences between the global population and blue or infrared populations. For this comparison, we can use measures of location for the distribution of the parameters. Here we use the standard mean and also robust measures of location, such as the median and α-trimmed means, which are less biased by outliers than the classic standard mean. In the same way we can use the classic standard deviation as a measure of dispersion around the mean, but we can also use more robust measures of dispersion, such as the normalised standarised median absolute deviation (NMAD). The mean value of the global population is 3.6, while the standard deviation gives a value of 0.5. Using only the blue or the infrared populations, the mean and standard deviation obtained are also 3.6 and 0.5. The median for the combined population also gives a value of 3.6, while the median values of the *B* and *H* populations are both of 3.7. The NMAD is computed to have a value of 0.4 in the three cases. In the case of the α-trimmed means we also obtain values of 3.6 for the three populations. Thus, our data allow us to conclude that there are no differences in the bars detected with *B* or *H* passbands using the Fourier technique. This is in agreement with the results obtained in Sect. 5. This is confirmed by statistical tests on the mean difference of the location measures for the three distributions. An standard *t*-test on the difference of means, assuming that the populations are normal is unable to detect any difference in the means of the three galaxy distributions. This is true also for the case of the non-parametric statistical tests on the difference of the median values as the Wilcoxon-Mann-Whitney test or the robust generalisation of this test proposed by Mee (1990). A global non-parametric test for the comparison of the distributions, such as the Kolmogorov-Smirnov test, is also unable to separate the entire population from the population in the *B* or *H* passbands at the 95% confidence level.

If we repeat our analysis but this time separate the three galaxies populations using their SA, SAB, and SB visual class, we obtain similar results. None of the robust tests are able to obtain any difference between the combined population and the population obtained from the *B* or *H* passbands. Thus, all the distributions can be considered equal from a statistical point of view. We can find no differences in the bar detection levels using the blue or infrared passbands with our technique. Contrary to the methods used by other authors (Laurikainen & Salo 2002; Marinova & Jogee 2007), our method seems to be able to detect bars irrespective of the filter used to obtain the galaxy image.

We can also compare the distribution of the values of the bar indicator B_M separately for the SA, SAB, and SB galaxies also using the standard and robust measures of location. For the SA population, the mean, median, and α-trimmed mean give values of 3.46, 3.51, and 3.51, respectively. In the case of SAB galaxies, these values are 3.59, 3.64 and 3.62, respectively, while in the case of SB galaxies, we obtain 3.74, 3.72, and 3.73. The differences between the SA, SAB, and SB are statistically significant at the 95% confidence level. The standard t-Student test on the difference of means give a confidence interval at the 95% level for the mean difference between SA and SB galaxies of $[-0.39, -0.15]$, excluding the zero value. This test is barely able to separate SA from SAB galaxies, giving a confidence interval of $[-0.23, 0.00]$, while it is able to separate the SAB from the SB population with a confidence interval of $[-0.27, -0.03]$. This could indicate that the SAB population is more similar to the SA than to the SB population, but confirms the idea that this galaxy type is a mixed bag of values. The robust tests on the mean differences agree with the classical test. Thus, the generalised robust Wilcoxon-Mann-Whitney test from Mee (1990) is also able to separate the SA from the SB populations, giving a confidence interval at the 95% level on the ratio of means of $[0.59, 0.72]$, excluding the 0.5 value. This test is also able to separate SA from the SAB populations with a confidence interval of $[0.52, 0.64]$ and the SAB from the SB galaxies with confidence level of $[0.51, 0.65]$. Thus our bar indicator B_M performs very well in detecting the bar components of galaxies and

A&A 601, A132 (2017)

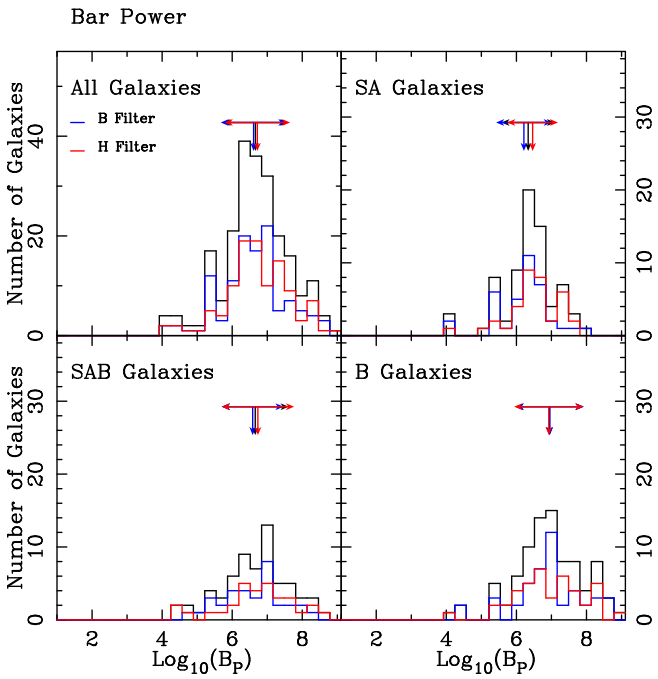

Fig. 14. Number of galaxies as a function of their bar power. The *upper left panel* includes all galaxies, while the three others are indicated separately for the SA, SAB, and SB families, respectively. The layout and symbols are as in Fig. 13.

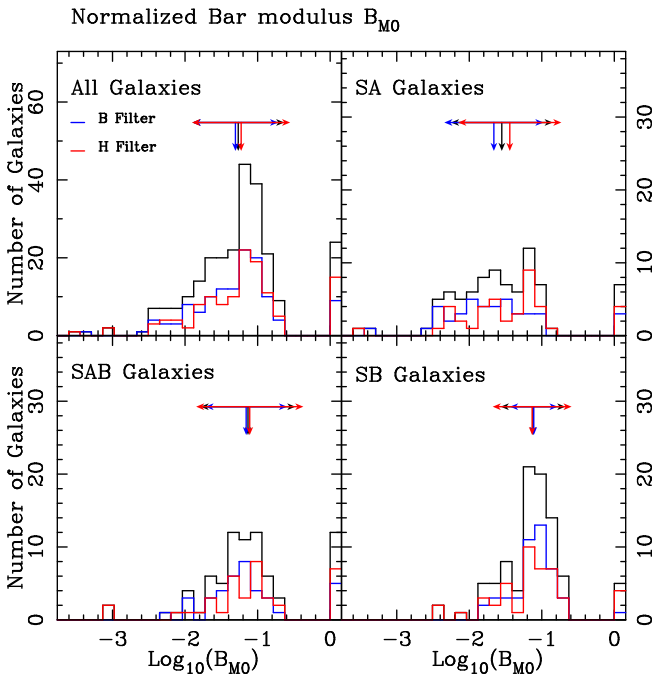

Fig. 15. Number of galaxies as a function of the natural logarithm of the B_{M0} bar indicator. The *upper left panel* includes all galaxies, while the three others are indicated separately for the SA, SAB, and SB families, respectively. The layout and symbols are as in Fig. 13.

is in overall good agreement with the visual classification of the RC3 catalogue from de Vaucouleurs et al. (1991). Similar results were found when using the bar power indicator instead of the bar modulus and are not given here for the sake of conciseness. The distributions and means obtained using this bar indicator are shown in Fig. 14, which shows the same layout as Fig. 13.

When we look at the distribution of our bar indicators, we can conclude that the relative strength of the bar in disc galaxies is a continuous parameter that is sometimes difficult to detect visually or with any qualitative measure. It is better to define the strength of the bar with a quantitative measure as the B_M or B_p parameters obtained from the Fourier analysis of the images. The values of this parameter in normalised images span about three orders of magnitude and could be used to define the degree of the bar phenomenon in a particular galaxy. Using the values from our analysis, we can define the set of non-barred galaxies as the galaxies with $\log_{10}(B_M) < 3$, the set of mildly barred galaxies as galaxies with $3 < \log_{10}(B_M) < 3.5$, and the set of barred galaxies as those with $\log_{10}(B_M) > 3.5$. This quantitative classification could be particularly useful when studying galaxies with no previous qualitative classification as any set of galaxies that is not included in the RC3 catalogue with cosmological interest.

We can try also to use the normalised bar indicators to see if these features can be enhanced. In Fig. 15 we show the distribution of the values of the natural logarithm of the normalised bar indicator B_{M0}, where we normalised the bar component modulus to the modulus of the $m = 0$ spectrum, which corresponds to the strength of the underlying disc. The layout of Fig. 15 is also similar also to that in Fig. 13. As for the former cases, the mean value of the total distribution cannot be distinguished from the mean value of the distribution of B or H passbands. Moreover, as in the case of the B_M indicator, the total distribution, the distribution of B passband images, and the distribution of H passband images cannot be differentiated from a statistical point of view.

As in the case of the non-normalised indicators the only significant effect is found when analysing the difference between the population of SA, SAB, and SB galaxies. The 95% confidence interval for the mean difference between SA and SB galaxies in a standard t-Student test is of $[-0.61, -0.37]$, clearly excluding the zero value and indicating a significant difference between SA and SB galaxies. This is true also for SA and SAB galaxies with a confidence interval of $[-0.38, -0.13]$ and for SAB and SB galaxies, with confidence interval $[-0.35, -0.11]$. The robust generalisation of the Wilcoxon-Mann-Whitney test performs equally well, clearly separating the three galaxy types. The normalised values seem to perform a bit better when trying to separate the galaxy types, but we must stress that all the differences between galaxy types result to be statistically significative despite any of our bar indicators used. If for instance, we use the normalisation by the sum of all the moments, i.e. the bar indicator $B_{M\Sigma}$, the results are again similar to the results obtained with any of the non-normalised indicators. The distributions for the values of the natural logarithm of $B_{M\Sigma}$ are shown in Fig. 16. A similar result is obtained using the B_{M2} indicator; see Fig. 17.

8. Discussion and conclusions

In this paper we have introduced a new method to study the spiral structure of disc galaxies. This method uses a two-dimensional FFT on galaxy images. It is based on a similar method initially proposed by Considère & Athanassoula (1982) for the HII region distribution and, independently, by Iye et al. (1982) who used this method on a photometric image of the galaxy NGC 4254. Later, Considère & Athanassoula (1988) used it on a sample of images of bright spiral galaxies. These authors considered only the maximum component of each spectrum but the galaxy spectra can be very complicated owing to the presence of various components of different multiplicities. The method

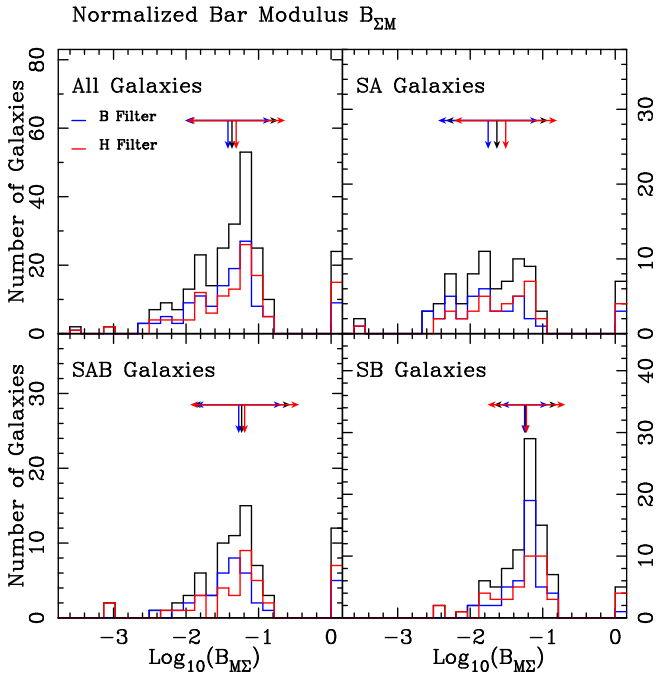

Fig. 16. Number of galaxies as a function of the natural logarithm of the $B_{M\sum m}$ bar indicator. The *upper left panel* includes all galaxies, while the three others are indicated separately for the SA, SAB, and SB families, respectively. The layout and symbols are as in Fig. 13.

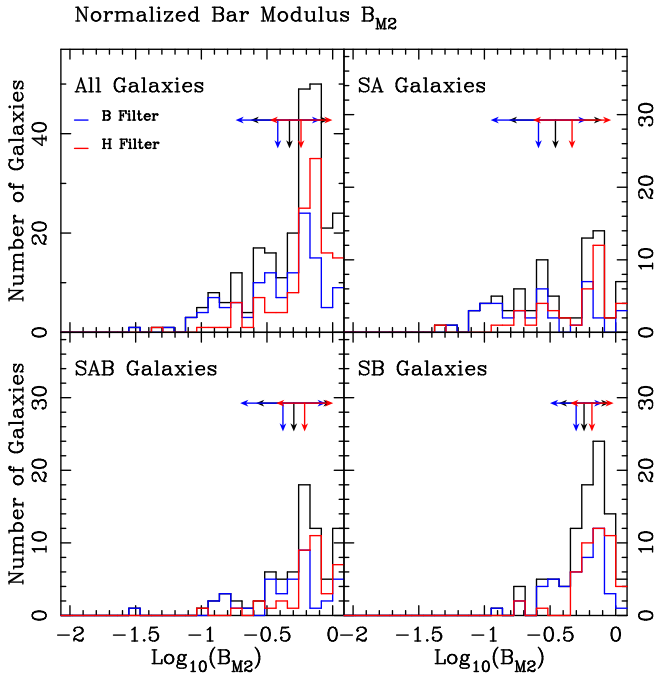

Fig. 17. Number of galaxies as a function of the natural logarithm of the B_{M2} bar indicator. The *upper left panel* includes all galaxies, while the three others are indicated separately for the SA, SAB, and SB families, respectively. The layout and symbols are as in Fig. 13.

was fully developed by García-Gómez & Athanassoula (1991) for the HII region distribution. These authors introduced the possibility of dealing with the whole complexity of the Fourier spectra, separating all the signals present in each spectrum. In this paper we adapted this method to be applied on photometric galaxy images. Some other authors also applied the two-dimensional FFT on photometric galaxy images, for instance, Block & Puerari (1999), Block et al. (2001), and Buta et al. (2003, 2004). In these papers however, only the maximum component was used for the analysis of the spiral structure. In a later paper, Buta et al. (2005) made an effort to include more components for each spectrum in a way similar to the present method. Our method is more general, however, as we are free to use as many components as necessary to obtain very good fits of the galaxy spectra, while we can recover the whole spiral structure of any galaxy image with great accuracy.

We used this method extensively on two large homogeneous galaxy samples, namely the Frei sample, Frei et al. (1996) and the Ohio State University Bright Spiral Galaxy Survey (OSU) Eskridge et al. (2002). In this particular paper, we only concentrated on the detection and analysis of barred structures. We introduced some bar strength indicators based on the Fourier decomposition of the galaxy images. These new bar indicators perform equally well from a statistical point of view as other bar indicators, namely the bar torque introduced by Buta & Block (2001) and Laurikainen & Salo (2002) and the bar strength measured by the $f_{\rm bar}$ introduced by Abraham & Merrifield (2000) and used by Whyte et al. (2002). Our bar indicators are not so well correlated with the bar ellipticities, as suggested by Athanassoula (1992), which were used in Marinova & Jogee (2007).

The first point to be stressed is that we are able to detect the barred component with comparable strength in any of the galaxy passbands used to obtain the galaxy images in the former samples. Thus, we do not find evidence of the case of a higher fraction of barred galaxies in the infrared as has been suggested by Eskridge et al. (2000) or Marinova & Jogee (2007). The distribution of bar strength for the galaxy images obtained in the blue cannot be distinguished from the distribution of the bar strength obtained for the galaxy images obtained in the infrared region of the spectrum. When using our bar indicators in the Ohio sample, there is a minor effect that is more statistically significant for the case of stronger bars in the blue than for the galaxies in the far-infrared . On the other hand, our bar indicators are able to statistically separate the SA, SAB, and SB population of galaxies in order with the visual classification of the galaxies in the RC3 catalogue. Our method is able to separate the bar component from the rest of the spiral components and in about the 95% of the galaxies is able to detect a bar component, irrespective of its galaxy type. Thus, the vast majority of galaxies seem to harbour a bar in its stellar disc.

The strength of this bar, however, can be measured within a range of about three orders of magnitude. Thus the visual classification of galaxies as barred or non-barred is clearly justified. Our parameters could be used, however, as the basis of a more quantitative classification of the bar phenomenon.

This is intended to be the first paper of series in which we want to study the spiral structure of disc galaxies deeply. We intend to extend our analysis to the other spiral components with the aim of searching any links between the global spiral structure and the dynamical properties of galaxy discs. Another possible application of out method could be the study of the strength of the bar in a set of galaxies of cosmological interest. We would be able to study whether galaxies at larger distances appear to be more barred than neighbouring galaxies. This Fourier technique could be also used for large samples of galaxies. In this case, major issues should be addressed. The first should be of course the determination of the deprojection angles,

as the Fourier technique should be used on a face on image of the galaxy. The deprojection methods used by different authors and using different methodologies can sometimes give very different results (Barberà et al. 2004; García-Gómez et al. 1991. Particularly for nearly face-on galaxies. For these cases, the PA could only be determined with some certainty using some information on the velocity field of the disc. For galaxies with inclination angles of values $40° < IA < 65°$ all the deprojection methods give comparable results and these galaxies could be deprojected using an automated procedure. A second important issue is to determine the parameter r_{min} used in our calculations, namely the size of the galaxy bulge. This value could be computed in a large sample using automated decomposition of the photometric galaxy profile. We have shown that the Fourier analysis is not very sensitive to this value as long as we clearly avoid the inner bulge. We think that this value could be computed with enough precision using the photometric profiles of the galaxies. The use of the Fourier analysis of the spiral structure in these large samples of cosmological interest could be very useful to understand the evolution of the spiral structure of galaxy discs.

Acknowledgements. We thank the anonymous referee for clear and acute comments, which have certainly improved the quality of this paper. We also thank David Block and Laura Whyte for providing us with the results of the Q_2 and F_b measurements, respectively. E.A. and A.B. acknowledge financial support to the DAGAL network from the People Programme (Marie Curie Actions) of the European Union's Seventh Framework Programme FP7/2007-2013/ under REA grant agreement number PITN-GA-2011-289313. We also wish to thank Ohio State University for the public release of the OSUBSGS galaxy sample.

References

Abraham, R. G., & Merrifield, M. R. 2000, AJ, 120, 2835
Abraham, R. G., Merrifield, M. R., Ellis, R. S., Tanvir, N. R., & Brinchmann, J. 1999, MNRAS, 308, 569
Aguerri, J. A. L. 1999, A&A, 351, 43
Aguerri, J. A. L., Beckman, J. E., & Prieto, M. 1998, AJ, 116, 2136
Aguerri, J. A. L., Muñoz-Tuñon, C., Varela, A. M., & Prieto, M. 2000, A&A, 361, 841
Aguilar, L. A., & Merritt, D. 1990, ApJ, 354, 33
Athanassoula, E. 1992, MNRAS, 259, 328
Athanassoula, E. 1996, in Barred Galaxies, eds. R. Buta, D. Crocker, & B. Elmegreen, ASPC conf. Ser., 91, 309
Athanassoula, E. 2002, ApJ, 569, L83
Athanassoula, E. 2003, MNRAS, 341, 1179
Athanassoula, E. 2005a, MNRAS, 358, 1477
Athanassoula, E. 2005b, Celest. Mech. & Dyn. Astron., 91, 9
Athanassoula, E., & Misiriotis, A. 2002, MNRAS, 330, 35
Athanassoula, E., Morin, S., Wozniak, H., et al. 1990, MNRAS, 245, 130
Barberà, C., Athanassoula, E., & García-Gómez, C. 2004, A&A, 415, 849
Binney, J., & Tremaine, S. 1987, Galactic Dynamics (Princeton University Press)
Block, D.L, & Puerari, I. 1999, A&A 342, 627
Block, D. L., Puerari, I., Knapen, J. H., et al. 2001, A&A, 375, 761
Block, D. L., Bournaud, F., Combes, F., Puerari, I., & Buta, R. 2002, A&A, 394, L35
Block, D. L., Buta, R., Knapen, J. H., et al. 2004, AJ, 128, 183
Buta, R., & Block, D. L. 2001, ApJ, 550, 243
Buta, R., Block, D. L., & Knapen, J. H. 2003, AJ, 126, 1148
Buta, R., Laurikainen, E., & Salo, H. 2004, AJ, 127, 279
Buta, R., Vasylyev, S., Salo, H., & Laurikainen, E. 2005, AJ, 130, 506
Buta, R., Laurikainen, E., Salo, H., Block, D. L., & Knapen, J. H. 2006, AJ, 132, 1859
Chapelon, S., Contini, T., & Davoust, E. 1999, A&A, 345, 81
Combes, F., & Sanders, R. H. 1981, A&A, 96, 164
Considère, S., & Athanassoula, E. 1982, A&A, 111, 82
Considère, S., & Athanassoula, E. 1988, A&AS, 76, 365
Danver, C. G. 1942, Ann. Obs. Lund, 10, 7
de Vaucouleurs, G. 1963, ApJS, 8, 31
de Vaucouleurs, G., de Vaucouleurs, A., Corwin, H. G., et al. 1991, Third Reference Catalogue of Bright Galaxies, RC3 (New York: Springer)
Durbala, A., Buta, R., Sulentic, J. W., & Verdes-Montenegro, L. 2009, MNRAS, 397, 1756
Elmegreen, B. G., & Elmegreen, D. M. 1985, ApJ, 288, 438
Eskridge, P. B., Frogel, J. A., Pogge, R. W., et al. 2000, AJ, 119, 536
Eskridge, P. B., Frogel, J. A., Pogge, R. W., et al. 2002, ApJS, 143, 73
Fisher, R. A. 1921, Metron, 1, 3
Frei, Z., Guhathakurta, P., Gunn, J., & Tyson, J. A. 1996, AJ, 111, 174
García-Gómez, C., & Athanassoula, E. 1991, A&AS, 89, 159
García-Gómez, C., Barberà, C., Athanassoula, E., Bosma, A., & Whyte, L. 2004, A&A, 421, 595
Grosbol, P., Patsis, P. A., & Pompei, E. 2004, A&A, 423, 849
Heller, C., Shlosman, I., & Athanassoula, E. 2007, ApJ, 657, L65
Huber, P. J. 1981, Robust Statistics (Wiley)
Iye, M., Okamura, S., Hamabe, M., & Watanabe, M. 1982, ApJ, 256, 103
Kennicutt, R. C., Jr. 1981, AJ, 86, 1847
Knapen, J. H., Shlosman, I., & Peletier, R. F. 2000, ApJ, 529, 93
Kormendy, J. 1979, ApJ, 227, 714
Laurikainen, E., & Salo, H. 2002, MNRAS, 337, 1118
Laurikainen, E., Salo, H., Buta, R., & Vasylyev, S. 2004, MNRAS, 355, 1251
Laurikainen, E., Salo, H., Buta, R., et al. 2006, AJ, 132, 1859
Ma, J. 2001, Chin. J. Astron. Astrophys., 1, 395
Marinova, I., & Jogee, S. 2007, ApJ, 659, 1176
Martin, P. 1995, AJ, 109, 2428
Martinet, L., & Friedli, D. 1997, A&A, 323, 363
Mee, R. W. 1990, J. Am. Stat. Assoc., 85, 793
Menéndez-Delmestre, K., Sheth, K., Schinnerer, E., Jarrett, T. H., & Scoville, N. Z. 2007, ApJ, 657, 790
Ohta, K. 1996, in Barred Galaxies, eds. R. Buta, D. A. Crocker, & B. G. Elmegreen (San Francisco: ASP), ASP conf. Ser., 91, 37
Ohta, K., Hamabe, M., & Wakamatsu, K. 1990, ApJ, 357, 71
Press, W. H., Teulkosky, S. A., Vetterling, W. T., & Flannery, B. P. 1994, Numerical Recipes (Cambridge University Press)
Regan, M. W., & Elmegreen, D. M. 1997, AJ, 114, 965
Rozas, M., Knapen, J. H., & Beckman, J. E. 1998, MNRAS, 301, 631
Sandage, A., & Tammann, G. A. 1981, A Revised Shapley-Ames Catalog of Galaxies (Washington: Carneige Inst.)
Seigar, M. S, & James, P. A. 1998, MNRAS, 299, 672
Shlosman, I., Peletier, R. F., & Knapen, J. H. 2000, ApJ, 535, L83
Speltincx, T., Laurikainen, E., & Salo, H. 2008, MNRAS, 383, 317
Sygnet, J. F., Tagger, M., Athanassoula, E., & Pellat, R. 1988, MNRAS, 232, 733
Tagger, M., Sygnet, J. F., Athanassoula, E., & Pellat, R. 1987, ApJ, 318, L43
Whyte, L. F., Abraham, R. G., Merrifield, M. R., et al. 2002, MNRAS, 336, 1281

Chapter 3

Conclusion and Further Work

3.1 Thesis Achievements

In this thesis we have applied Fourier techniques to develop tools to quantitatively analyze the morphology of spiral disk galaxies. We have developed methods to deproject disk galaxies and to measure the strength of any spiral component including bar perturbations in disk galaxies showing a bar component. As we are interested in a quantitative analysis, we need data samples big enough and over a wide range of different types of disk galaxies, which could allow us to perform deep statistical studies to fully exploit our methods. With this objective in mind, we started by using HII regions catalogues (76 sample number) which have been used to check our two deprojecting methods. This first work concluded that our two methods are as good as the other methods used so far and can give equally reliable estimations of the deprojection angles. Furthermore, our two methods are well correlated not only with other methods relying on similar principles, but also with methods based on kinematics which are considered the most reliable ones, specially for determining the position angle, PA.

In order to improve our statistical studies, we looked for richer catalogues and we moved to galaxy image catalogues which provide huge and complete information from all the galaxy components. Using information from galaxy images brings us new challenges and opportunities to verify our two deprojecting methods and to go further in our study of the morphological structure of disk galaxies. So, thanks to the use of galaxy images, we can carry out more accurate studies and prove that our two deprojecting methods perform

particularly well when determining the inclination angle, IA. Our two methods, continue to work well when determining the position angle, PA for galaxies with inclinations greater than 55 degrees. For less inclined galaxies, the major source of uncertainty is the bar strength. For non-barred galaxies our methods perform well up to inclinations of 30 degrees. Therefore, our two methods provide good results when determining IA. They are in good agreement with other methods in the literature and show the same limitations as others when trying to determine PA. It is worth noting that our methods do not introduce any bias on the deprojection angles. Moreover, the richness of the galaxy image catalogues allows us to use images from different samples and with different passband. So, we can confirm the robustness of our methods which can be used with confidence.

Our methods are based on the assumption that galactic disks are thin and circular. Assumptions shared by most of the other methods in the literature. The thickness and the instabilities of the disk are related to the mass placed in the halo. Comins *et al.* (1997) showed that massive halos help to suppress disk instabilities and recommended a halo containing 75% of the total mass of the galaxy. In addition to that, determining the ellipticity of the disk on spiral galaxies is a statistical issue as showed in Ryden (2004). If disks are oval, our results will need to be revised as the results from all the deprojection methods in the literature.

We would like to point out that we do not assume that the disk spiral structure is logarithmic. We fit the disk spiral structure to a basis of logarithmic functions because using those basis functions, we get less Fourier's terms than using other basis. If some spiral structure is not adequately represented by a logarithmic spiral, our technique will simply use a certain additional number of components in order to describe it accurately.

Our methods have the ability to provide good results with few information from the disk. This has been shown when deprojecting galaxies with a strong bar component where we need to remove all the circular fraction of the image affected by the bar. Consequently, the remaining area of the disk where to apply our methods can be small. This, however, has proved to be not a major difficulty. Moreover, thanks to this ability, we can apply our methods on low resolution images allowing to perform studies with catalogues of distant galaxies. This can have important implications to the study of spiral structure in a cosmological context.

When using our methods to measure the strength of the bar component, we proved that

we can isolate the bar component regardless of the filter used to obtain the galaxy image, and regardless of the strength of the bar component. These features provide results in good agreement with different bar indicators used in the literature and show good agreement with the morphologial classification in three categories: non-barred (SA), mildly barred (SAB) and barred (SB) galaxies. In addition to this agreement, we have a numerical measure of the bar strength showing a clear difference between the two classes, SA and SB, and a continuous transition halfway between them, that can be merged in the SAB class.

After all those statistical analysis proving the performance and robustness of our methods, we can start applying them to huge galaxy image catalogues to classify and characterize disk galaxies.

3.2 Further Work

Thanks to the ability to work with low resolution images, we can focus on larger catalogues of galaxy images including distant galaxies. We want to enlarge our database of spirals galaxies calculating their deprojection angles, and describing quantitatively their whole structure. This may allow us to perform studies of cosmological interest.

In orther to go deeper in the characterization of spiral structure, we will modify our methods for quantifying spiral arms. As we are able to isolate the arms, we can proceed studying them individualy. The first parameter which we can measure is the pitch angle, which will be compared to other galactic parameters to test spiral arms genesis theories. We will continue measuring the arm's width for a better understanding of spiral structure and its relation with other galactic properties like its mass distribution. Meanwhile, we are interested in the bar arms interaction with all the concerning implications on galaxy formation. We are now in the position to study how arm structures and amplitudes vary with radius, Hubble type and different bar properties.

Bibliography

Arp, H., 1964, ApJ, 139, 1045

Bertin, G., Lin, C.C., Lowe, S.A., Thurstans, R.P., 1989, ApJ, 338, 78

Bertin, G., Lin, C.C., Lowe, S.A., Thurstans, R.P., 1989, ApJ, 338, 104

Buta, R. 1989, in World of Galaxies, ed. H. G. Corwin, Jr. & L. Botinelli (New York: Springer-Verlag)

Cepa, J., Beckman, J.E., 1990a, A&A 114,7

Cepa, J., Beckman, J.E., 1990, ApJ 349,497C

Comins, N., 1981, MNRAS, 194, 169

Comins, N., Lovelace, R., Zeltwanger, T., Shorey, P. 1997, ApJ, 484, 33

Considère, S., Athanassoula, E., 1982, A&A, 111, 82

Considère, S., Athanassoula, E., 1988, A&AS, 76, 365

de Vaucouleurs, G. 1959 "Classification and Morphology of External Galaxies", Handbuch der Physik, 53, 275

Danver, C.G., 1942, Ann. Obs. Lund, Vol. 10, Pag. 7

Dixon, M.E., 1971, ApJ, 164, 411

Dixon, M.E., Ford, V.L., Robertson, J.W., 1972, ApJ, 171, 35

D'Onghia, E., Vogelsberger, M., Hernquist, L., 2013, ApJ, 766, 34

Elmegreen, B.G., Lada, C.J., 1977, ApJ, 214, 725

Elmegreen, D.M., Elmegreen, B.G. 1982, MNRAS, 201,1021

Elmegreen, D.M., Elmegreen, B.G. 1984, ApJS, 54, 127

Elmegreen, D.M., Elmegreen, B.G. 1987, ApJ, 314, 3

Elmegreen, B.G., Elmegreen, D.M. 1989, ApJ, 342, 677

Elmegreen, B.G., Elmegreen, D.M., Seiden, Ph.E., 1989, ApJ, 343, 602

Elmegreen, D.M., Elmegreen, B.G. 1995, ApJ, 445, 591

Elmegreen, D.M., Chromey, F.R., Bissell, B.A., Corrado, k., 1999, ApJ, 118, 2618

Eskridge, P.B., Frogel, J.A. 1999, Astrophysics and Space Science, 269/270, 427-430

Frei, Z., Guhathakurta, P., Gunn, J., Tyson,J.A., 1996, AJ, 111, 174

Gerola, H., Seiden, Ph.E., 1978, ApJ, 223, 129

Gnedin, O.Y., Goodman, J., Frei, Z., 1995, Aj, 110, 1105

Goldreich, G., Lynden-Bell, D., 1965 MNRAS 130,97

Hausman, M.A., Roberts W.W.,jr. 1984 ApJ 282,106

Hubble, E., 1926, ApJ, 64, 321

Iye, M., Okamura, S., Hamabe, M., Watanabe, M., 1982, ApJ, 256, 103

Junqueira, S., Combes, F., 1996, A&A, 312, 703

Kalnajs, A.J., 1975 *La Dynamique des Galaxies Spirales* Ed. Weliachew, actes du colloque International du C.N.R.S., 241, 103

Kimura, T., Tosa, M. 1985 PASJ 37 669

Levinson, F.H., Roberts, W.W.,jr, 1981 ApJ 245,465

Lin, C.C.,Shu, F.H., 1964 ApJ 140,646

Lin, C.C.,Shu, F.H., 1966 Proc. Natl. Acad. Sci. USA 55,229

Lindblad, B., 1929, Astronomische Nachrichten, vol 236, issue 12, 181

Miller, R.H., 1978, ApJ, 226, 81

Mueller, M.W., Arnett, W.D., 1976, ApJ, 210,670M

Nozakura, T., Ikeuchi, S., 1984, ApJ, 279,40N

Oort, J.H., 1962 "Interstellar Matter in Galaxies", ed. L. Woltjer (W.A. Benjamin Press) p. 334

Ryden, B. S. 2004 ApJ 601, 214

Roberts, W.W.,jr. 1969 ApJ 158,123

Roberts, W.W.,jr., Hausman, M.A. 1984 ApJ 277,744

Roberts, W.W.,jr., Stewart, G.R. 1987 ApJ 314,10

Schweizer, F., 1976, ApJS, 31, 313

Seiden, Ph.E., Schulman, L.S., Feitzinger, J.V., 1982, ApJ, 253,91

Sellwood, J.A., Carlberg, R.G., 1984, ApJ, 2882,61

Sellwood, J.A., 2012, ApJ, 751, 44

Sellwood, J.A., Carlberg, R.G., 2014, ApJ, 785,137

Simien, F., Athanassoula, E., Pellet, A., Monnet, G., Maucherat, A., Courtès, G., 1978, Astr.Ap., 67, 73

Takase, B., Kodaira, K., Okamura, S., 1984 *An Atlas of Selected Galaxies* Univ. of Tokio Press, VNU Sciences Press, p. 14

Thornley, M.D., 1996, ApJ, 469, L45

Toomre, A., 1969 ApJ 158,899

Toomre, A., 1969 "The Structure and Evolution of Normal Galaxies" eds. S.M. Fall D. Lyndel-Bell. (Cambridge Univeristy Press)

Yuan, C., Grosbol, P., 1981, IEEE *Transactions on Computers* C-20, No. 1

Zaritsky, D., Hans-Walter, R., 1997, ApJ, 477, 118

UNIVERSITAT ROVIRA I VIRGILI
ANALYSIS OF THE SPIRAL STRUCTURE IN DISK GALAXIES USING THE FFT TRANSFORM
Carlos Barberà Escoí

UNIVERSITAT ROVIRA I VIRGILI
ANALYSIS OF THE SPIRAL STRUCTURE IN DISK GALAXIES USING THE FFT TRANSFORM
Carlos Barberà Escoí

UNIVERSITAT ROVIRA I VIRGILI
ANALYSIS OF THE SPIRAL STRUCTURE IN DISK GALAXIES USING THE FFT TRANSFORM
Carlos Barberà Escoí

UNIVERSITAT
ROVIRA i VIRGILI